THE UNIVERSITY OF HULL

Advanced Computer Modeling of Abdominal Aortic Aneurysms to Predict Risk of Rupture.

Being a Thesis submitted for the Degree of PhD

In the University of Hull

By

(OMAR ALTUWAIJRI)

Supervisor: Prof. Michael Fagan

University of Hull, United Kingdom, 2012

ABSTRACT

An abdominal aortic aneurysm (AAA) is an abnormal enlargement of the aorta which is related to weakness of the vessel wall (associated with degradation of connective tissue), and if left untreated will lead to rupture and cause death in 78% to 94% of cases. Approximately 7,000 deaths each year in the United Kingdom are caused by AAA rupture.

AAA repair requires surgical intervention but the surgery itself has a mortality rate of about 5% in patients with stable AAA. The decision to undertake the surgery is made depending on the aortic maximum diameter of ≥5 cm. However, it is observed that rupture sometimes occurs in aneurysms with smaller diameter, thereby creating the need for better criteria for surgical intervention. Therefore, (biomechanical) indicators of AAA rupture were introduced as a superior criterion to the maximum diameter for predicting the risk AAA rupture. Several studies that have been conducted on abdominal aortic aneurysms have suggested that peak wall stress may be a more reliable predictor of the risk of AAA rupture.

This thesis is a continuation of a previous study undertaken at the University of Hull which investigated a number of biomechanical factors that affect the AAA wall stress magnitude and distribution. Novel results were gained which may help in the understanding of AAA growth and rupture events. For the first time, it is proposed that aspect ratio has an effect on the stress magnitude, location and distribution of the outer wall of AAA. These findings were used to introduce an empirical relationship between the aneurysm aspect ratio and maximum wall stress. This empirical relationship could be used as an additional clinical indicator to predict the location and magnitude of maximum wall stress where a rupture may develop.

Analysis of the porosity of the thrombus was introduced for the first time in this work using the simulation of mass transport of blood flow in an AAA, showing novel results for the possible role of blood flow on the site of growth and rupture for AAA.

Furthermore, the results of this research may also explain the conflicting views on aneurysm shape and the role of the thrombus as previously reported in the literature.

The work carried out in this research used simplified AAA geometries to allow the isolation of specific aneurysm parameters. Clearly, the next stage would include the application of the ideas and results developed here to more complex patient-specific geometries.

ACKNOWLEDGEMENTS

Firstly, I would like to express my deep and sincere gratitude to my supervisor, Professor Michael Fagan, Director of the Centre for Medical Engineering and Technology, University of Hull. His broad knowledge and logical way of thinking have been of great value to me. His understanding, encouragement and personal guidance have provided a good basis for the present thesis. Furthermore, I have gained a great deal of knowledge and skills in the past four years from working in the same centre while improving my academic career skills.

My appreciation is given to all staff and postgraduate students of the Centre for Medical Engineering and Technology who were always supportive and assisted me with academic and personal enquiries.

I am very grateful to my parents and my family who gave me the chance to complete my education in the UK and were, at all times, enormously supportive of me. I am also grateful to my wife, who gave me infinite support during these four years and helped me to complete this thesis.

I would also like to take this opportunity to convey my gratitude to my friends for always being there for me and I would like to particularly acknowledge Mahdi for his constant support and willing effort.

I am also sincerely grateful for the opportunity to use the electronic library of Hull University who provided me with most of my much needed books and resources.

Finally I would like to thank my sponsor, King Saud University, for the financial and logistic support they provided during my study.

I dedicate this work to my parents and to my small family, Rayda and Sofanah, in appreciation of the constant help and support and the way they understood my need to sacrifice my time so that I could put more effort into completing this project.

TABLE OF CONTENTS

LIST OF ABBREVIATIONS

AAA: Abdominal aortic aneurysm

CAD: Computer Aided Design

CFD: Computational Fluid Dynamics

CT: Computed Tomography

ECs: Endothelial Cells

FEA: Finite Element Analysis

ILT: Intraluminal Thrombus

MMPs: Matrix metalloproteinases

RMS: Root Mean Square

TIMPs: Inhibitors of matrix metalloproteinases

VSMCs: Vascular smooth muscle cells

LIST OF FIGURES

LIST OF TABLES

Chapter 1
Introduction

An abdominal aortic aneurysm (AAA) is a cardiovascular health disease that occurs when the aorta becomes weak and develops into a balloon-like structure and usually occurs below the renal bifurcation (Sanfelippo, 2003). The aneurysm diameter can be up to four times the normal aortic diameter and can enlarge at a rate of 0.2 - 1.0 cm/year until it suddenly ruptures if left untreated (Wolf and Bernstein, 1994). The estimated prevalence for AAAs in older males is in the order of 3% to 5% (Crawford et al., 2003) and the mortality rate for ruptured AAA is between 78% and 94% (Hall et al., 2003). AAA is the 13th leading cause of adult mortality and the 3rd leading cause of sudden death in men older than 65 years of age (Cowan et al., 2006). The British Heart Foundation recently reported that Aortic aneurysms cause around 7,000 deaths in the United Kingdom every year (British Heart Foundation Media News, 2011).

AAAs occur in the infrarenal segment of the aorta between the renal arteries and the iliac bifurcation, as shown in Figure 1-1. Men are affected more than women by a ratio of 4:1 and the prevalence of the disease has not decreased even with highly advanced medical surgeries and technology, while the mortality and morbidity caused by AAA are still increasing (Karkos et al., 2000).

One of the major problems with AAAs is that they are often asymptomatic until rupture, which is why AAA is called the "silent killer". When an AAA is small, periodic observation to monitor the aneurysm is the only available treatment. But when it becomes larger and at risk of rupture, surgical treatment is required which by itself has a mortality rate of between 2% and 5% (Hollier et al., 1992).

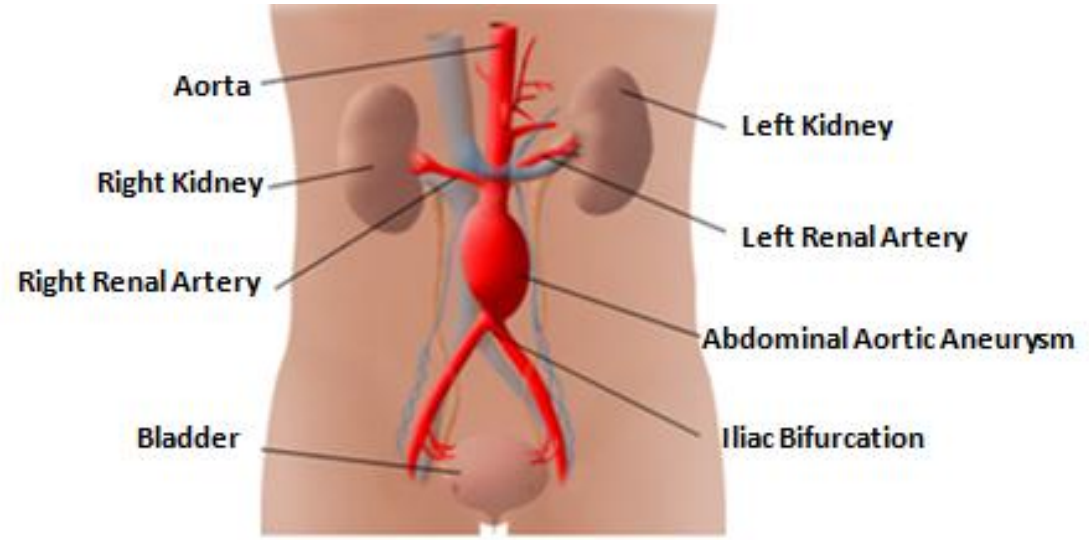

Figure 1-1: Abdominal aortic aneurysm. (Adapted from www.jeffersonhospital.org/Tests-and-Treatments/abdominal-aortic-aneurysm-repair.aspx)

Because of the high cost and risk of the surgical treatment it may be a more serious threat to life than a stable AAA. Therefore, watchful management is the first choice for any new patient with elective surgery should only be chosen when rupture risk is high (Katz et al., 1992).

Currently, the decision of when to operate is made depending on the diameter of the AAA. It is recommended that the operation be performed when the diameter of the AAA exceeds 5 cm. The surgery is also recommended for aneurysms that are less than 5 cm diameter with average growth rates of more than 0.5 cm/year. However, it is difficult to decide when the risk is sufficiently high due to the lack of reliable rupture risk indicators. The reason for this lack of indicators is the natural history and development of individual AAAs. They can either be stable, expanding slowly, or they can expand rapidly. An accurate identifier of patients with a high risk AAA would therefore reduce medical costs and save lives.

Rupture to the AAA is the worst possible outcome and causes death in more than 80% of the cases (Thomas and Stewart, 1988). The rupture is a biomechanical event that occurs when the mechanical stresses applied on the inner wall of the aorta exceeds the failure strength of the wall (Heller et al., 2000; Lombardi et al., 2004; Speelman et al., 2007). Out of these two factors (wall strength and wall stresses), it is

only possible to assess the wall stresses using different approaches but there is a lack of a non-invasive method to measure wall strength.

The current assessment of AAA risk of rupture is still largely based on a maximum diameter criterion (when the maximum transverse diameter of AAA exceeds 5 cm) which is a simple indicator. In medical practice, it is observed that AAAs with diameters less than 4 cm are found to rupture. But the abdominal aorta diameter does not vary with body size, which does not explain the rupture of smaller aneurysms (Alcorn et al., 1996; Fillinger et al., 2003; Peppelenbosch et al., 2004).

In the current literature there are a number of studies and experiments reporting that wall stress may be a better indicator of the development of the disease and that the stress is greatly influenced not only by the diameter of the AAA wall but also by blood pressure, the AAA shape, aneurysm wall local curvature, aneurysm wall thickness and presence of thrombus inside AAA.

A significant amount of research has been carried out investigating the biomechanics of AAA using a range of computational models. Over the past few decades the state-of-the-art in AAA simulation has evolved from simple analytical models involving cylindrical geometry to fully coupled fluid-solid interaction simulations using patient specific geometries and anisotropic finite strain constitutive relations for AAA tissues. However, a number of factors which may have an effect on AAA risk of rupture were not discussed, while other factors were neglected for the purpose of simplicity. In this current work, some of these factors will be investigated as detailed below.

While the relationship between the length of the aneurysm and the diameter of the normal aorta (aneurysm aspect ratio) seems to have an effect on wall stress distribution, no studies in the literature have assessed this relationship. This current work is therefore the first to study this relationship, whereby an investigation is carried out on how the aspect ratio of the aneurysm could change magnitude and the location of maximum wall stress to aid in AAA diagnosis.

Additionally, a common assumption among previous numerical simulations which modelled the thrombus inside the AAA is that the thrombus has been given solid material properties, while in reality the thrombus is a porous permeable material. This work suggests that modelling the thrombus as porous media can provide additional information on the biomechanical environment within the AAA.

Two recent studies have modelled the thrombus as a porous medium (Ayyalasomayajula et al., 2010; Polzer and Bursa, 2010) and have provided further insight into the impact of thrombus porosity on AAA biomechanics. However, both these studies neglect the actual dynamics of blood flow in the aneurysm sac and its transfer into the thrombus. This current work is the first to implement mass transport of the blood into porous thrombus to investigate how blood flows from the blood lumen through the thrombus, providing additional information and possible mechanisms for AAA growth and improvements in AAA diagnosis.

The role of the thrombus in AAA has been investigated in a number of studies, but there is a conflict between the conclusions reported by researchers and further investigation is required. This work contributed to this field of study because it uses non-complex geometries to examine a variety of factors, providing a clear understanding about the possible role of the factors examined.

This work also provides additional information about the role of the aneurysm shape on its pathology.

1.1 Organisation of the thesis

This thesis begins with an introductory Chapter on the abdominal aortic aneurysm with some statistics of its prevalence, growth rate and mortality in general (especially in the United Kingdom), followed by a summary description of the clinical problem and how it is assessed in clinics and a discussion on the limitation of this assessment method. The study then briefly demonstrates the indicators researchers have used to provide a better method of assessment and how this work can contribute to the current body of knowledge. Chapter one also includes an overview of the organisation of this thesis.

Chapter two includes a literature review of AAA, beginning with a discussion on the anatomy of the aorta and its wall structure, followed by a review of the abdominal aortic aneurysm, including a chart showing the pathogenesis of an abdominal aortic aneurysm. A brief description is also included of the treatment of AAAs and a discussion of the rupture mechanism.

Chapter two includes a detailed description of the biomechanics of the AAA to understand how wall stresses are developed. This description includes an illustrated study on blood flow patterns inside the aneurysm using steady and pulsatile flow. The flow-induced stresses and pressure are discussed in terms of their effect on the rupture mechanism. The aneurysm shape is then discussed to understand its effect on the wall stresses.

Chapter two also details the role of the intraluminal thrombus, which exists in most AAAs, by examining its structure then examining how intraluminal thrombus affects wall strength and how it alters oxygen diffusion in the aneurysm.

Chapter three discusses in detail the methodology used to perform the simulations undertaken in this thesis. Chapter three begins with a discussion of the finite element analysis technique followed by a detailed description of the models used for this method. The study of the convergence for this method is then described to confirm that the results obtained were taken at acceptable approximations prior to a validation study of the simulation. A brief background on the strategy of computational fluid dynamics techniques is then demonstrated with details of the models used for flow studies followed by convergence and validation studies.

Chapter four, using finite element analysis (FEA) and computational fluid dynamics (CFD), investigates the effects of basic aneurysm geometry to understand how aneurysm shape can affect wall stresses and blood flow patterns. An intensive study of the aneurysm aspect ratio is then taken using three shapes with three different diameters for each shape.

Chapter five outlines the intensive investigation of the role of thrombus presence, thickness, structure, material properties and porosity on wall stresses and its possible relationship to growth using FEA and CFD.

Chapter six includes a discussion on the effect of aneurysm shapes on wall stress and blood flow. The chapter then outlines some novel findings of the aneurysm aspect ratio relationship with maximum wall stress followed by a discussion of the effect of the inclusion of thrombus with different thicknesses and material properties. A discussion is then given on the effect of thrombus porosity on wall stresses followed by a description on how the flow of blood within the porous thrombus can contribute more information to understand the reasons of the rupture risk.

Chapter seven concludes the results of this work and discusses possible areas of future work to be continued.

1.2 Research aims

The aims of the research may be summarised as follows:

- To prove that maximum diameter is not the best predictor of rupture.
- To understand how blood behaves inside the aneurysm and how this may affect the risk of rupture of AAA.
- To investigate and understand the effect of aneurysm shape especially the aspect ratio of the aneurysm on wall stresses.
- To investigate and understand the effect of thrombus presence on wall stresses.
- To investigate the effect of thrombus porosity on aneurysm wall stresses and on the blood flow within the aneurysm.

Chapter 2
Review of the anatomy and biomechanics and Abdominal Aortic Aneurysm

2.1 Clinical Anatomy

AAA is a localised abnormal dilatation of the abdominal aorta. The normal aorta is 19 to 22 mm in diameter, while aneurysms as large as 7 cm in diameter have been recorded (Imray, 2006).

When the aorta enters the abdomen it is then called the abdominal aorta. The abdominal aorta supplies five main vascular branches from its beginning until its end by the two iliac arteries (Gray, 1918). The abdominal aorta branches in addition to the two iliac arteries including celiac trunk, superior mesenteric artery, and two renal arteries (Gray, 1918), as shown in Figure 2-1.

The renal arteries start approximately 1 cm inferior to the superior mesenteric artery and 90% of the AAA starts inferior to the renal arteries and continues until it reaches the iliac arteries (Finol and Amon, 2001). Abdominal aorta geometry varies from one individual to another, and depends on sex and age (Lee et al., 1982).

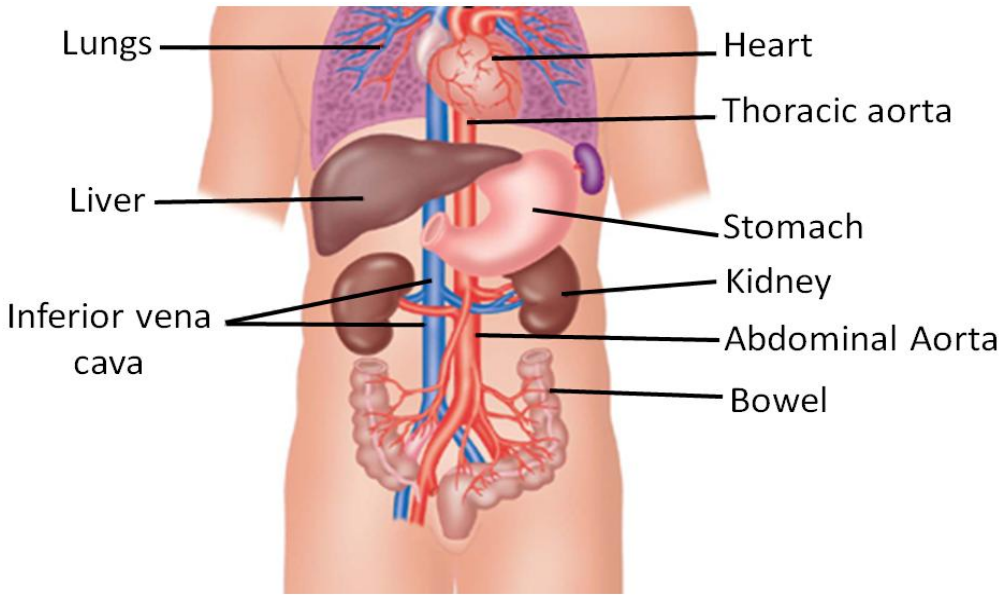

(a)

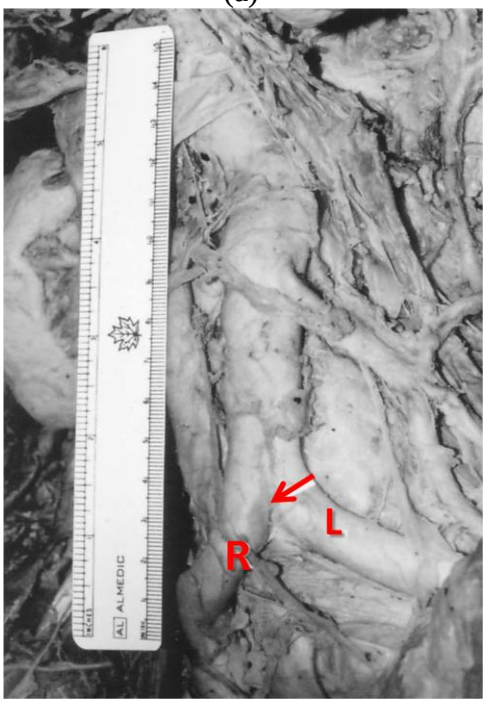

(b)

Figure 2-1: (a)Tthe anatomy of the abdominal aorta (from http://familydoctor.co.uk/aortic01). (b) Normal aorta, iliac bifurcation (arrow) and right (R) and left (L) iliac (Crawford et al., 2003).

2.2 Structure of the Aortic wall

The aorta wall consists of three layers (Fung, 1993), as shown in Figure 2-2.

- Tunica adventitia: this is the strong and elastic external covering of the aorta. It is composed of connective tissue as well as collagen and elastic fibres which give the aorta strength and elasticity.

- Tunica media: this is the middle layer of the aortic wall and is composed of smooth muscle and elastic fibres.
- Tunica intima: this is the inner layer of the aorta and is composed of spongy connective tissue that secretes a layer of elastic collagen and endothelium that consists of flat and smooth epithelial cells. This layer is in direct contact with the blood and responds to changes in the blood pressure by altering the vessel diameter.

Dysfunction of these tissues is an important factor of the pathology of the aorta, as described in the following sections.

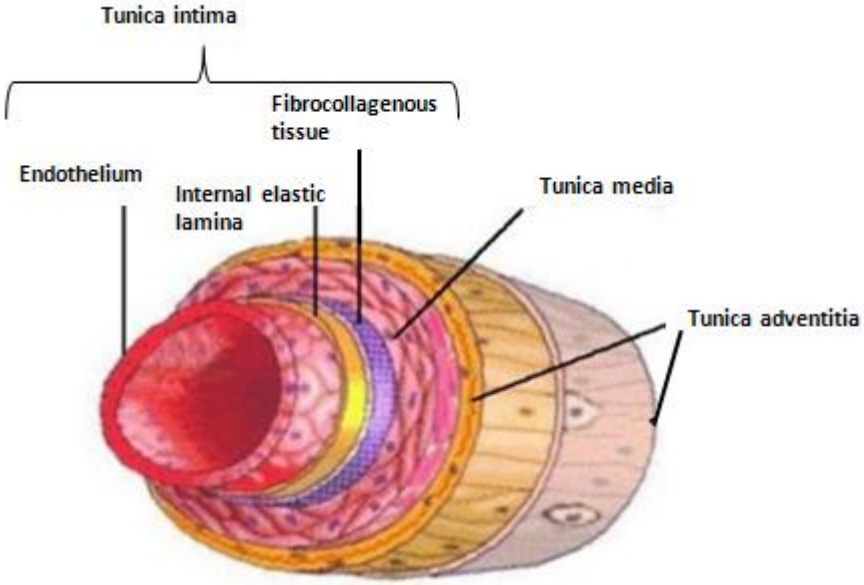

Figure 2-2: The structure of the aorta, (adapted from http://fau.pearlashes.com/anatomy/Chapter32/Chapte32.htm)

2.3 AAA Pathophysiology

AAA is a pathologic, irreversible dilatation of a segment of the aorta, caused by a congenital or acquired weakness. The difference between a healthy and diseased aorta is the difference in the wall structure. A large decrease in aortic elastin, an increase in collagen production and degradation, inflammatory changes and imbalances in the structure of the wall can occur in the diseased wall. Family history and genetic factors play a role on the pathophysiological process of the disease,

especially in disorders such as Marfan disease[1] (Crawford et al., 2003; Wang et al., 2001).

Normally, arterial blood pressure and flow velocity cause high stresses on the aortic wall which, with the help of other factors, can cause changes to the wall. From a mechanical point of view, how the development of AAA occurs is not yet fully understood. However, it is known that many factors together play a role in the formation of AAA (Alcorn et al., 1996; Bonert et al., 2003; Buchanan et al., 2003; Cheng et al., 2003a; Wang et al., 2001; Fleischmann et al., 2001).

The process of AAA development includes an initial weakening of the wall in combination with other factors that are already known to be stress generators. Figure 2-3 shows the pathogenesis of AAA (Crawford et al., 2003). Aneurysms are believed to be caused by the degradation of elastin in the aortic wall causing the vessel to lose its elasticity and recruit the non elastic collagen fibres. Failure of collagen will then lead to dilatation of the aorta (Crawford et al., 2003).

The most commonly known factors in the pathophysiological process include: atherosclerosis, hypertension, breakdown of elastin and collagen, inflammation, male sex, chronic obstructive pulmonary disease, tobacco smoking, age, poor diet, genetic factors and family history (Crawford et al. , 2003; Wang et al. , 2001; Wang et al., 2002).

When the aorta is weaker it becomes more prone to expand due to blood pressure and a larger aneurysm is likely to have higher stresses due to the fundamental principles as explained in the law of Laplace:

$$\sigma = \frac{pD}{2\tau} \qquad \text{(Eq 2.1)}$$

For this equation, it has been observed that the hoop stress σ increases when diameter D increases if the pressure p and wall thickness τ are constants, which may explain why large aneurysms grow at faster rates (Wang et al., 2002; Elger et al., 1996).

[1] The Marfan syndrome is a connective tissue disorder whereby tendons, ligaments, blood vessel walls, cartilage, heart valves and many other structures are not as stiff as they should be.

Medical literature explains that the anatomic and physiologic properties of the aorta change with age. The aorta becomes thicker, stiffer, and less distensible. Arterial elastin fibres degrade and the collagen fibres increase, which may lead to a loss of load-bearing capacity and cause vessel dilation. The decrease of aortic dispensability is faster and occurs at an earlier age in men, which explains why more men suffer from AAA than women (Cheng et al., 2003a). African-Americans and persons with diabetes have lower prevalence of AAA (Cheng et al., 2003b). People suffering from other diseases or problems may become more prone to develop AAA. For example "post-traumatic" above-knee amputees are 5 times more likely to develop AAA 40 years after the injury than normal individuals, while spinal cord injury patients seem to be twice as likely to experience AAA formation approximately 20 years following their injury. This is explained by the significant haemodynamic changes which occur in people having these kinds of diseases (Ernst, 1993). Haemodynamics and its role is discussed in further detail later in this thesis.

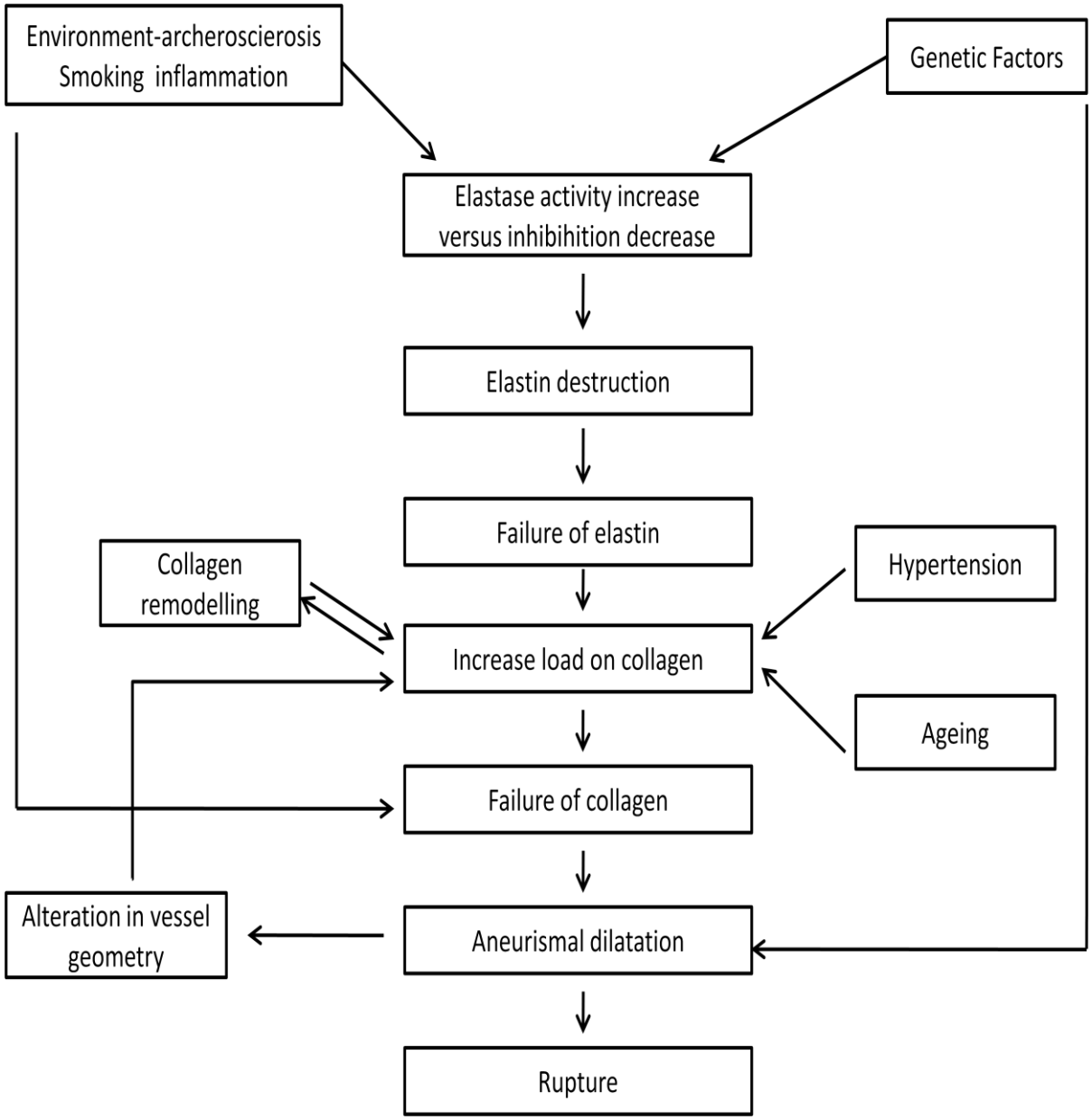

Figure 2-3: Chart showing the pathogenesis of an abdominal aortic aneurysm (adapted from Crawford et al., 2003)

2.4 Matrix metalloproteinases and AAA

Matrix metalloproteinases (MMPs) are an ever-expanding family of endopeptidases with proteolytic activity towards one or more components of the extracellular matrix. Of the 25 MMPs identified in vertebrates, 23 are found in humans (Birkedal et al., 1993; Visse and Nagase, 2003).

The activity of MMPs is regulated at three levels (Visse and Nagase, 2003):

1. Transcriptional regulation.

2. Pro-enzyme activation.
3. Inhibition of proteolytic activity by endogenous inhibitors of matrix metalloproteinases (TIMPs).

Endothelial cells (ECs), vascular smooth muscle cells (VSMCs) and adventitial fibroblasts and all other vascular cells secrete MMPs in their normal activities. Macrophages and lymphocytes can be additional sources of MMPs. MMPs are responsible for normal tissue remodelling but have various other important roles in many biological processes such as embryogenesis, wound healing and angiogenesis as well as in diseases such as atheroma, arthritis, cancer and tissue ulceration. In normal conditions, MMP activities are controlled by their inhibitors TIMP, but an imbalance between MMPs and their inhibitors TIMPs, may lead to matrix degradation (Liapis and Kadoglou, 2004).

Increased levels of MMP expression and activity have been found in the aortic wall of AAA leading to matrix degradation (Wassef et al., 2001). In normal conditions, MMPs play an important role in the remodelling process of the aortic wall by degrading extracellular matrix proteins such as elastin and collagen, both of which are needed to maintain structural integrity and favourable mechanical properties (Ailawadi et al., 2003).

It is speculated that MMP production within the aneurysm wall may be released into the systemic circulation and then could be used to diagnose AAA severity or rupture risk. In addition, plasma MMPs could be used to evaluate the effectiveness of AAA surgeries (Liapis and Kadoglou, 2004).

The blood flow may have a role in concentrating the MMPs in specific sites of the AAA wall or its adjacent thrombus and hence increase the chance of pathogenesis of AAA as discussed later in this thesis.

2.5 Treatment

One of the major problems with AAAs is that they are often asymptomatic until rupture, which is why AAA is called the "silent killer". However, some symptoms of AAA can develop such as pain in the abdomen, back or chest area. AAAs can be felt

as a pulsating or throbbing mass in the abdomen (Ernst, 1993; Lermusiaux et al., 2001).

When an aneurysm does rupture, the symptoms include:

- Sudden severe back or abdominal pain.
- Loss of colour from the face.
- Thirst and dryness of the mouth or skin.
- Nausea and vomiting.
- Shaking, dizziness, fainting, sweating, and rapid heartbeat.

When an AAA is small, periodic observation to monitor the aneurysm is the only available treatment. However, when the AAA becomes larger and at risk of rupture, surgical treatment is required which in itself is risky as it has a mortality rate of between 2% and 5% (Hollier et al., 1992).

Two procedural options are available: open surgical repair and endovascular repair. Open surgical repair is the most common treatment for large, non-ruptured aneurysms. In this operation the surgeon cuts the aorta and places a synthetic graft inside the aneurysm connecting the two ends of the healthy aorta by sutures, as shown in Figure 2-4. Endovascular repair is less invasive as the surgeon places an endovascular graft inside the aneurysm making the graft a new lumen for the blood, as shown in Figure 2-5. The graft is delivered via a catheter. Endovascular repair requires more accurate morphological information and detailed measurements than open repair (Engellau et al., 2003).

Endovascular repair is associated with a high frequency (17-26%) of endoleakage[2] with the possibility of recurrence and/or rupture during the 18 month follow-up period (Sangiorgi et al., 2001). Observing endoleakage involves significant effort which greatly increases the cost of endovascular repair treatment (Sangiorgi et al., 2001; Bargellini et al., 2005; Bieth, 2001).

[2] Endoleaks are defined as a persistent blood flow leaking into the aneurysm sac and outside the graft lumen; they represent the most frequent complication after endovascular aneurysm repair (Engellau et al., 2003).

Because of the high cost and risk of the operation, the operation may be a more serious threat to life than a stable AAA. Therefore, watchful management is the first choice for any new patient with elective surgery and should only be chosen when rupture risk is high (Katz et al., 1992).

Currently, the decision of when to operate is made depending on the diameter of the AAA. It is recommended that the operation is performed when the diameter exceeds 5 cm. The surgery is also recommended for aneurysms that are less than 5 cm diameter with average growth rates of more than 0.5 cm/year. Approximately 20% of aneurysms expand faster than 0.4 mm/year, while the remaining 80% expand at slower rates (Brady et al., 2004; Breeuwer et al., 2004). However, it was observed in clinics that AAA with diameters of less than 4 cm were found to rupture (Fillinger et al., 2003; Peppelenbosch et al., 2004). It is difficult to determine when the risk of rupture is sufficiently high due to the lack of reliable rupture risk indicators. The reason for this lack of indicators is the natural history and development of individual AAAs. They can either be stable, expanding slowly or they can expand rapidly. An accurate identifier of patients with high risk AAA would therefore reduce medical costs and save lives.

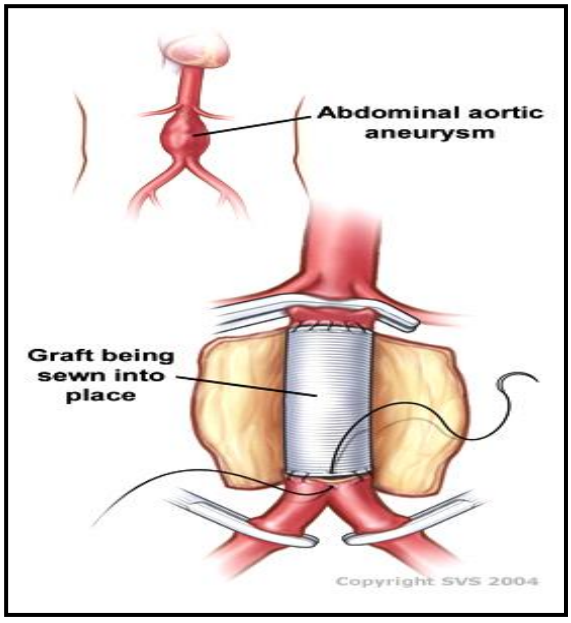

Figure 2-4: Open surgical repair showing the synthetic graft inside the aneurysm connecting the two ends of the healthy aorta by suture.
(from http://www.vascularweb.org/vascularhealth/Pages/SurgicalAneurysmRepair.aspx).

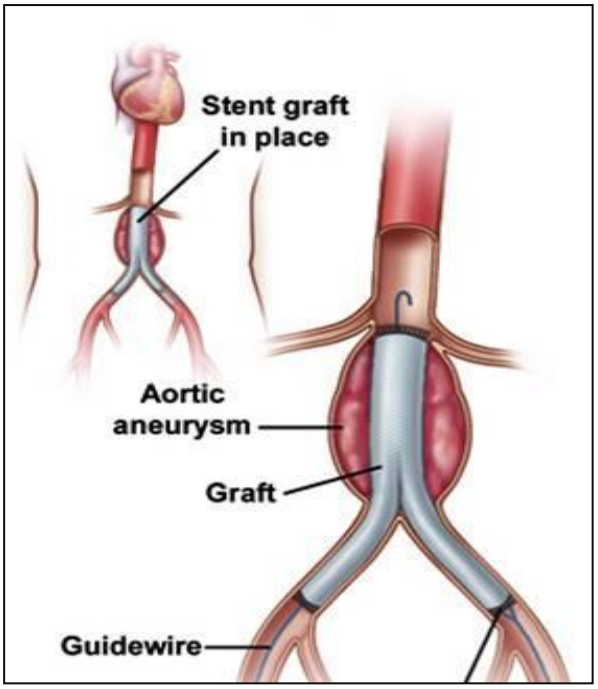

Figure 2-5: Endovascular repair showing the endovascular graft inside the aneurysm making the graft a new lumen for the blood (From http://www.metrohealth.org/body.cfm?id=1448).

2.6 AAA rupture

Rupture to the AAA is the worst possible outcome and causes death in more than 80% of the cases (Thomas and Stewart, 1988). Mortality rates for ruptured AAA are still high even with the current advances in medical surgeries and technologies. The rupture is a biomechanical event that occurs when the mechanical stresses applied on the inner wall of the aorta exceed the failure strength of the wall (Lombardi et al., 2004; Heller et al., 2000; Speelman et al., 2007).

The current indicator of high rupture risk (when the maximum transverse diameter of AAA exceeds 5 cm) is a simple indicator. Other more complex indicators include aneurysm shape, wall thickness, flow dynamics and vessel mechanical properties. However, ostensibly these are too complex for use because they can differ between aneurysms of the same diameter (Finol and Amon, 2001).

As mentioned earlier, it has been observed that AAAs with diameters of less than 4 cm can rupture. However, the abdominal aorta diameter does not vary with body size, which does not explain the rupture of a smaller aneurysm (Alcorn et al., 1996; Fillinger et al., 2003; Peppelenbosch et al., 2004).

Biomechanical analysis of blood dynamics could be used in addition to maximum transverse diameter as an indicator for rupture risk of the aneurysm. In particular, the fluid stress on the internal wall of the aneurysm may be an indicator of when a particular aneurysm will rupture (Wang et al., 2001; Fillinger et al., 2002).

2.7 Biomechanics of the AAA

Blood flow dynamics, known as "haemodynamics," create forces applied on the internal wall of the aneurysm which can lead to rupture. Haemodynamic forces are generated by the flow of blood through the aorta. Therefore, the study of haemodynamics of the AAA is a very important factor for understanding the characterization of the biomechanical environment of aneurysms (Taylor et al., 1998).

2.7.1 Flow patterns

Flow patterns within the AAA can strongly influence the magnitude and distribution of all components of the (flow-induced) forces on the aneurysm wall (Walsh et al., 2003; Finol and Amon, 2003). Several experimental and numerical studies have examined the flow patterns inside the AAA using steady and pulsatile flows (Yu et al., 1999; Yu, 2000).

Yu et al. (1999) studied the haemodynamics of models of the AAA using particle image velocimetry. Their study of the steady flow in an AAA model shows the upstream flow on the tube before the aneurysm consisting of two parts: a large core across the tube and a secondary thin boundary layer attached to the wall, as shown in Figure 2-6. When the flow enters the aneurysm it consists of a stream surrounded by recirculation vortices. These vortices are a result of the adverse pressure gradient caused by the increase in cross-sectional area at the bulge. The velocity inside these vortices is relatively slow. The vortices are closer to the downstream side of the aneurysm (Yu et al., 1999). Interestingly, the size of the aneurysm did not significantly alter the flow patterns. These findings are similar to those of Budwig et al. (1993).

In the same study, Yu et al. (1999) repeated the experiments, this time using pulsatile flow and found that boundary layer thickness in the tube before the aneurysm decreases as the flow rate increases. After the peak of the flow rate, the boundary layer thickness slightly increases. When the flow reaches a minimum it is still attached to the wall (Yu et al., 1999).

When the flow enters the aneurysm and immediately in the proximal end of the aneurysm, a small recirculation vortex develops at the beginning of the cycle, which then moves to the distal end of the aneurysm after the peak flow rate of the systolic cycle, as shown in Figure 2-6. Compared to the steady state condition, the pulsatile flow pattern did not change significantly, except that the recirculating vortex grew slightly stronger as the flow continued to accelerate towards the point of peak flow rate. Again, the size of the bulge did not alter the flow features, although the strength of the vortex was greater if the size of the bulge was larger (by about 20% at every point over a cycle) and the location of the centre of the vortex was not constant as it was in steady flow. As a result, the regions of high shear stresses and low shear stresses in pulsatile flow were not stable and wall shear stress fluctuation could occur.

Yu et al. (1999) did not find any vortex formation in their small AAA model with low flow rate condition. It is speculated that vortex formation inside the aneurysm sac helps the thrombus to form in those regions. In addition, vortexes at the exit of the bulge cause high-pressure regions to become potentially prone to rupture. They then hypothesized that the vortex formation during the diastole may be responsible for “tearing the wall tissue” leading to thrombus formation (Yu, 2000; Yu et al. 1999).

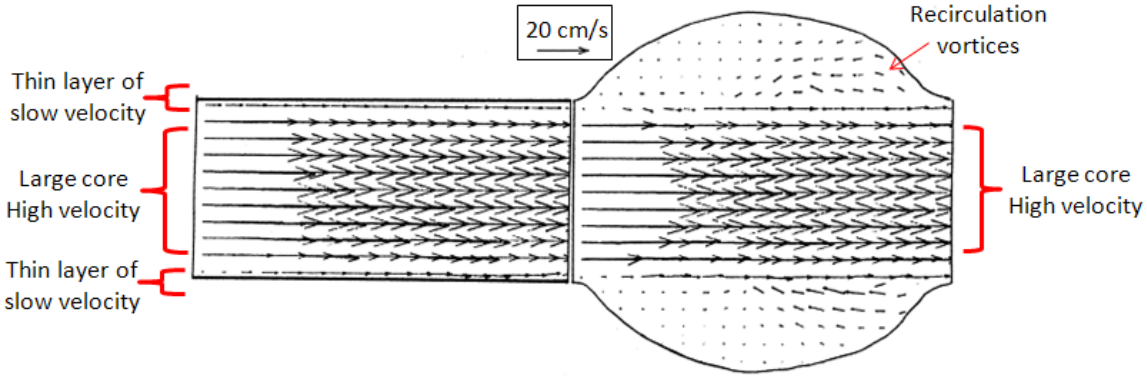

Figure 2-6: Velocity vector plots under steady flow condition (Yu, 2000).

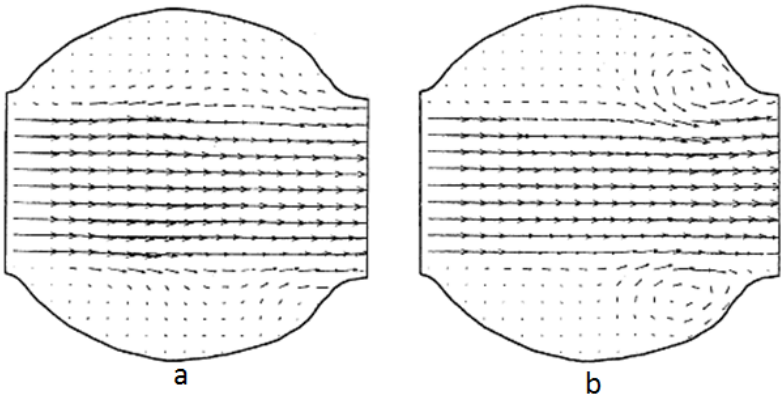

Figure 2-7: Velocity vector plots under pulsatile flow condition, a) at the beginning of the systolic cycle, b) after the peak of flow rate (Yu, 2000).

2.7.2 Wall shear stresses

Wall shear stresses (WSS) are the tangential forces on the surface of the aneurysm, along the axis of flow. A numerical study of a realistic AAA undertaken by Papaharilaou et al. (2007) for pulsatile flow found that most of the AAA wall surface was under a very low wall shear stress during the cardiac cycle. Only the proximal and distal necks of the AAA bulge were under a high WSS, as shown in Figure 2-8.

These findings were similar to those of Peattie et al. (2004) who established in an experimental study of 7 AAA models that WSS seemed to be constant in the upstream tube and suddenly decreased in the bulge, then increased again at the distal end of the bulge where sharp velocity gradients occur, which leads to a sharp increase in shear stresses at the distal bulge end with values of 1.5 to 2 times those at the proximal end.

Peattie et al. (2004) reported in an experimental flow study that the increase in large distal wall shears is dependent on flow spreading into the bulge the maximum shear stress may therefore be expected to be affected by the bulge diameter. In their study, the maximum systolic shear stress (19 dynes/cm^2) was at the distal bulge end of AAAs with a diameter of 4 cm. With aneurysms of 5 cm diameter, the maximum systolic shear stress was found to be 12 dynes/cm^2, which is higher than the maximum systolic shear stress recorded for aneurysms of 3, 5.5 and 6 cm diameter. Hence, Peattie et al. (2004) proposed that these 'medium' sized AAAs are more prone to maximal shear stress than the very small or very large sized AAAs, as shown in Figure 2-9.

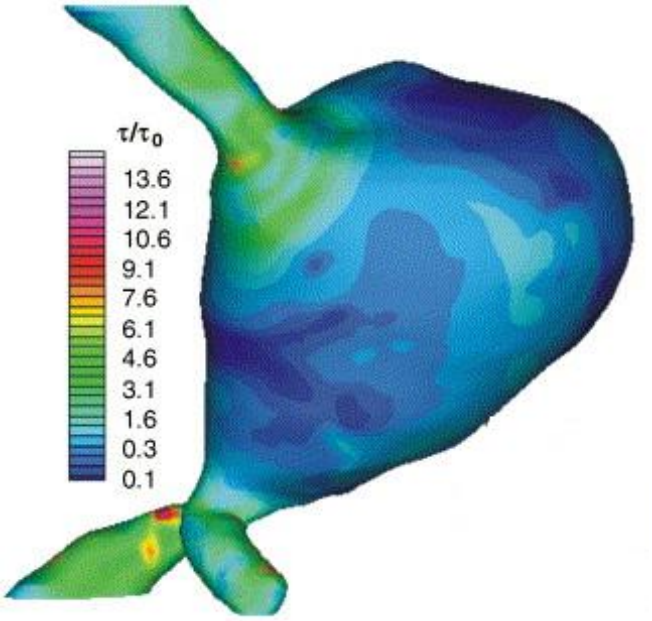

Figure 2-8: Wall shear stresses normalized to the inlet straight pipe (Papaharilaou et al., 2007).

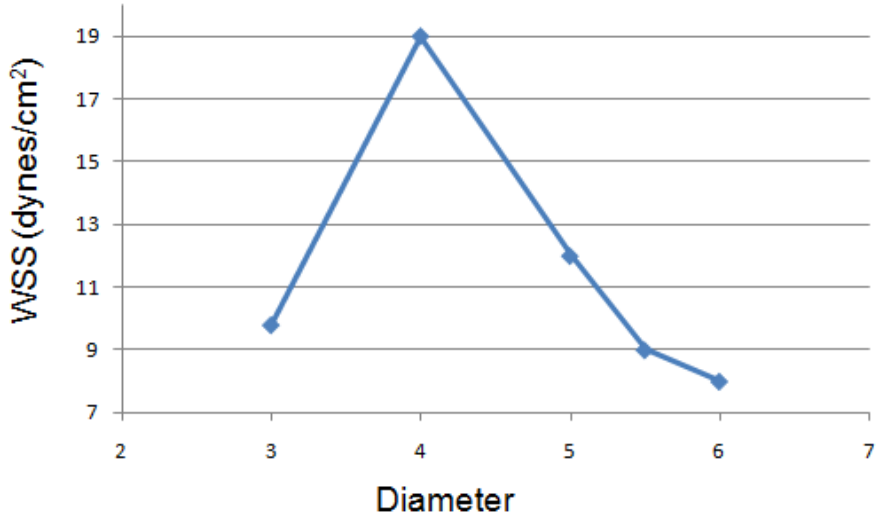

Figure 2-9: Dependence of the maximum systolic wall shear stress on aneurysm diameter (reproduced from Peattie et al., 2004).

However, in earlier experimental investigations, Peattie et al. (1996) showed that the flow in AAAs may become unstable and show random velocity fluctuations even under steady flow conditions. Furthermore, when instability occurs, peak immediate shear stresses at the wall may reach 20 times their mean value. Thus, turbulent flow may significantly increase wall shear stresses at the aneurysm distal end. From this it could be concluded that the relationship between size and rupture in AAAs may be due to higher wall stresses caused by more frequent and severe unstable flow in the larger aneurysms (Peattie et al., 1996). WSS depends very much on AAA geometry (bulge shape and diameter) and AAA geometry varies from patient to patient.

2.7.3 Wall stresses and pressure distribution

Several attempts to derive a reliable AAA rupture risk indicator have been based on the assessment of the arterial wall stress distribution. In a number of studies, maximum wall stress has been speculated to be a better predictor of rupture than diameter (Raghavan et al., 2000; Fillinger et al., 2003; Venkatasubramaniam et al., 2004).

Using finite element analysis (FEA), Raghavan et al. (2000) carried out a wall stress study using non-linear hyperelastic wall material properties on aneurismal and normal aorta and found that wall stress was higher in the aneurismal aorta compared to the normal aorta. They also found that stresses on the aneurismal wall were distributed in

a complex way with large regional variations compared to those of the normal aorta, which was lower and more uniformly distributed, as shown in Figure 2-10.

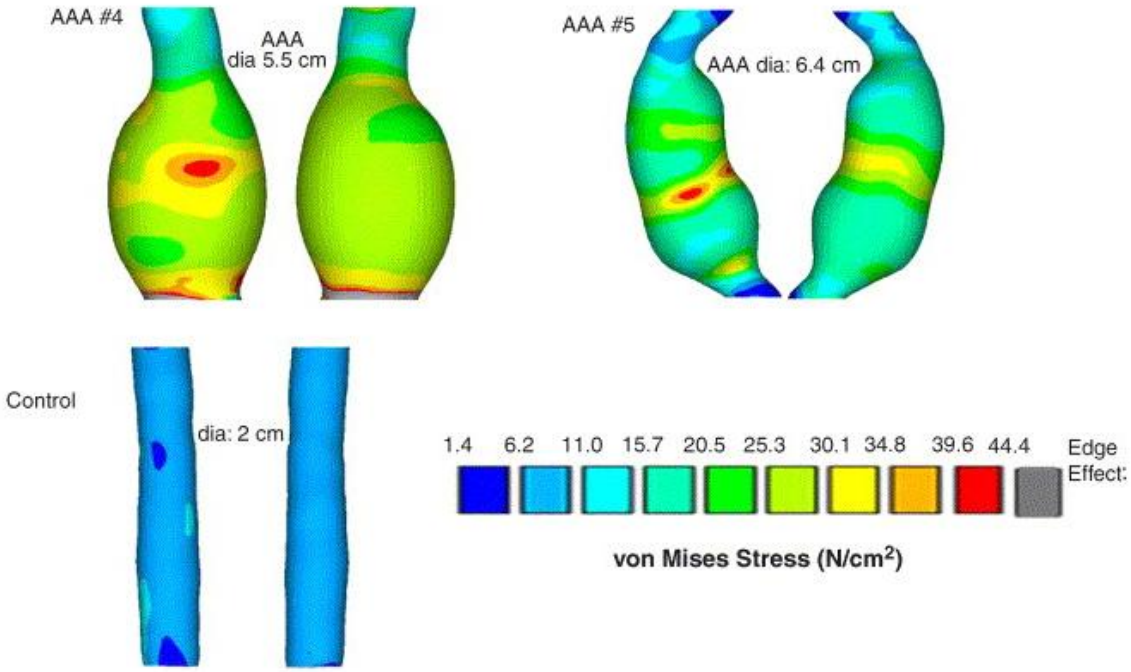

Figure 2-10: Wall stress distributions for two AAA (top) and one non-aneurismal aorta (bottom). Two images are shown for each aorta. The left image is the posterior surface, while the right image is the anterior surface. The maximum diameter of the AAA at the top left is 5.5 cm, while that at the top right is 6.4 cm (Raghavan et al., 2000; Vorp, 2007).

Fillinger et al. (2003) used Clinical Computed Tomography (CT) scan images used to create patient specific finite element models in order to investigate whether these models can predict AAA rupture. Computed Tomography (CT) scans from 103 aneurysms were analyzed for patients with AAA when observation was planned for 6 months. Three-dimensional computer modelling and finite element analysis (nonlinear hyperelastic model depicting aneurysm wall behaviour) were used and blood pressure was taken during observation. Fillinger et al. (2003) found that finite element analysis of AAA wall stress is a better predictor of higher stresses regions than the diameter of the AAA for patients with high risk of rupture who later required emergent repair.

Fillinger et al. (2003) have reported that the distribution of diameter measurements as shown in Figure 2-11 demonstrates that 90% of AAAs in the study had a diameter larger than the lowest recorded diameter for AAAs that consequently ruptured or became symptomatic, which was (4.4 cm) in maximum diameter. In the ruptured or symptomatic group, 5 of 22 AAAs were 5 cm or less in maximum diameter. The results gained from maximum wall stress was showed better prediction for ruptured or symptomatic aneurysms as shown in Figure 2-11. The box plot for maximum wall stress demonstrates that 75% of AAAs in this study had stress lower than the lowest recorded stress for AAAs that consequently ruptured or became symptomatic.

Venkatasubramanium et al. (2004) used finite element analysis to study twenty seven AAA patients divided into ruptured and non-ruptured groups. In their study, 3D geometries of AAA were derived from CT scans of 27 patients (12 ruptured and 15 non-ruptured). AAA geometry, systolic blood pressure and material properties derived from the literature, were utilised to calculate the wall stress for individual AAAs. They reported that peak wall stress was notably higher in the ruptured AAA (mean 1.02 MPa) than the non-ruptured AAA (mean 0.62 MPa). In patients with an identifiable location of rupture on a CT scan, FEA was able to predict the area of peak wall stress that correlated with the rupture site as shown in Figure 2-12.

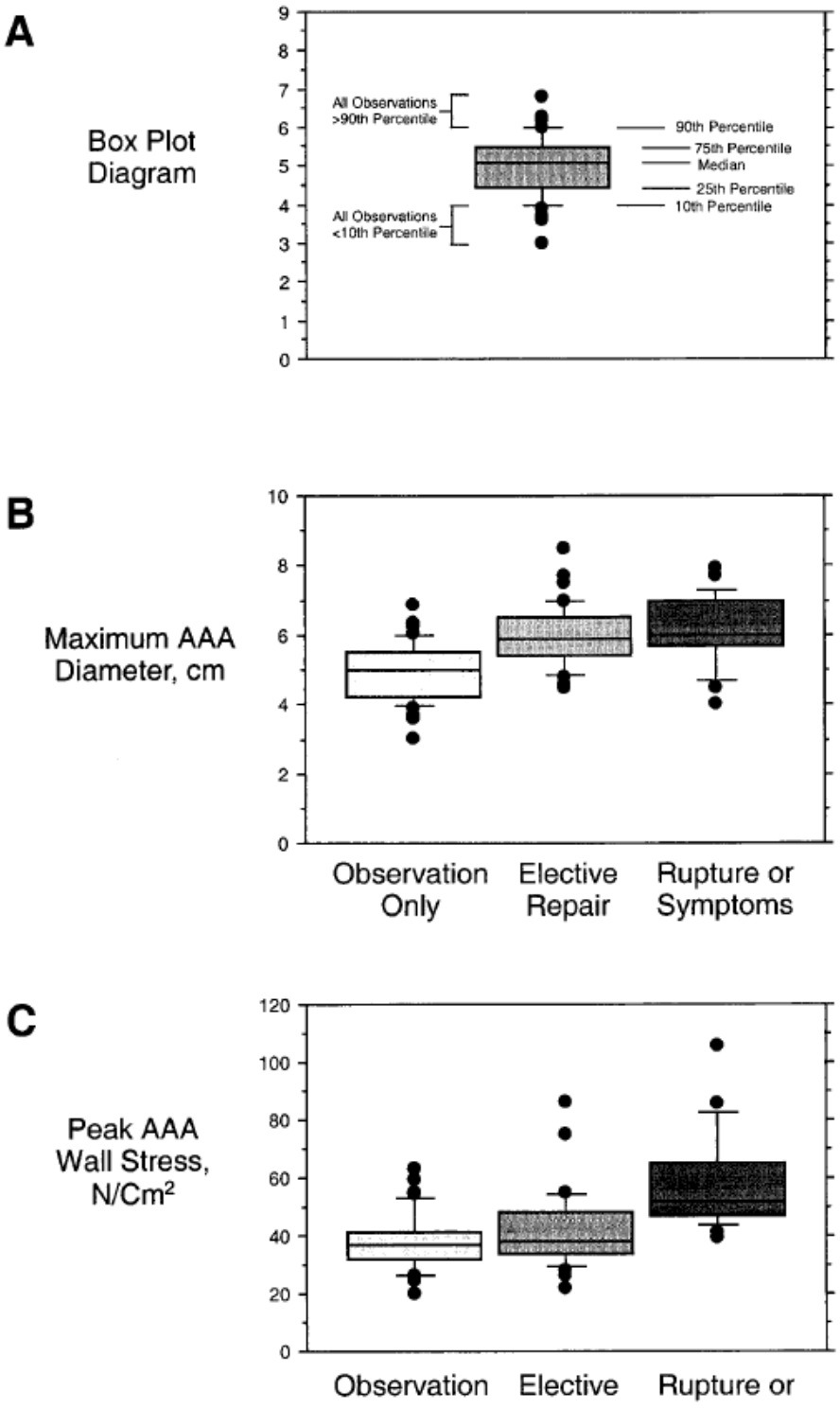

Figure 2-11: (A) Box plot. Rectangles, 25th to 75th percentile of data; horizontal bar within rectangles, median of data; short horizontal bars outside rectangles, 10th and 90th percentiles of the data; solid circles, any value below the 10th or above the 90th percentile. (B) Box plot for AAA diameter demonstrates that 90% of AAAs under observation have diameter larger than the lowest recorded diameter for an AAA that subsequently ruptured or became symptomatic, which was 4.4 cm in maximum diameter. (C) Box plot for peak AAA wall stress demonstrates that 75% of AAAs under observation have stress lower than the lowest recorded stress for an AAA that subsequently ruptured or became symptomatic.

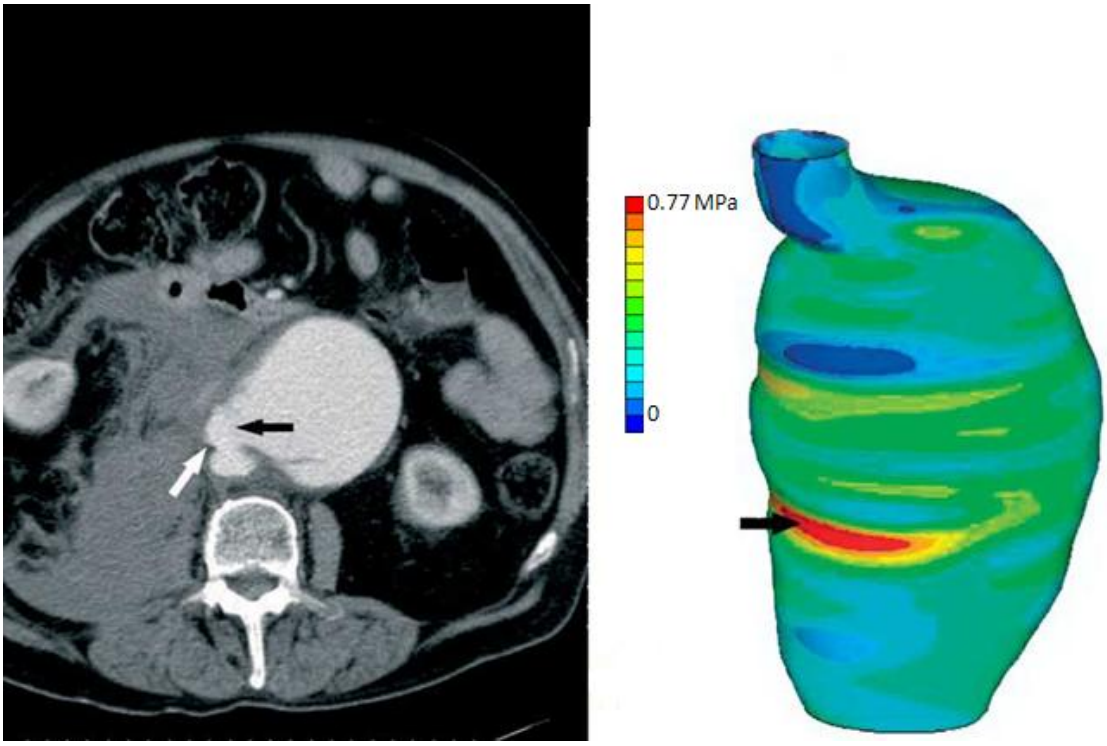

Figure 2-12: (Lift) Point of rupture in CT (Right) correlated with area of high stress in FEA model. Sight of rupture and area of high stress are indicated by arrows (Venkatasubramanium et al., 2004).

2.7.4 AAA shape

The AAA geometry may play a role in rupture. Asymmetry and geometry irregularities appear to have an important role in rupture; some attention should be therefore be given to the overall shape of the aneurysm (Breeuwer et al., 2004).

Elger et al. (1996) and Vorp et al. (1998) proposed that the stresses acting on the AAA wall are highly affected by the aneurysm shape (e.g., curvature, tortuosity and asymmetry) of the specific AAA. Hence, AAAs with the same diameters could have largely different stress distributions, which clearly means that the maximum diameter criterion and the Law of Laplace cannot effectively describe the risk of rupture of an aneurysm on a patient-specific basis (Vorp, 2007).

AAAs can assume a variety of different shapes. They can resemble a balloon with one side of the wall expanded, a fusiform gradual dilation of the complete circumference of the artery, or a cylindrical form. However, when the aneurysm is more than 4.5 cm diameter, it is difficult to keep its fusiform or axisymmetric shape as it becomes irregular and asymmetric. The obvious reason for this is that the AAA does not

develop in an empty peripheral space. All other surrounding organs may play a role in the deformation of the AAA. Also, there is no documented evidence to suggest that the shape of the aneurysm is related to any cardiovascular disease or other background (Lee et al., 1982; Elger et al., 1996).

The regions of high curvature within the wall may be directly linked to high stresses acting on the wall. Sacks et al. (1999) found that the formation of focal regions of high curvature is associated with AAA tortuosity which can lead to high stresses on the wall with AAA tortuosity leading to an increase or decrease in the spatial distribution and focal area of surface curvatures. They show that more curvature and a more complex AAA geometry may increase focal areas compared to smoother areas, as shown in Figure 2-13. They proposed that the degree of tortuosity of the AAA may play a more important role in rupture than its diameter (Sacks et al., 1999).

*K is curvature parameter as its sign indicates the general shape of the surface. Specifically, K>0 indicates an elliptical surface, K=0 a cylindrical surface and K<0 is a hyperbolic.

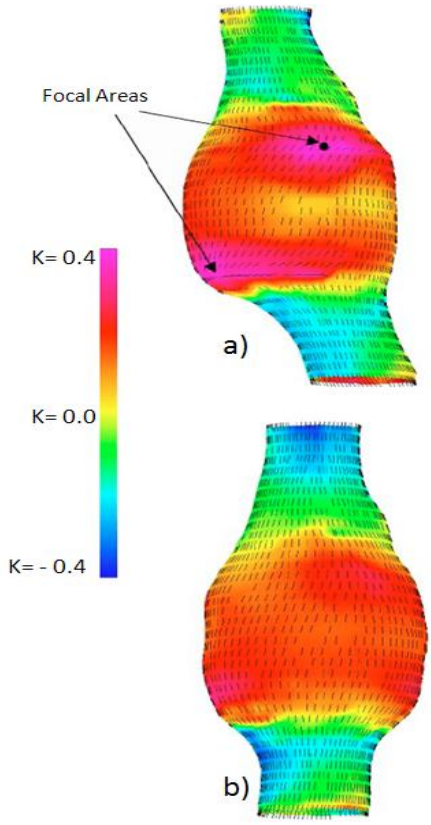

Figure 2-13: AAA Tortuosity, a) unmodified AAA geometry, and b) after the removal of tortuosity. Adapted from (Sacks et al., 1999).

2.8 Role of intraluminal thrombus

An intraluminal thrombus (ILT) is found in most ruptured AAA's. This section will discuss the specific role played by ILT in AAA and how the presence of an ILT can change the biomechanics of the AAA. It is important to understand ILT in detail because of its possible role in changing the magnitude and distribution of stresses on the aortic wall and dynamics of the blood flow. Fluid mechanics are the main cause of ILT formation as discussed earlier in this chapter (Di Martino et al., 2001; Bernad et al., 2009).

2.8.1 ILT structure

ILT is a fibrin structure composed of blood cells, platelets, blood proteins and cellular debris. It can be divided into three layers: luminal, medial and abluminal, as shown in Figure 2-14. The first layer, luminal, has direct contact with the blood stream and has the most influence and has a blood-like colour. The second layer, medial is white and is stiffer than the first layer. The third layer, abluminal is attached to the wall and is dark brown in colour (Wang et al., 2001).

The mechanical properties of ILT are isotropic since it can be observed from scanning electron microscopy (SEM) images that there is no clear privileged direction in the material texture and it has the same mechanical behaviour and material properties longitudinally and circumferentially. However, it is inhomogeneous because the abluminal mechanical behaviour and properties are more structurally stable compared to those of the luminal and medial (Wang et al., 2001). Ashton et al., (2009) reported that the abluminal layer (Young's modulus = 19.3 kPa) is stiffer than the medial (Young's modulus = 2.49 kPa) and luminal (Young's modulus = 1.54 kPa) layers.

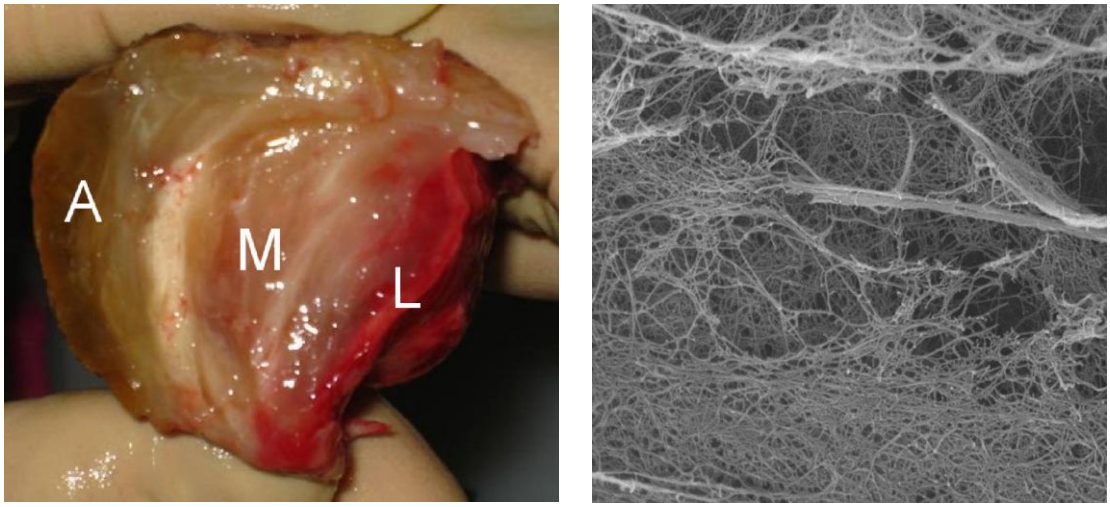

Figure 2-14: Cross-sectional cut of ILT specimen with abluminal (A), medial (M), luminal (L) layers and scanning electron microscopy (SEM) images of ILT (Ashton et al., 2009)

2.8.2 Role of ILT on wall mechanical strength

ILT is a factor that could change the stresses applied on the internal wall of the aneurysm. However, it is not yet clear whether the ILT causes more stresses on the internal wall and hence increases the risk factor of rupture, or whether it could be considered a supporter of the wall against stresses (Speelman, 2007). The role of ILT in AAA rupture is controversial. Some studies suggest that ILT increases the risk of rupture as it weakens the wall while other studies suggest that the presence of ILT may work as a cushion to the wall and decrease the risk of rupture. However, some other studies suggest that there is no relation between the presence of ILT and the rupture of AAA (Wang et al., 2002).

Wall mechanical strength can be decreased in the presence of an aneurysm, but the mechanism of this decrease is not yet clear. Vorp et al. (2001) found that the wall adjacent to a thick layer of ILT is weaker than others with a thin ILT, as shown in Figure 2-15. From clinical statistics, ILT is greater in thickness in ruptured aneurysms than in non-ruptured aneurysms.

In a finite element study, Wang et al. (2002) showed that ILT reduces peak wall stress and changes wall stress distribution. The effect of thrombus on the wall stress was investigated with models derived from CT scan images of real aneurysms. Finite element models of four AAA patients whose aneurysms consisted of intraluminal

thrombus were analysed both with and without the presence of thrombus. All the models showed a significant decrease in the wall stress in the presence of thrombus and also the stress distribution was found to be altered in all the models with intraluminal thrombus when compared to the same model without intraluminal thrombus, as shown in Figure 2-16 and Table 2-1. The degree of significance however can differ from one individual to another.

These results and analyses conflict because, as mentioned above, there are two factors which control the mechanism of rupture, the stress in the wall and the strength of the wall. An AAA will rupture only when the stresses applied on the aneurysmal wall exceed the strength of the wall. The inputs and outputs of these two factors are interrelated and cannot be separated. While ILT can reduce the peak stresses on the aneurysmal wall, it can also affect the strength of the wall. Also, the precise role of ILT in AAA haemodynamics remains unclear (Dalman, 2003). The balance between the above two factors is discussed in detail in this research.

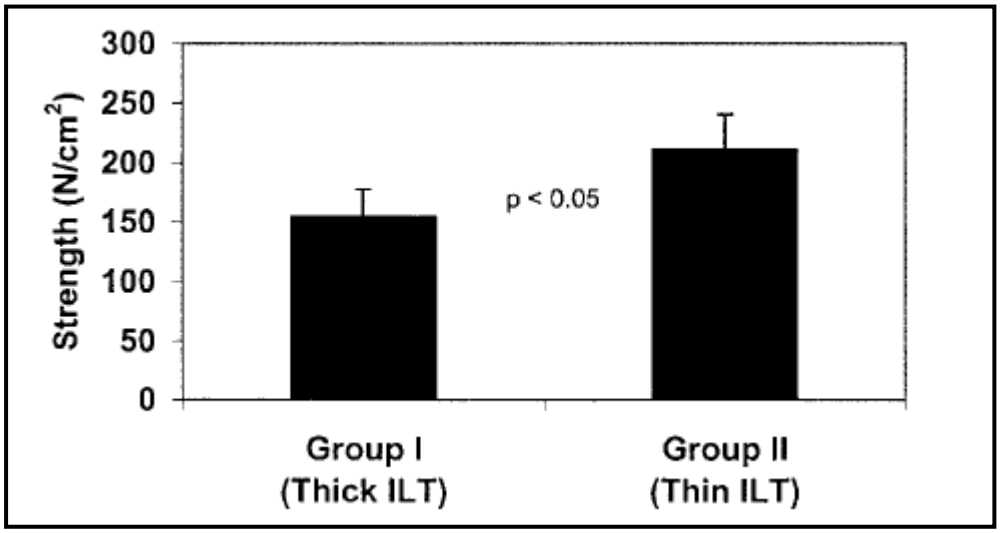

Figure 2-15: Association of wall strength with ILT thickness (Vorp et al., 2001).

These results and analyses conflict because, as mentioned above, there are two factors which control the mechanism of rupture, the stress in the wall and the strength of the wall. An AAA will rupture only when the stresses applied on the aneurysmal wall exceed the strength of the wall. The inputs and outputs of these two factors are interrelated and cannot be separated. While ILT can reduce the peak stresses on the aneurysmal wall, it can also affect the strength of the wall. Also, the precise role of

ILT in AAA haemodynamics remains unclear (Dalman, 2003). The balance between the above two factors is discussed in detail in this research.

Patient	Peak Stress without ILT *(N/cm2)*	Peak Stress with ILT *(N/cm2)*	Decrease of Peak Stress
1	36	34	6%
2	30	19	36%
3	40	37	6%
4	44	28	38%

Table 2-1: Peak wall stress for each patient with and without ILT. Adapted from (Wang et al., 2002).

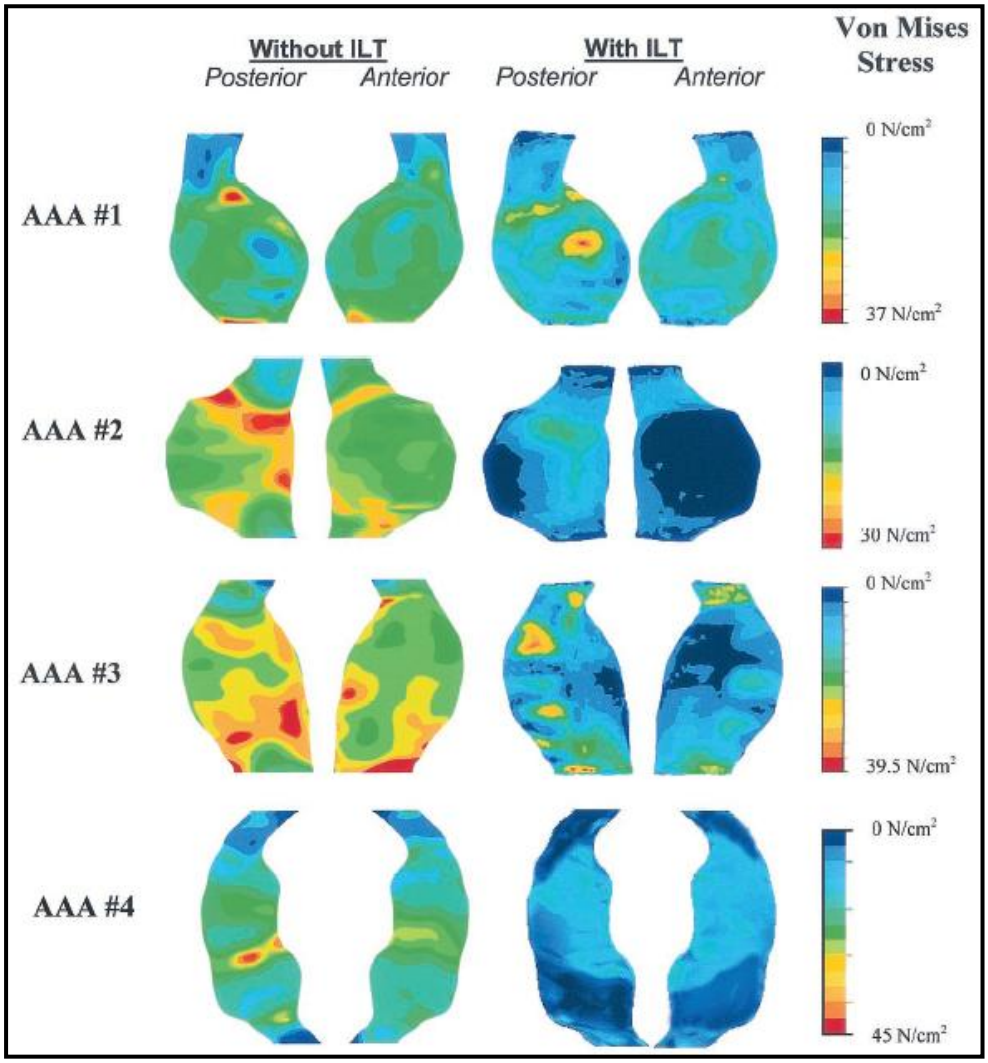

Figure 2-16: Comparison of 3D wall stress distribution between AAA models with and without ILT. Individual colour scales (right) indicate von Mises stress for each AAA. Both posterior and anterior views are shown for each case (Wang et al., 2002).

2.8.3 Role of ILT on oxygen diffusion

Vorp et al. (1996a, 1996b, 2001) indicated that the presence of ILT alters the normal pattern of oxygen supply to the AAA wall. ILT may isolate oxygen diffusion between the blood stream and the internal layers of the wall which could lead to hypoxic cell dysfunction in the AAA wall, subsequently weakening the wall and increasing the risk of rupture. This weakening of the wall might be caused by the combination of a number of factors (Wang et al., 1999; Vorp et al., 2001). When the oxygen supply is affected, inflammatory regions develop which can lead to an increase in the local proteolytic activities of the wall, typically weakening the wall. In vivo studies report an increase of inflammation on the aortic wall on thick ILT compared to thin ILT (Vorp et al., 2001). Figures 2-17 and 2-18 show how thick ILT can significantly decrease oxygen in the wall (Vorp et al., 2001; Sun et al., 2009).

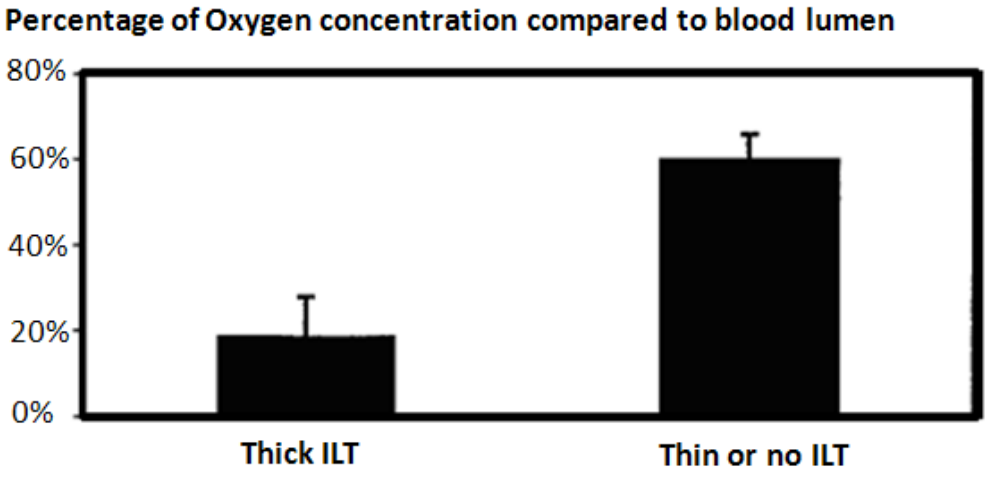

Figure 2-17: Comparison of in vivo Oxygen measurements for AAA wall adjacent to thick ILT versus AAA wall adjacent to thin or no ILT. Adapted from (Vorp et al., 2001).

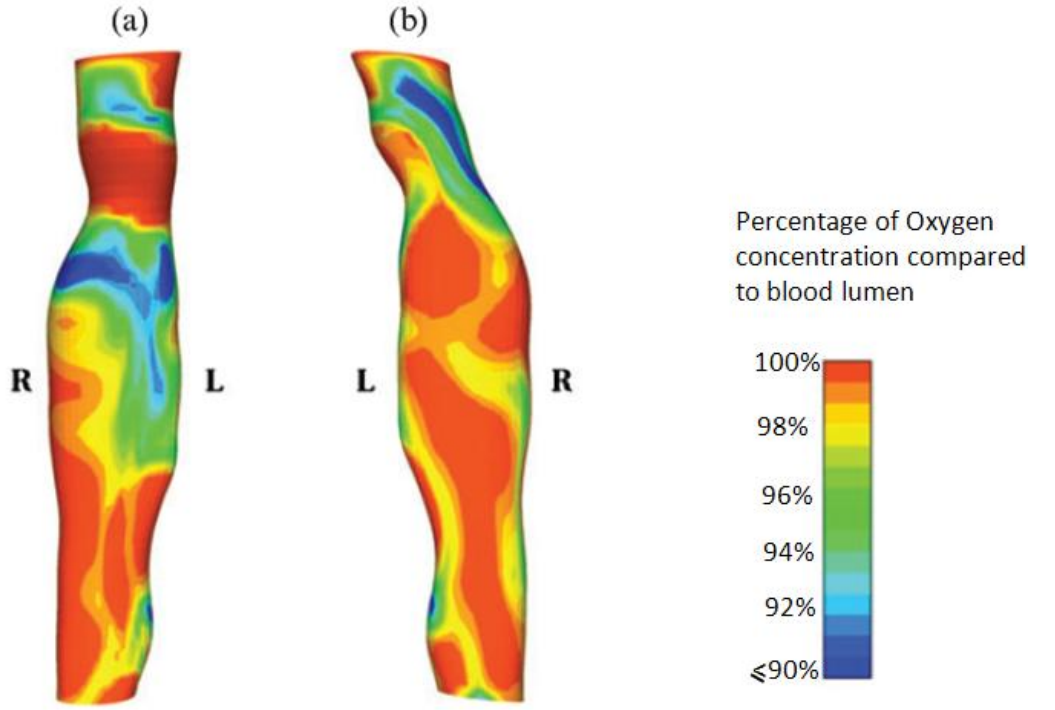

Anterior (a) and posterior (b) views of normalised oxygen concentration distribution at the lumen–thrombus interface in the abdominal aortic aneurysm model.

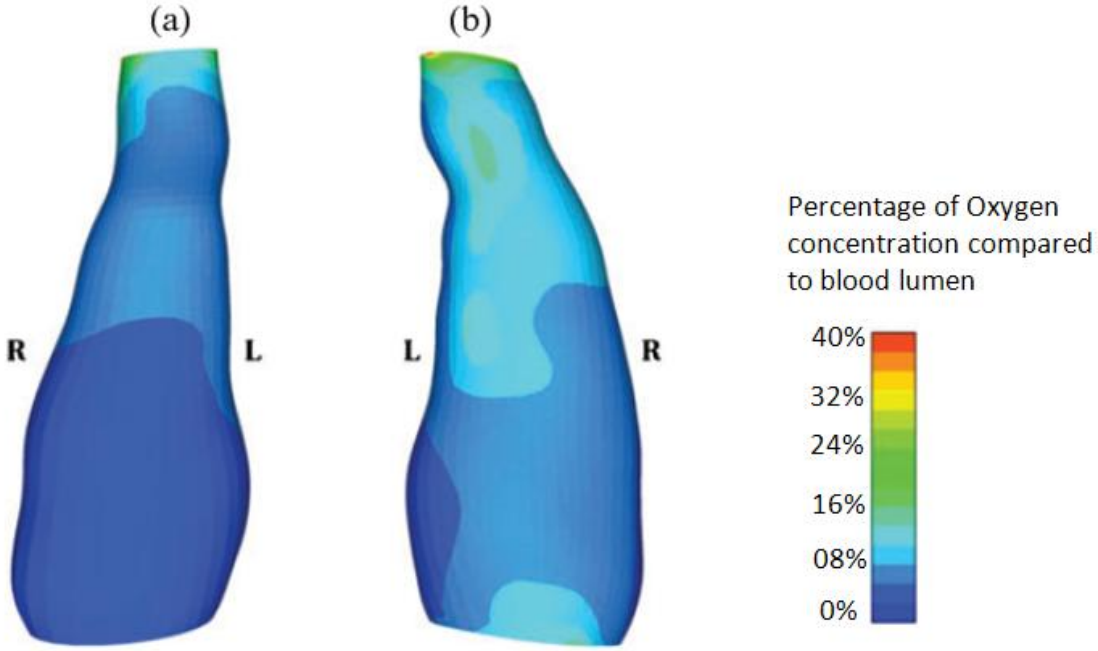

Anterior (a) and posterior (b) views of normalized oxygen concentration distribution at the thrombus–wall interface in the abdominal aortic aneurysm model.

Figure 2-18: Comparison between oxygen concentrations at two locations; (top) lumen–thrombus interface, (bottom) thrombus–wall interface (Sun et al., 2009).

2.9 Summary

From a discussion on AAA pathology and treatment, it was found that the current method of AAA assessment in clinics which use the diameter of the aneurysm to determine when to operate is unstable indicator and there is therefore a real need to find a better method for assessment of AAA at a high risk of rupture.

Because the rupture occurs when the stresses applied on the internal wall exceed the wall strength and because there is no non-invasive method to measure the wall strength, the best option for researchers is to study the stresses on the AAA wall.

Several attempts to derive a reliable AAA rupture risk indicator have been based on the assessment of the arterial wall stress distribution. In a number of studies, maximum wall stress has been speculated to be a better predictor of rupture than AAA diameter but maximum stress on the wall is affected by a number of factors. This work will investigate the relationship among wall stresses, aneurysm shape and aneurysm aspect ratio. It will also investigate the effect of ILT presence, thickness and material properties. The porosity of ILT will also be investigated to examine its effect on wall stresses and to examine its effect on blood flow inside the ILT and possible role of hemodynamic in AAA pathology.

Chapter 3
Methodology

The methodology used to perform the simulations and analysis to gain results is discussed and explained in this chapter. Two main techniques have been used to apply blood pressure and to simulate blood flows. The two methods are finite element analysis (FEA) and computational fluid dynamics (CFD).

In this chapter, a brief background of each technique will be presented, as well as an outline on the methods used to apply the technique followed by a convergence study for each method to confirm that the results were achieved to a sufficient degree of accuracy. The initial validation of each method is then undertaken

3.1 Structural solids analysis with finite element analyses

The FE method was developed and has been widely used and improved since the 1950's. In order to apply the FEA method to investigate the stress distribution in an aneurysm for example, the AAA geometry is divided into a finite number of subdivisions called elements, which are connected together at nodes which together produce the FEA mesh (Figure 3-1). The material properties and the governing relationships are considered over these elements and are expressed in terms of unknown values at the nodes. An assembly process duly considering the results of the loading and constraints is shown in a set of equations. The solution of these equations gives the approximate behaviour of the complete AAA geometry (Logan, 2006).

Once the individual elemental equations are combined to define the behaviour of the entire AAA geometry, the overall system of equations takes the following form:

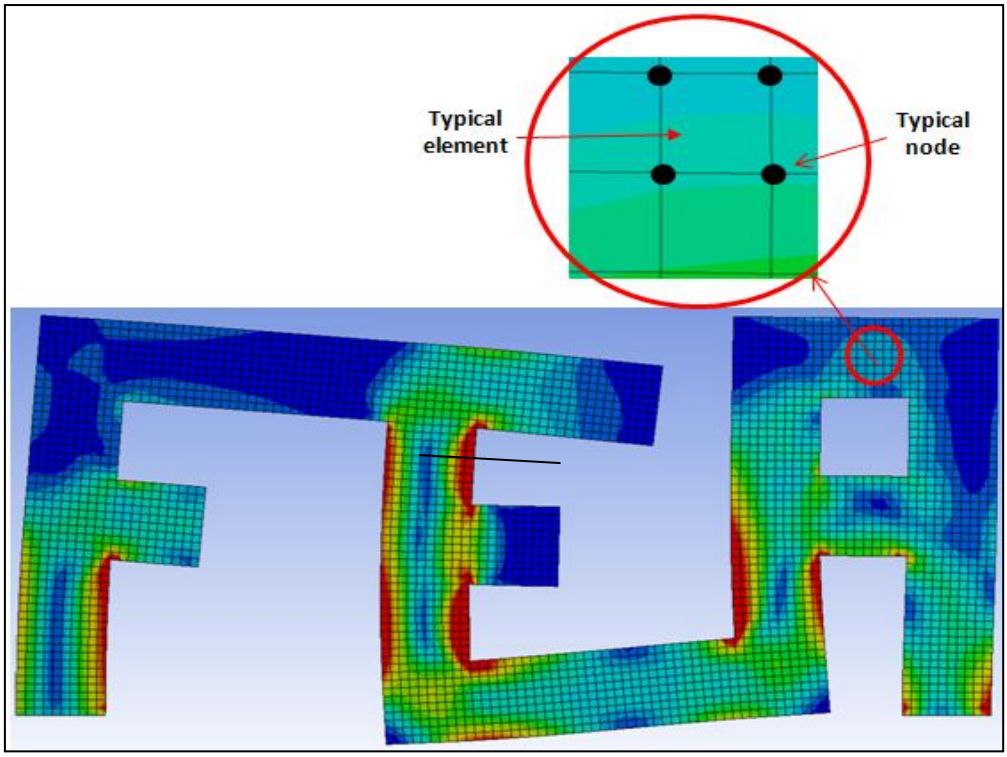

Figure 3-1: Typical finite element mesh showing elements and nodes.

After applying the boundary conditions (i.e. anatomical constraints, internal blood pressure), the system of equations is solved and the whole process is normally carried out in commercial or open source software.

In order to obtain the most accuracy for the AAA results using the FEA method, it is necessary to provide an accurate representation of the AAA geometry with optimum FEA element type as well as a definition of the correct material properties that can model in-vivo properties. In FEA models, the size and number of elements used to represent the geometry need to be carefully chosen. As the number of elements increases, the number of equations to be solved in the system increases, which usually leads to more accurate results, although simultaneously increasing the solution time and cost. For AAA stress analysis, thin shell elements are the most suitable type of element, as they are capable of modelling both bending and membrane effects (Fagan, 1992).

3.1.1 Models

Twelve fusiform axisymmetric three-dimensional aneurysms with constant inlet diameter, d = 2.0 cm, variable maximum aneurysm diameter, D = 4 - 7.0 cm, total length of the model TL=30 cm and variable aspect ratio (L/d) were considered as shown in Figure 3-2. Details of each model and the wall curvatures of each aneurysm were derived from the equations shown in Table 3-1. The shapes were taken from Elger et al., (1996). The ANSYS finite element package (Version 12) was used for all the FEA studies reported in this thesis. Details of the mathematical equations for meridional curves of the models can be seen in Table 3-2.

ANSYS shell elements (type: Shell63) are found to be suitable for modelling problems such as pressure vessels due to their ability to include both membrane and stretching effects (Fagan, 1992). All aortic walls in this research were considered to have linear elastic behaviour and thin wall thickness, making these shell elements suitable due to their reliability (widely used and validated element) and efficiency.

For the thrombus within the AAA, solid elements were used to capture the in depth stress distribution developed in the bulk parts of the thrombus. In models that have thrombus; the wall was modelled using the solid-shell element, "Solsh190". This element is known to suit thin and moderately thick walled structures and can be used to model a non-constant wall thickness if necessary while preserving the flexibility offered by the shell elements.

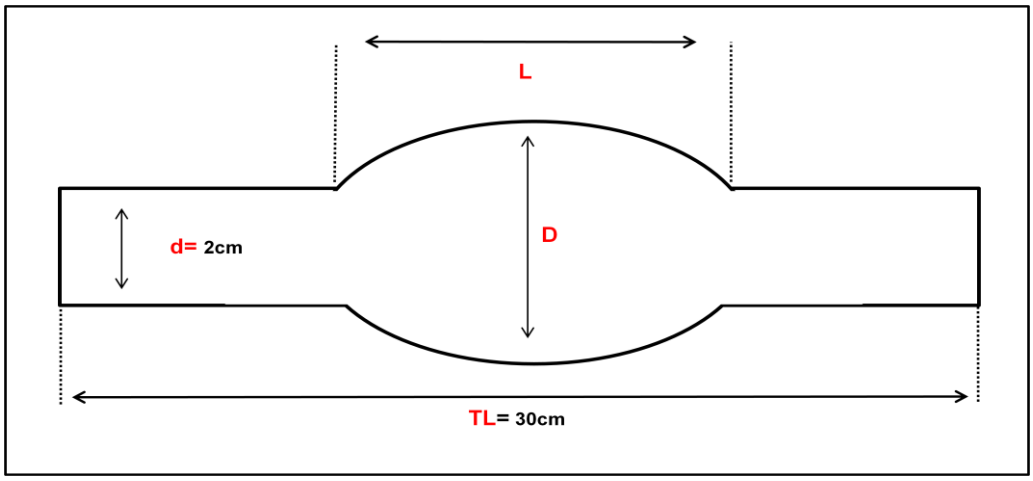

Figure 3-2: Basic aneurysm geometry where inlet diameter, d = 2.0 cm, maximum aneurysm diameter, D, and aspect ratio (L/d), total model length TL=30 cm.

Model Name	D (cm)	Aspect ratio	Wall curvature	Thrombus thickness (mm)	Type and number of elements
SO	5	4	Open-sphere	Zero	10,600 Shell elements
SE1	5	4	Exponential	Zero	10,877Shell elements
SC1	5	4	Cosine Exponential	Zero	11,274Shell elements
SP1	5	4	Parabola-Exponential	Zero	12,040 Shell elements
SE4 (A,B,C)	4	3,4, 5	Exponential	Zero	9,678 Shell elements
SC4 (A,B,C)	4	3,4, 5	Cosine Exponential	Zero	9,878 Shell elements
SP4 (A,B,C)	4	3,4, 5	Parabola-Exponential	Zero	10,892 Shell elements
SE5 (A,B,C)	5	3,4, 5	Exponential	Zero	10,877Shell elements
SC5 (A,B,C)	5	3,4, 5	Cosine Exponential	Zero	11,274Shell elements
SP5 (A,B,C)	5	3,4, 5	Parabola-Exponential	Zero	12,040 Shell elements
SE7 (A,B,C)	7	3,4, 5	Exponential	Zero	12,664Shell elements
SC7 (A,B,C)	7	3,4, 5	Cosine Exponential	Zero	13,112Shell elements
SP7 (A,B,C)	7	3,4, 5	Parabola-Exponential	Zero	14,244 Shell elements
SENLT	5	4	Exponential	Zero	10,017 Solid-shell elements
SLT2.5	5	4	Exponential	2.5 mm	26,490 Solid-shell and Solid elements
SLT5	5	4	Exponential	5 mm	32,190 Solid-shell and

					Solid elements
SLT7	5	4	Exponential	7 mm	35,324 Solid-shell and Solid elements
SLT15	5	4	Exponential	15 mm	69,373 Solid-shell and Solid elements
SLTV	5	4	Exponential	3 – 5 mm Variable	39,081 Solid-shell and Solid elements

Table 3-1: Details of all 37 models used for the FEA calculations in this thesis

Model	Wall curvature equation
Open-sphere	$y(x) = \sqrt{D^2 - x^2} : if \lvert x \rvert < \sqrt{D^2 - d^2}$, *otherwise* $y(x) = d$
Exponential	$y(x) = (D - d)\, e^{-\lvert c_1 x/d \rvert\, c_2} + d$ C_1=0.667, C_2=4
Cosine Exponential	$y(x) = e^{-c_1 \lvert \frac{x}{d} \rvert c_2} \left[\frac{(D - d)}{2} \left(\cos\left(\frac{\pi x}{c_3 d} \right) + 1.0 \right) \right] + d$ C_1=0.025, C_2=5.44, C_3=5
Parabola-Exponential	$y(x) = e^{-c_1 \lvert \frac{x}{d} \rvert c_2} \left[(D - d) - C3(\frac{x2}{d}) \right] + d$ C_1=1.38x10-10, C_2=17.3, C_3=0.94

Table 3-2: Mathematical equations for meridional curves of the models. Taken from Elger et al. (1996)

3.1.1.1 Creation of models

The models were created using two approaches: manual mesh generation and using the solid modelling capabilities of ANSYS.

For AAA idealized models (homogeneous fusiform), modelling using a two-dimensional axisymmetric model could be sufficient to gain the desired FEA results; however, in this study the complete model was used for ease of visualization and low modelling cost due to the non-complex nature of the geometry. Furthermore, these models will be used later for blood flow and the assumptions of axisymmetric

modelling of blood flow in idealised geometries could not be validated (Jamison et al., 2009).

Approach one (manual mesh generation)

Four nodes were created and one element of the four nodes was then created using the following steps:

1. Create two-dimensional curves of nodes (points) as shown in Figure 3-3.

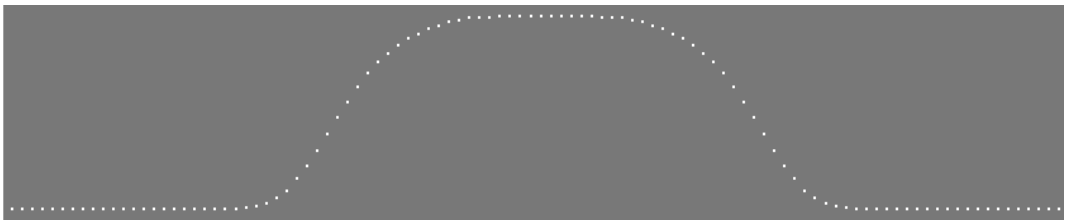

Figure 3-3: XY view of the points showing the curvature of the aneurysm

2. Rotate and copy the original line of nodes about the z-axis by 10 degrees, as shown in Figure 3-4.

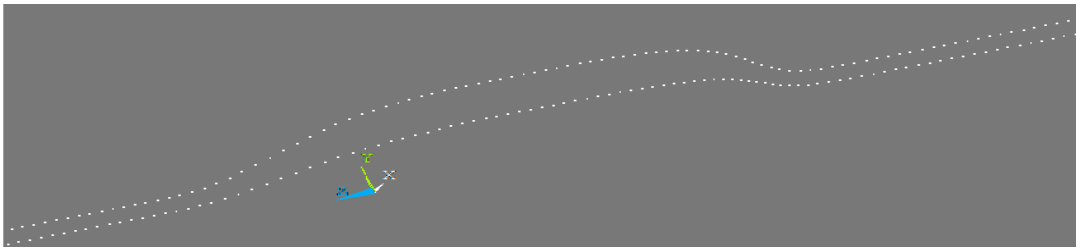

Figure 3-4: Three-dimensional top view of the two lines of points

3. Create one element from each of the 4 nodes, as shown in Figure 3-5.

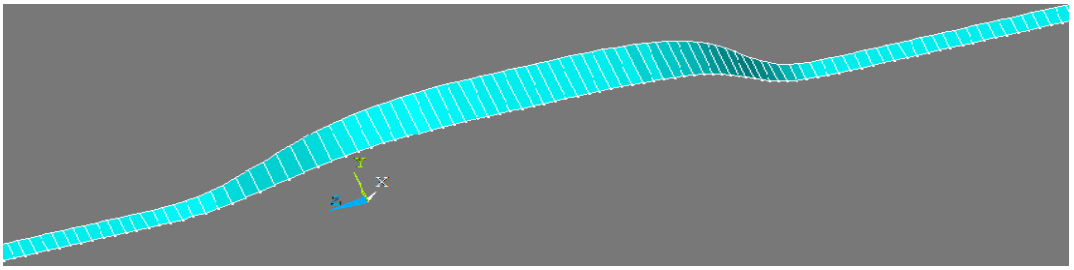

Figure 3-5: Three dimensional top view of one element along the curve

4. Rotate and copy the node and element patterns 36 times to create the full 360 degree geometry, as shown in Figure 3-6.

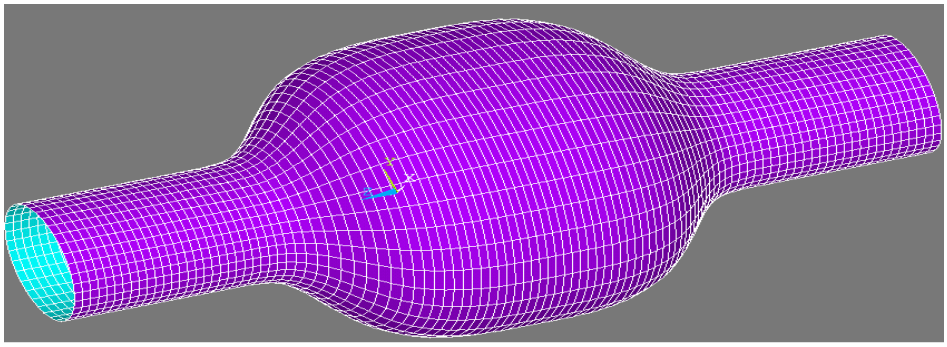

Figure 3-6: Three-dimensional top view of model showing 36 elements of each X position of the aneurysm.

Approach two (solid modelling capabilities)

In this approach, the aneurysm geometry was created using the ANSYS CAD package (ANSYS Design Modeller) and then divided (meshed) into the elements using the following steps:

1. Create the XY curve using points details, as shown in Figure 3-7.

Figure 3-7: XY view showing the curvature of the aneurysm.

2. Rotate the line about the x-axis to create the model surface, as shown in Figure 3-8.

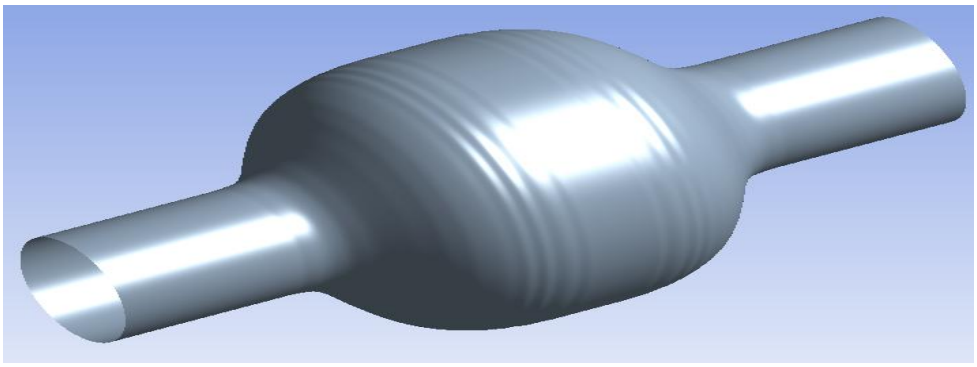

Figure 3-8: Surface model result from revolving the line.

3. Divide the surface into elements, as shown in Figure 3-9.

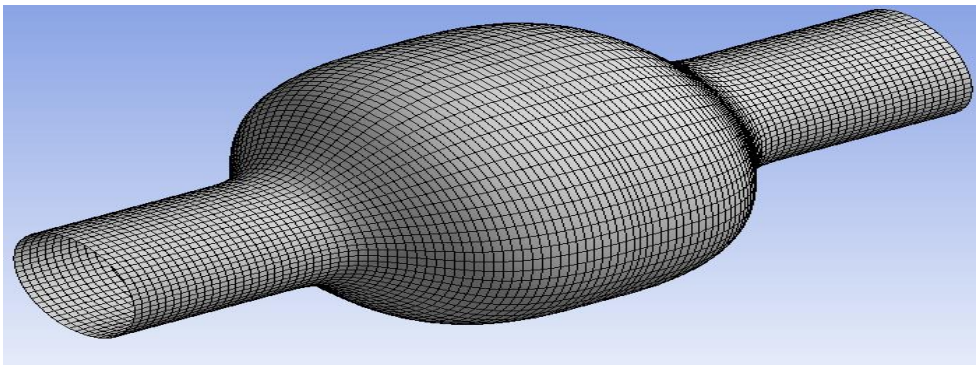

Figure 3-9: Model is divided into elements (meshed) and elements are given a thickness.

3.1.1.2 Thrombus creation

The second approach was used to create a thrombus inside the aneurysm. The model was then filled with the thrombus and, depending on the thrombus thickness needed blood lumen was then created inside and subtracted from the CAD. Figure 3-10 shows a longitudinal (X axis) section of the model. Bonded contact was used to connect the wall geometry with the thrombus and the details of this type of contact are shown in Table 3-3.

Characteristic name	Value used
Type	Bonded
Behaviour	symmetric
Algorithm	pure penalty

Table 3-3: Wall to thrombus contact characteristics.

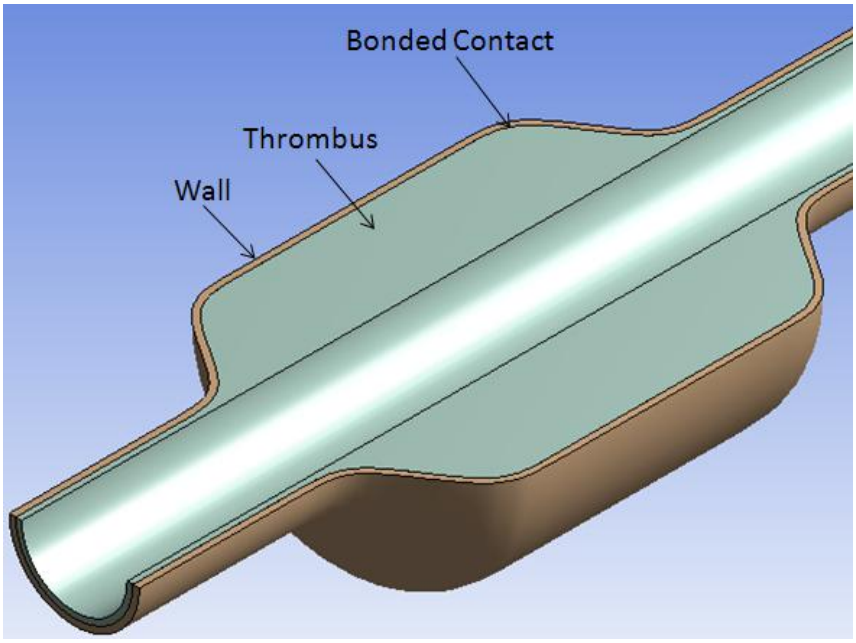

Figure 3-10: Thrombus was created by filling the hollow between the wall and lumen with solid material.

3.1.2 Boundary conditions

An AAA wall thickness of 1 to 1.5 mm has been used in many previous studies (Vorp et al., 1998; Scotti et al., 2005; Raghavan et al., 2006; Leung et al., 2006) while a thickness of 2.0 mm has been used in other studies (Sacks et al., 1999; Venkatasubramaniam et al., 2004). In this project, walls were assumed to have a uniform thickness of between 1.0 – 2.0 mm for all models (to allow comparison with previous work). The wall materials were modelled as linearly elastic isotropic (Poisson's ratio, μ = 0.45, Young's Modulus = 2.7 MPa). These material properties have been used in many previous works (Di Martino et al., 2001; Scotti et al., 2005). A homogeneous pressure between 120 to 145 mmHg (Outten et al., 2003; Kelly and O'Rourke, 2009) was applied to the internal surface of the models as shown in Figure 3-11. This value represents the peak systolic pressure of a 'normal' patient and a homogeneous pressure of between 120 and 145 allow comparison with previous work.

The thrombus inside the aneurysm was modelled as an incompressible, isotropic, homogeneous, linear elastic material with a Young's modulus E = 0.11 MPa and a Poisson's ratio μ = 0.45. These values of E and μ represent population mean values

obtained from uniaxial loading tests performed on ILT specimens harvested during AAA surgery by Di Martino et al. (1998).

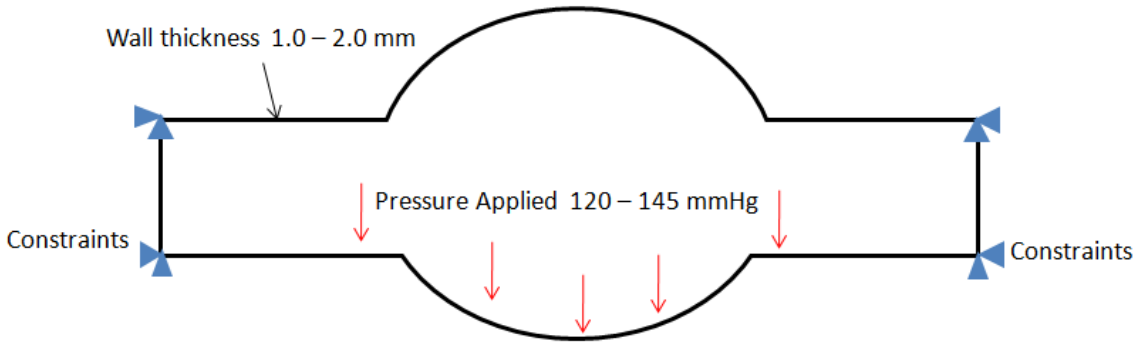

Figure 3-11: Basic aneurysm geometry showing the boundary conditions applied in this project.

Three directional (XYZ), fixed points were applied at the ends of the models to represent the anatomical constraints, fixing the AAA in the abdominal region. The stress value is represented as Von Mises stress, which is a method used to combine the stresses in three-dimensions to calculate the failure criteria. Von Mises stress is widely used in the assessment of AAA stresses for most FEA studies to calculate the failure of the AAA wall. Hoop and longitudinal stresses were also used to study the aneurysm shape effects and to validate the results of this work by comparing them with previously published results. Hoop stresses were used to investigate in more depth the causes of the aspect ratio effect discussed in Chapter 4.

3.1.3 Convergence studies

In FEA modelling, a higher number of elements (and therefore a finer mesh) usually results in a more accurate solution. However, the computation time increases as the mesh becomes finer. Researchers and engineers tend to use a reasonable number of elements which balance the accuracy of results and time needed to complete analysis. For this purpose, a convergence study of sufficient number of elements was undertaken for each model to confirm the stability of the results, particularly in maximum stress and maximum displacement.

Model SE1 was used to demonstrate the convergence study in this section with the number of elements varying from 1,176 to 28,560 as seen in Figure 3-12.

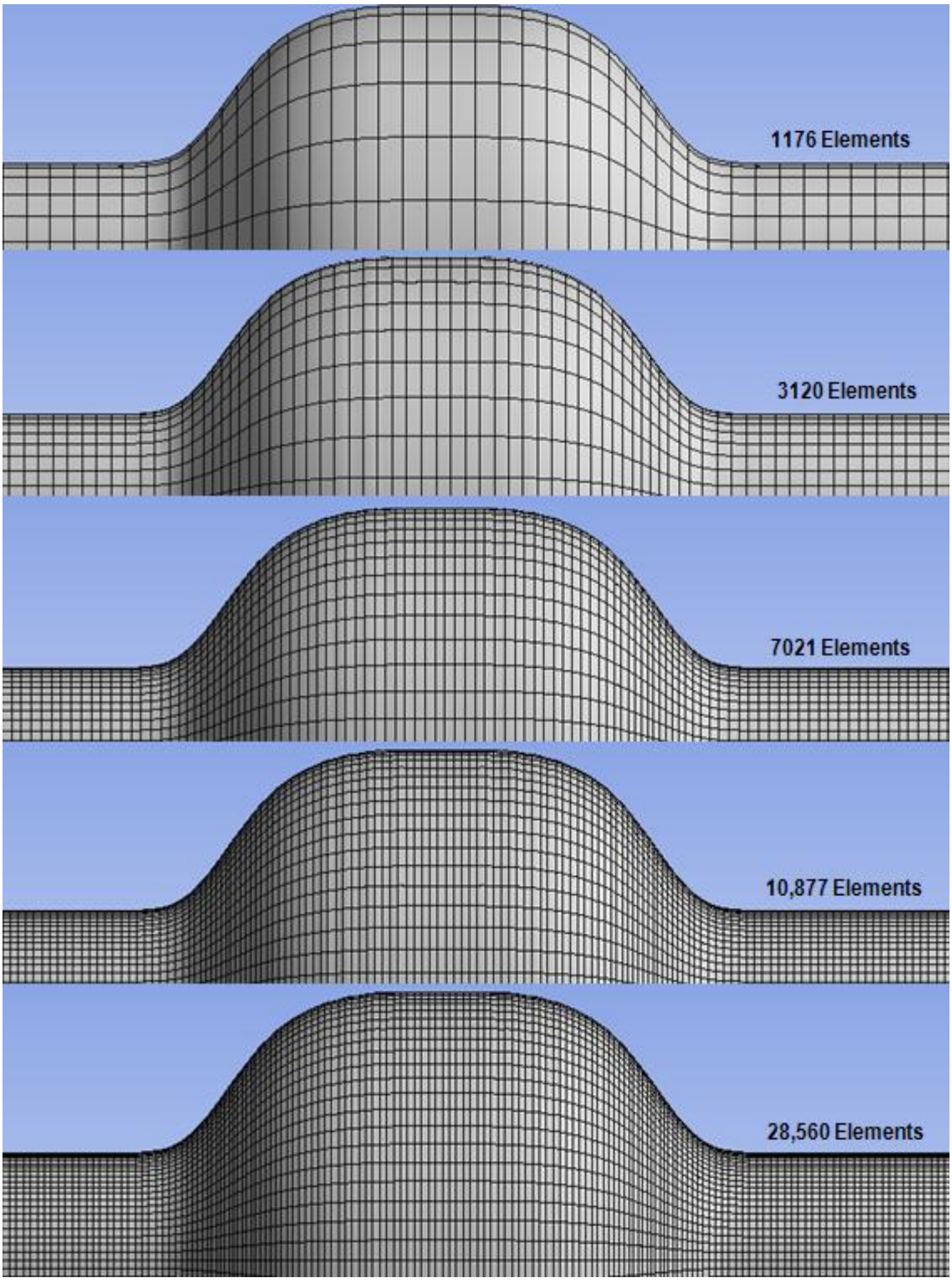

Figure 3-12: Element density increases from 1,176 to 28,560 elements (only top half of model shown to allow zooming).

3.1.3.1 Maximum stress

Table 3-4 and the Figure 3-13 show the relationship between the number of elements and the maximum stress value and location for the model.

Number of elements	Maximum stress Value (MPa)	Maximum stress location
1,176	0.2900	Proximal and distal ends of aneurysm
3,120	0.2849	Proximal and distal ends of aneurysm
7,021	0.2829	Proximal and distal ends of aneurysm
10,877	0.2825	Proximal and distal ends of aneurysm
28,560	0.2824	Proximal and distal ends of aneurysm

Table 3-4: Relationship between the number of elements and the maximum stress value and location in the model.

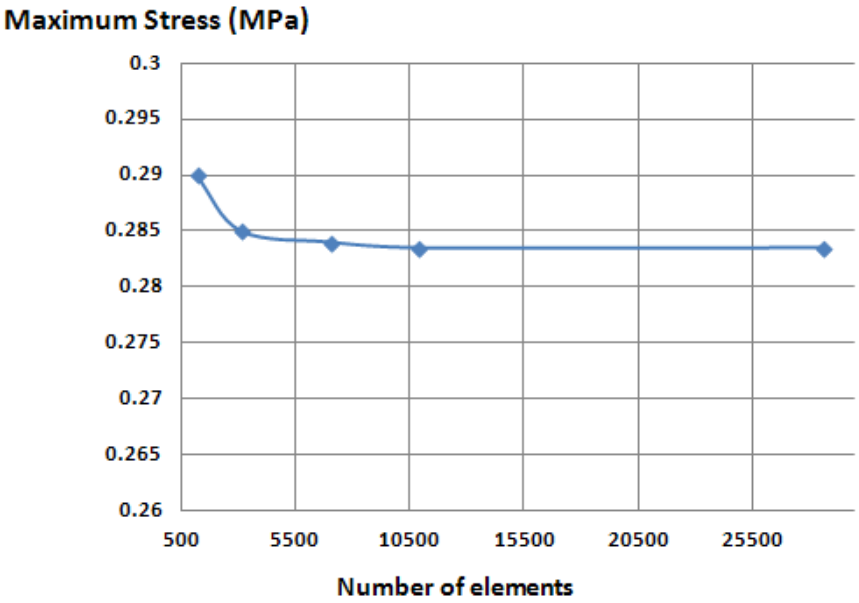

Figure 3-13: Graph showing the relationship between the number of elements and the maximum stress. Convergence was obtained at 10,877 elements.

3.1.3.2 Displacement

Table 3-5 and Figure 3-14 show the relationship between the number of elements and the maximum displacement (deformation) value and location for model SE1.

Number of elements	Maximum displacement (mm)	Maximum displacement location
1,176	1.999	Middle
3,120	1.991	Middle
7,021	1.990	Middle
10,877	1.989	Middle
28,560	1.988	Middle

Table 3-5: Relationship between the number of elements and the maximum displacement value and location for the model.

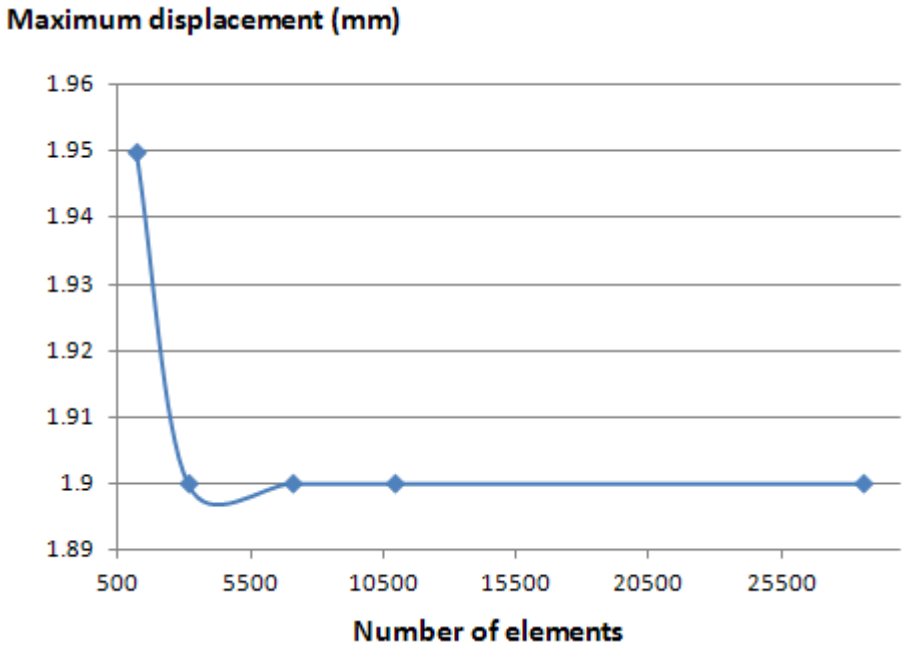

Figure 3-14: Graph showing the relationship between the number of elements and the maximum displacement in the model.

From the results shown above, it can be seen that for maximum stress and maximum deformation, the results of the model differ by less than 1% from the mesh of 10,877 elements and 28,560 elements but has the advantage of a large difference in the time of calculation. Thus, it was considered that results obtained from the model of 10,877 elements are sufficient for calculations in this study. In this study, similar convergence studies have been conducted to ensure all the results obtained are sufficient number of elements (converged).

3.1.4 Validation Study

Previous studies have shown validation of FEA results in terms of quantitative wall stress correlations using idealized geometries by comparing the FEA to experimental results (Morris et al., 2004; Callanan et al., 2005). Other studies were validated qualitatively by correlating rupture locations or maximum stress locations and regions of higher deformation (Doyle et al., 2010).

In the scope of this project, it was not possible to undertake a detailed experimental validation of the results. Therefore, validations for the results of the FEA simulations undertaken in this project, were compared to theoretical calculations of hoop and longitudinal stresses as well as the maximum stress gradient of Elger et al. (1996), who provided one of the pioneering analytical studies to understand the effect of aneurysm shapes on AAA. Validation was achieved on both amplitude of stress-quantitative and stress gradient location-qualitative results.

Three models (SO, SE1 and SC1) as shown in Table 3-1 were used with the same boundary conditions as those given in Section 3.1.2. The results were then compared to Elger et al. (1996).

3.1.4.1 Quantitative analysis

Tables 3-6 and 3-7 illustrate the maximum hoop and longitudinal stresses respectively in both the FEA and Elger et al.'s (1996) calculations; the values of stresses were calculated in terms of stress on the normal aorta before the aneurysm begins to form.

Model	Maximum hoop stress ratio (Elger)*	Maximum hoop stress ratio (FEA)*
Model S0	2.5	2.6
Model S2	2.7	2.8
Model S3	1.8	1.9

*Stresses values were normalized by stress on normal aorta

Table 3-6: Maximum hoop stresses of the FEA and Elger et al.'s (1996) calculations for the three models.

Model	Maximum longitudinal stress (Elger)*	Maximum longitudinal stress (FEA)*
Model S0	1.0	1.05
Model S2	1.2	1.3
Model S3	0.97	1.01

*Stresses values were normalized by stress on normal aorta

Table 3-7: Maximum longitudinal stresses of the FEA and Elger et al.'s (1996) calculations for the three models.

Results from the hoop and longitudinal stresses of FEA simulation have a maximum error of less than 5% compared to Elger et al.'s (1996) calculations which are acceptable in the scope of this project.

3.1.4.2 Qualitative analysis

The stress profile along the AAA wall in the three models was compared using the two methods; stress variations on each model are shown in Figure 3-15 for hoop stresses and in Figure 3-16 for longitudinal stresses. The location of maximum stress is the same in all models. In addition, the profiles of the FEA calculations have similar maximum and minimum locations for each aneurysm. It should be mentioned that hoop and longitudinal stresses for Elger et al.'s (1996) shapes were only investigated for the aneurysm and not for the normal aorta; consequently, a sharp increment from 1 to 2.5 was noticed on the first model shown in Figure 3-15. Comparisons of the FEA and Elger et al.'s (1996) shapes will be discussed in more detail in a discussion on the effect of shape on AAA in Chapter 4.

Overall, the qualitative and quantitative comparisons between Elger et al.'s (1996) calculations and the FEA results generated in this study suggest that FEA is capable of predicting the magnitude and location of high risks of rupture for AAA. The FEA model has the advantage of dealing with more realistic and complex geometries in a remarkably efficient manner.

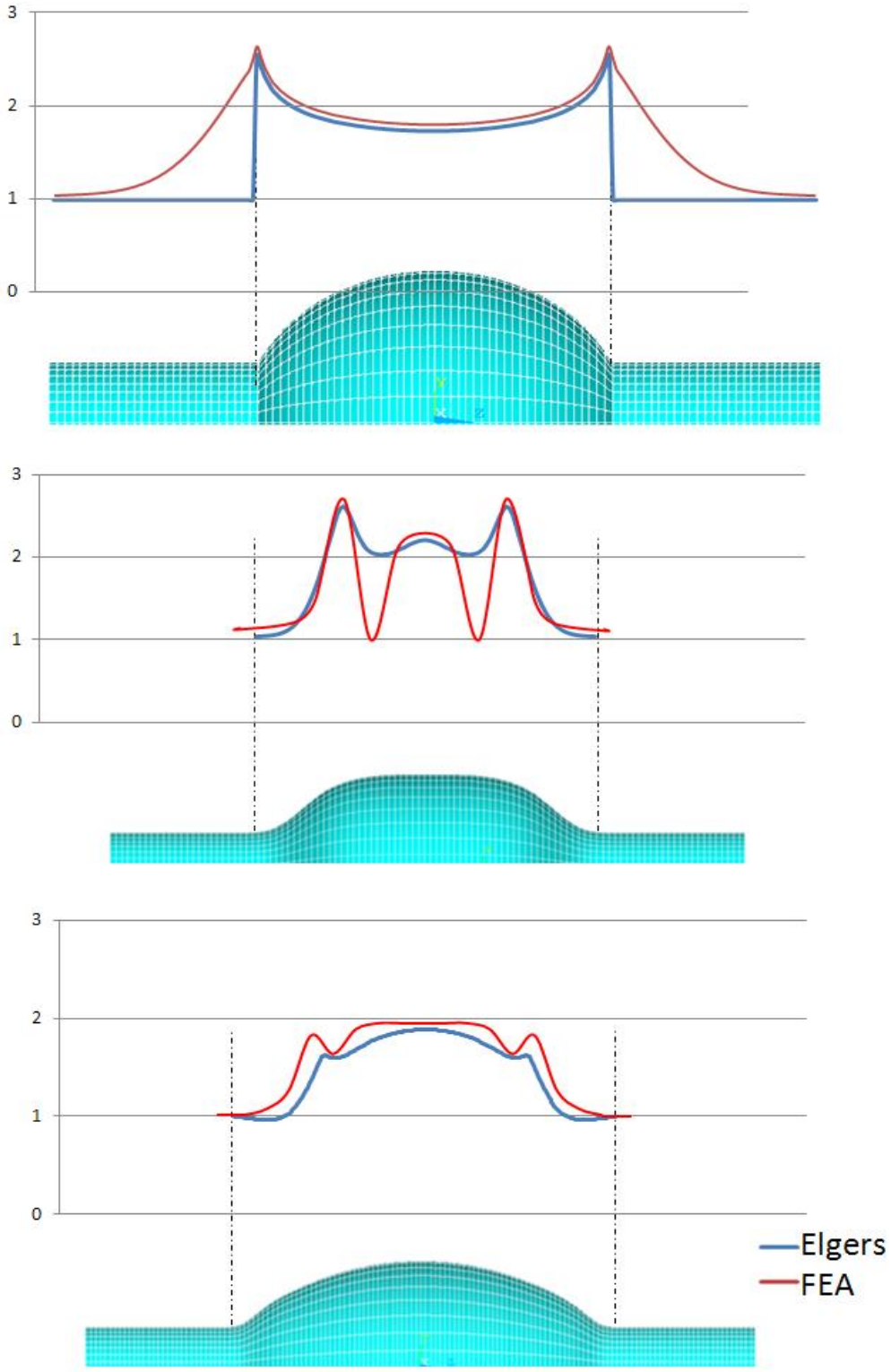

Figure 3-15: Hoop stress variation in the three models compared to the results of Elger et al. (1996). Values of stresses were normalised based on the stress value of normal aorta before the aneurysm begins to form.

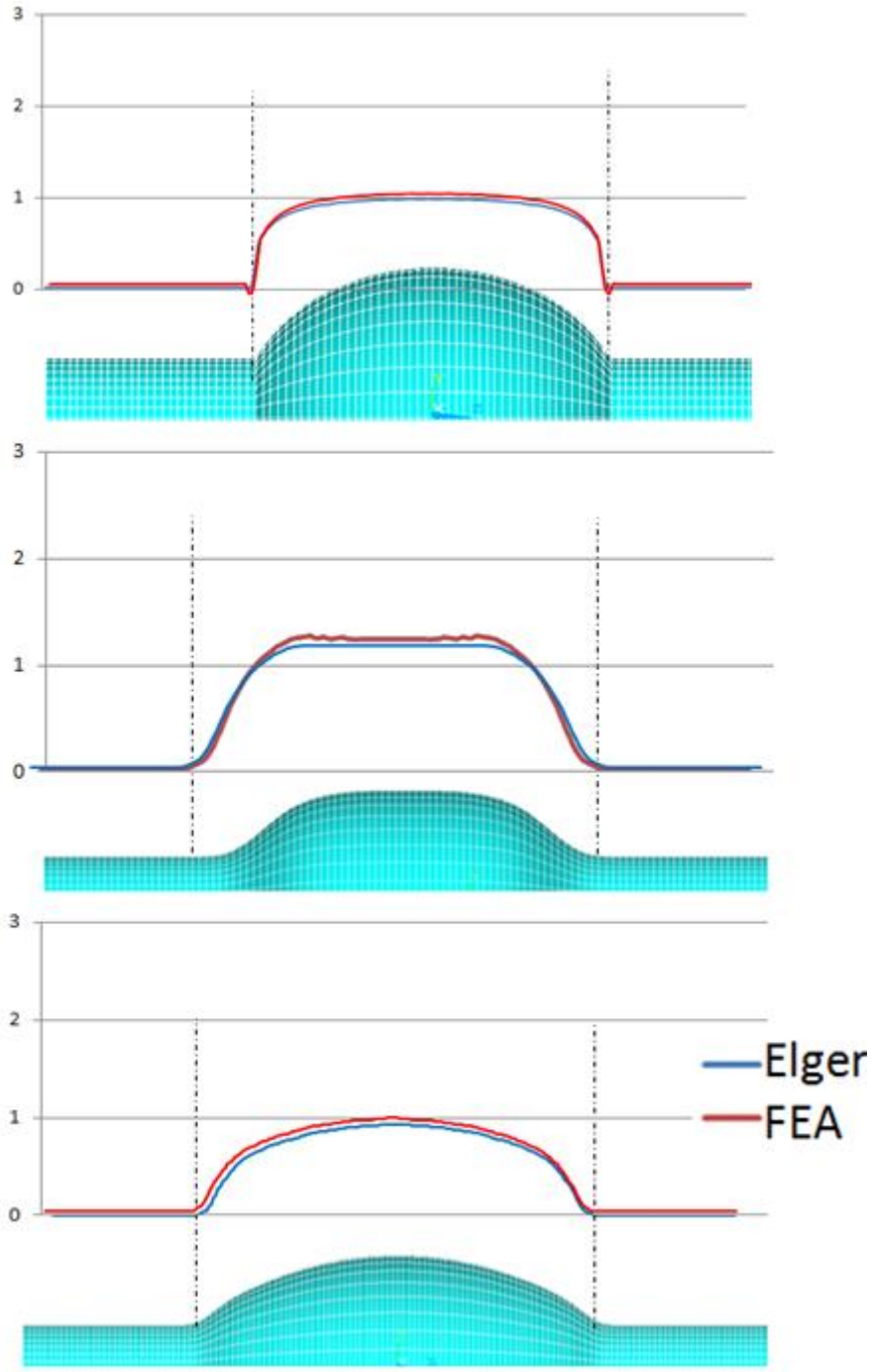

Figure 3-16: Longitudinal stress variation in the four models compared to the results of Elger et al. (1996).

3.2 Computational fluid dynamics

Computational Fluid Dynamics (CFD) is a method of analysis of the systems involving fluid flow and heat transfer by means of computer based simulations. This technique is very powerful and has been in wide use in research and industrial

applications (Versteeg and Malasekera, 1995). CFD methods are concerned with the solution of equations of motion of the fluid as well as with the interaction of the fluid with solid bodies (Blazek, 2001). Advancement in the computer industry has generated significant interest in CFD and this has consequently rendered a dramatic improvement in the efficiency of the computational techniques. Consequently, CFD is now the preferred means of testing alternative designs in many branches of engineering and a powerful tool for researchers (Fletcher, 1990).

The strategy of CFD is to replace the continuous problem domain with a discrete domain using a grid. In the continuous domain, each variable of the flow is defined at every single point in the domain. For example, the pressure p in the continuous one-dimensional domain shown in Figure 5-16 would be given as:

$$p = p(x),\ 0 < x < 1 \qquad \text{(Eq. 3-1)}$$

In the discrete domain, each flow variable is defined only at the grid points.
Therefore, in the discrete domain shown below, the pressure would be defined only at the N grid points:

$$pi = p(xi),\ i = 1, 2, \ldots, N \qquad \text{(Eq. 3-2)}$$

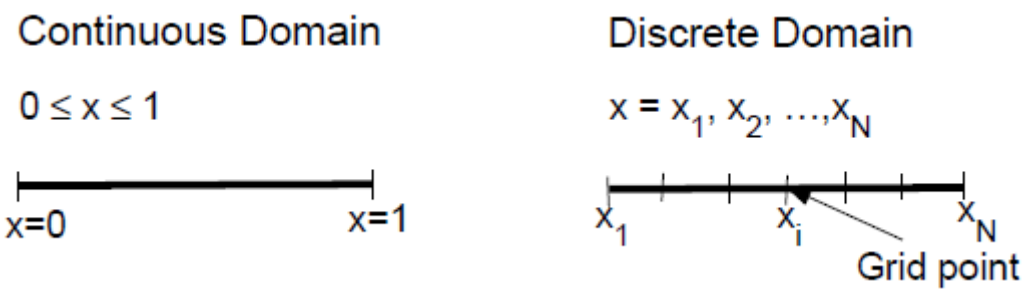

Figure 3-17: Continuous and discrete domains showing possible values of (x) (Bhaskaran, 2002).

In a CFD solution, one would directly solve the relevant flow variables only at the grid points. The values at other locations are determined by interpolating the values at the grid points (Bhaskaran, 2002).

3.2.1 Model creation

Eight fusiform axisymmetric three-dimensional aneurysms with constant inlet diameter, d = 2.0 cm, variable maximum aneurysm diameter, D = 3.76 - 7.0 cm, and constant aspect ratio of 4 were considered. Curvatures of the wall of all aneurysms were derived from the equations shown in Table 3-2. Details of each model are shown in Table 3-8.

Models for CFD were created using the second approach as discussed in section 3.1.1.2 with the additional step of filling the internal lumen of the aorta and aneurysm with solid material in the CAD model which is then meshed to finite volume cells as seen in Figure 3-18. The length of a normal tube (15 cm) before and after the aneurysm is modelled to allow the flow to develop to more parabolic shapes before entering the aneurysm.

Inflation layers, which are widely used in CFD, were added near the wall region to increase the number of cells and hence the accuracy in these areas as shown in Figure 3-19.

Model	D	Wall curvature	Thrombus thickness	Number of Elements
F0	3.76	Cosine Exponential	Zero	56782
F1	4	Parabolic	Zero	63003
F2	4	Exponential	Zero	68513
F3	5	Cosine Exponential	Zero	75894
F4	5	Exponential	Zero	83406
F5	7	Cosine Exponential	Zero	129878
F6	7	Exponential	Zero	146035
F7	5	Exponential	5 mm	150246

Table 3-8: Details of all eight models used for the CFD calculations in this research.

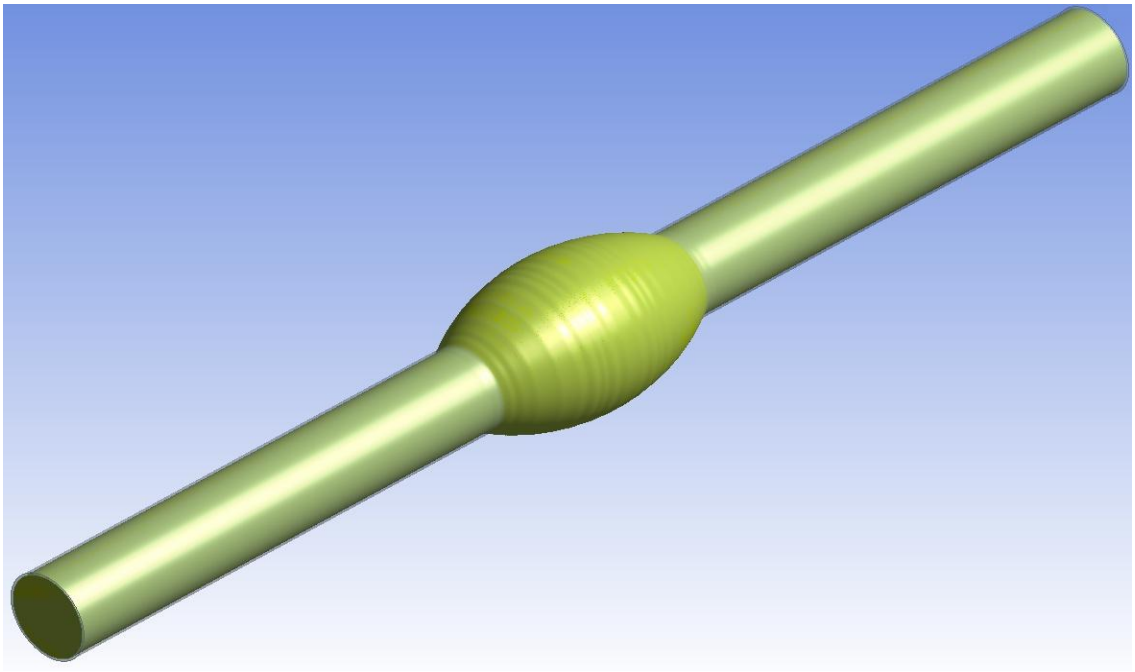

Figure 3-18: CAD model for flow analysis showing the inside of the tube filled with solid material.

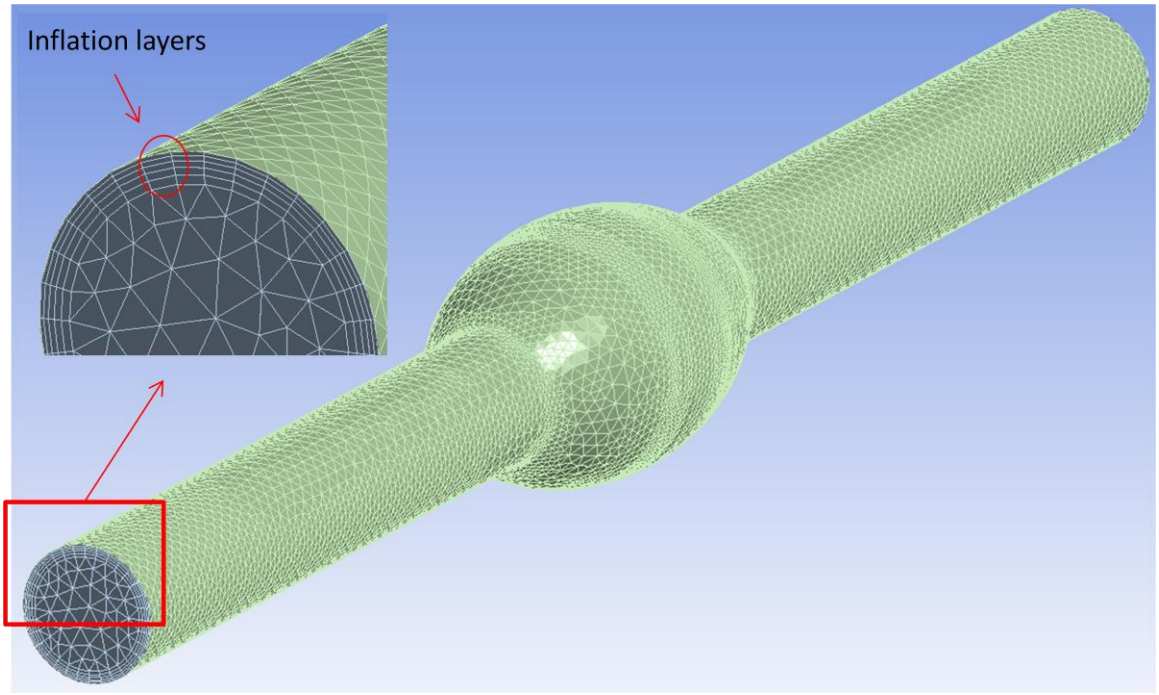

Figure 3-19: Mesh view of internal flow and the outside wall showing the inflation layers near the wall.

3.2.2 Boundary conditions

The ANSYS CFX (Version 12) computational fluid dynamics solution was used for all the fluid computational studies reported in this thesis. The governing equations for blood flow are the Navier–Stokes formulations with the assumptions of an incompressible, homogeneous laminar flow.

Because the aorta has a diameter greater than 0.5 mm, an assumption of Newtonian flow is reasonable due to the fact that blood viscosity is relatively constant at the high rates of shear typically found in the healthy aorta (Scotti and Finol, 2007). Steady flow with constant velocity at the inlet and blood pressure of 120 to 145 mmHg at the outlet (see Figure 3-20) was used with blood density, 1121 kg/m3 and blood dynamic viscosity, 0.0035 Poiseuille (Pa.s) (Yu, 2000):

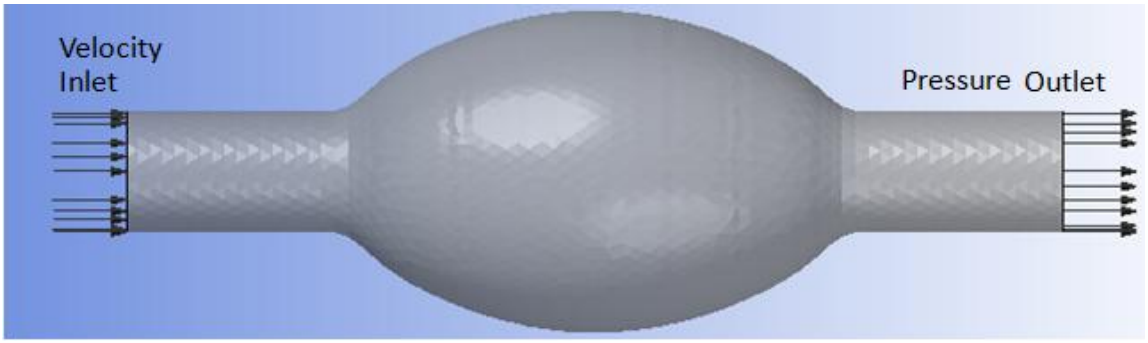

Figure 3-20: Model with inlet of steady state flow and outlet of constant pressure. (Note the actual lengths of the inlets and outlets were longer than that shown in the figure but in this figure only region of interest is shown)

3.2.3 Convergence studies

A convergence study has been undertaken, similarly to the study described earlier in section 3.1.3; the parameters to be tested here were pressure and velocity. The models show convergence when the number of elements exceeds 50,000.

Convergence history

Prediction of CFD solutions significantly depends on the numerical convergence of the coupled partial differential equations (Navier-Stokes equations) on a mesh structure. A measure of how well the solution is converged can be obtained by plotting the residuals for each equation at the end of each numerical iteration, for steady state simulations or at time-step for transient simulations. A reasonably converged solution requires a maximum residual level no higher than $5.0e^{-04}$ (ANSYS CFX help documents).

The root mean square (RMS) residual is obtained by squaring all the residuals throughout the simulation domain, taking the mean, and then taking the square root of the mean. This should present an idea of a typical magnitude of the residuals.

Convergence of the numerical solution requires a trade-off between simulation time and minimum level of RMS value which predicts the solutions with desired accuracy.

Considering the laminar nature of the flow, the RMS value was set to a standard of $1e^{-04}$ for all the flow variables. Figure 3-21 below shows the convergence history of the numerical solution, which indicates that all the flow variables reached an RMS value of $1e^{-04}$ and at this point the numerical iterations were stopped. The figure indicates the convergence history of the variables in the momentum equations (Navier-Stokes equation) and the Pressure (P-Mass) and velocities in the x-, y-, and z-directions (U-Mon, V-Mon and W-Mon).

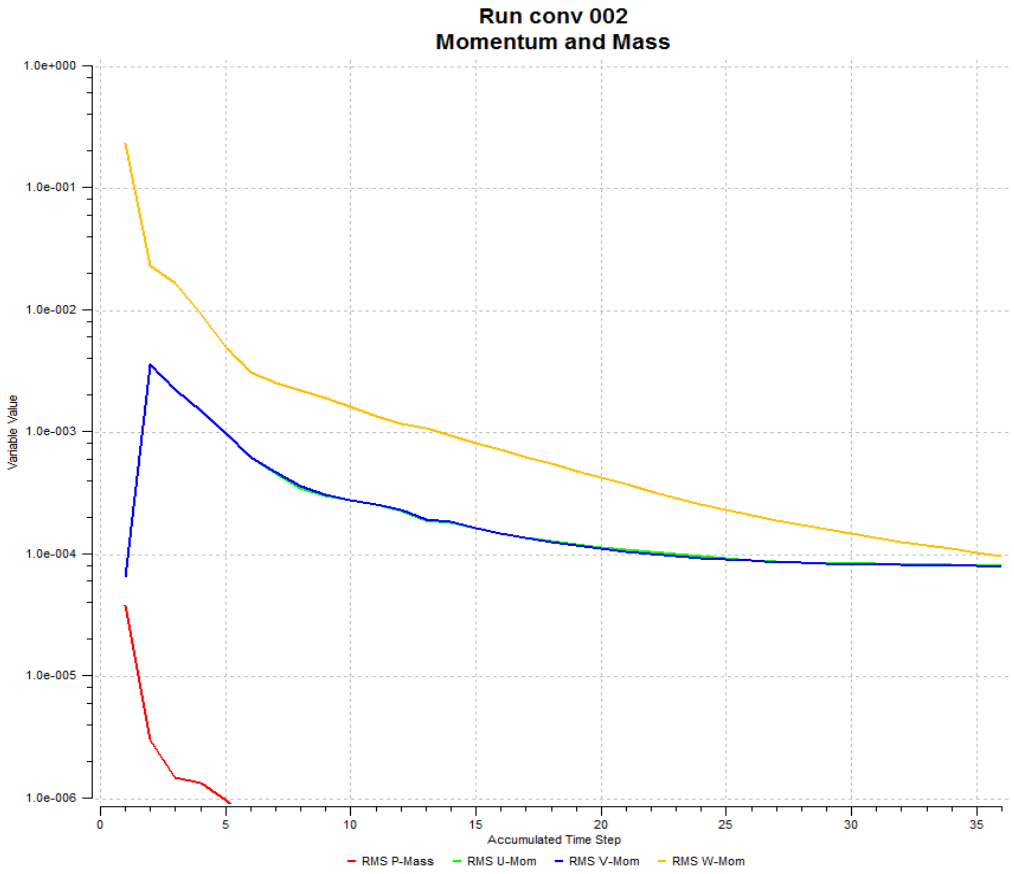

Figure 3-21: RMS values for the CFD numerical simulations

3.2.4 Validation studies

Previous studies have provided validation of CFD results using quantitative method by comparing the experimental and numerical results of axial velocity profiles and qualitative method by comparing velocity vector plots from the CFD simulation with experimental flow visualization results (Kelly and O'Rourke, 2009). Again, it was not

possible in the scope of this project to undertake a detailed experimental validation of the results. Therefore, validations for results of CFD simulations undertaken in this project were compared to the experimental results of steady flow performed by Peattie et al. (1996). Validation was achieved for both the velocity amplitude (quantitative) and flow behaviour (qualitative) results.

Model F0 from Table 3-8 was used with the same boundary conditions as above with an inlet speed of 10 cm/s to match the Peattie et al.'s (1996) study. Results were then compared to Peattie et al., (1996). The dimensions of the model were sourced from Peattie et al. (1996) and the shape was derived by digitizing the AAA model shown in their study.

Quantitative analysis

A quantitative comparison was made between the experimental and numerical results by comparing the velocity at 9 points at the middle of the aneurysm where X=0 and at the two ends of the aneurysm where X = 4 and -4 respectively. At each axial position, 3 points with different radial positions were chosen and are shown in Figure 3-22.

Table 3-9 and Figures 3-23, 3-24 and 3-25 present the velocity (in cm/s) for the nine points in the CFD model compared to the same positions of the experimental model.

X position	X=-4			X=0			X=4		
Y Position	A	B	C	A	B	C	A	B	C
Exp	5	10.6	5	-1	10	-1	4	10.6	3.5
CFD	4.9	10.3	4.8	-0.95	9.6	-0.95	4.2	10.3	3.6

Table 3-9: Velocity in X-direction (cm/s) for the nine points in the CFD model compared to the same positions in the experimental model.

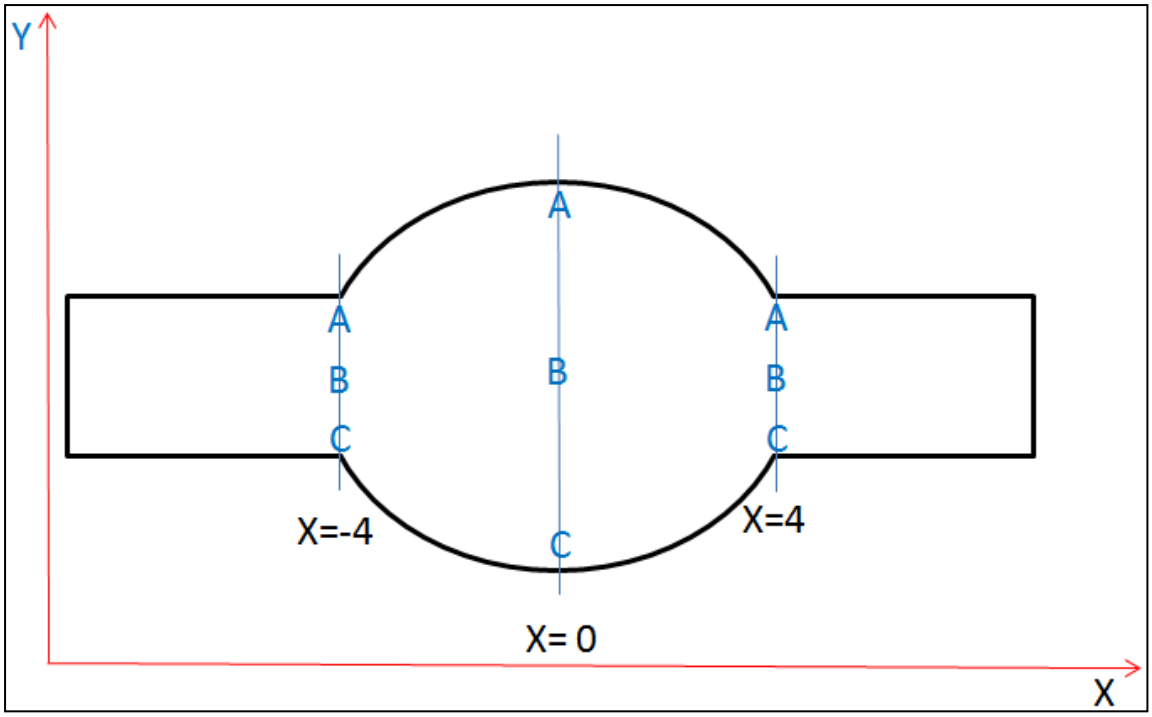

Figure 3-22: Axial and radial positions where measurements were taken.

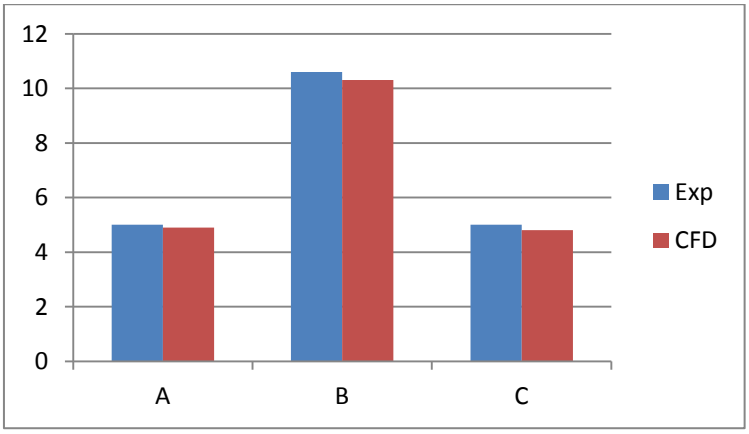

Figure 3-23: Velocity in X-direction (cm/s) for the three points at (X= -4) in the CFD model compared to the same positions in the experimental model.

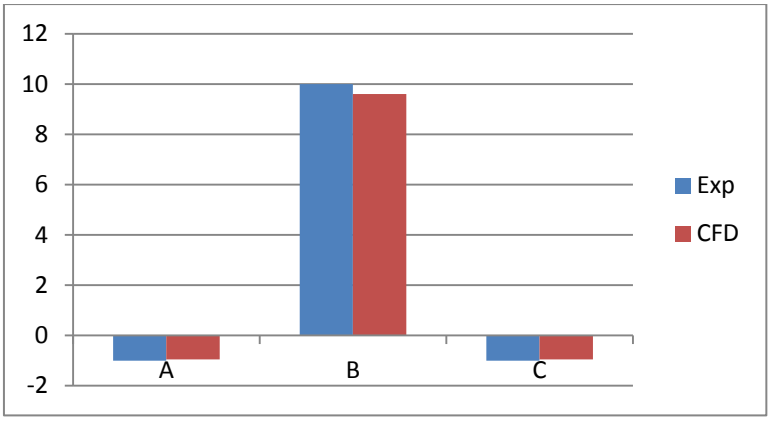

Figure 3-24: Velocity in X-direction (cm/s) for the three points at (X= 0) in CFD model compared to the same positions in the experimental model.

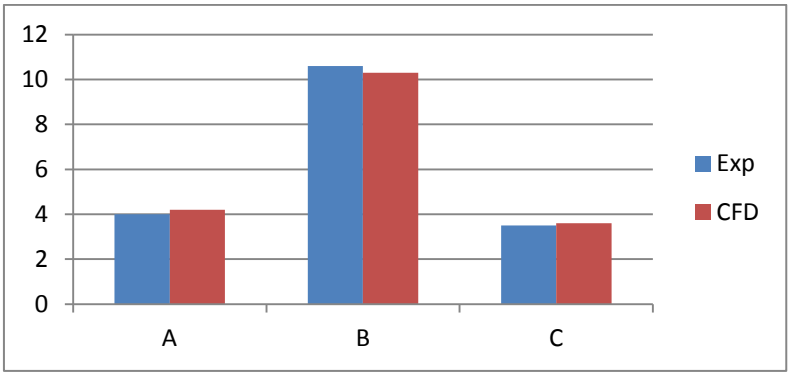

Figure 3-25: Velocity in X-direction (cm/s) for the three points at (X= 4) in CFD model compared to the same positions in the experimental model.

From the above, it could be concluded that CFD was able to predict the magnitude and the direction of velocity in all positions. The average error for all points is less than 5%, which is acceptable for the scope of this study.

Qualitative analysis

A qualitative comparison was undertaken between the experimental and numerical results by comparing flow behaviour and streamlines.

Peattie et al. (1996) reported a core of smoothly flowing fluid passed through the centre of the aneurysm surrounded by vortices in the external part of the aneurysm. These were also found in the CFD model shown in Figure 3-26. Parabolic flow also noticed at the inlet of the models before the aneurysm began in both CFD and experimental models.

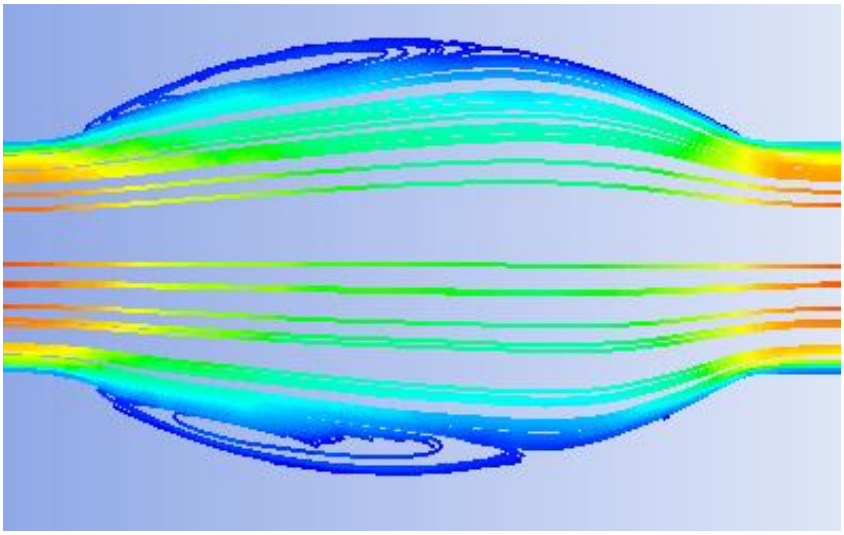

Figure 3-26: Velocity streamlines for the CFD flow within the model.

Overall, the qualitative and quantitative comparisons between the Peattie et al. (1996) calculations and the CFD predictions suggest that CFD is capable of predicting the magnitude and direction of the velocity within this idealized aneurysm geometry.

3.3 Summary

This chapter presented the theoretical background and the methodology undertaken in this research, along with extensive details about the geometry, material properties and the boundary condition used to allow other researchers to redo the work. The dimensions and the wall curvature were given for each model plus the element type used and number of elements.

A convergence study was presented for each technique to prove that the analyses were performed at the sufficient number of elements. A validation for each technique was undertaken to ensure that the simulations can predict the desired results.

Chapter 4
Effects of aneurysm shape and dimensions

4.1 Introduction

As discussed earlier in this thesis, aneurysm wall stress is generally considered to be a better way to differentiate patients with a high risk of abdominal aortic aneurysms than using the aneurysm diameter. The earlier AAA numerical studies used either patient specific AAA shapes or simple symmetric or asymmetric AAA shapes. Stringfellow et al. (1987) and Mower et al. (1993) used finite element analysis to calculate the stress distribution in simplified AAA model geometries and they found that the complexity of the geometry influences the stress distribution and that applying the law of Laplace (stress is proportional to diameter, see Eq 2.1) to AAA is not accurate. This finding is in agreement with Elger et al.'s (1996) hypothesis that the risk of rupture depends on AAA shape. Elger et al. (1996) used an analytical models and found that the wall stress distribution is mainly influenced by the shape of AAA with maximum stress correlated to wall curvature.

Hua and Mower (2001) examined some simple geometric characteristics to assess the risk of rupture on AAA using six FEA models with different shapes and they reported that simple geometric criteria is unreliable in predicting AAA stresses. However they found that AAAs having circular cross sections exhibited lowest wall stresses, whereas stresses increased as the cross sections became more elliptical. It seems that they have neglected the effect of the aneurysm shape by examining single parameter but not using the same shape which will not be surprising results.

Thus, geometric characteristics play a vital role in the variation of wall stress values and location. In the first part of this current study, fusiform axisymmetric three-dimensional (3D) AAA shapes were created. Simple and non-complex shapes rather than realistic shapes were used in order to concentrate on only one factor at a time to determine the effect of the shape in isolation of other factors effects.

In this chapter, the effect of AAA shapes will be investigated by using different shapes with the same dimensions to determine how this can affect the magnitude or distribution of the stresses on the AAA wall. A study of the aspect ratio for AAA will then be undertaken to conclude its effect on stress magnitude or distribution and to suggest how this can be useful in the assessment of the AAA.

The purpose of all investigations in this chapter was to study the relationship between wall stress values and specific geometric parameters; this may lead to further understanding of the effect of each value and parameter and improve the assessment of AAA with high risk of rupture.

The stress value is represented as hoop and longitudinal stresses were also used to study the aneurysm shape effects and to validate the results of this work by comparing them with previously published results. Hoop stresses were used to investigate in more depth the causes of the aspect ratio effect discussed in Chapter 4.

4.2 The effect of aneurysm shape

In clinics, AAA is found in a variety of shapes (Elger et al., 1996) which could itself be an assessment factor of the disease and lead to different assessments of severity. To understand the basic effects of aneurysm shapes on wall stress, four different shapes of the same diameter aneurysm were chosen to investigate the effect of shape.

4.2.1 Method

All the available shapes in this work (open sphere, exponential, cosine-exponential and parabola-exponential) shown in Figure 4-1 were investigated to provide an understanding of the behaviour of a variety of shapes. Methodology and all boundary conditions were the same as described earlier in 3.1.2 with a wall thickness of 1 mm and an internal pressure of 144 mmHg. Further details about the numerical models were given in Chapter 3.

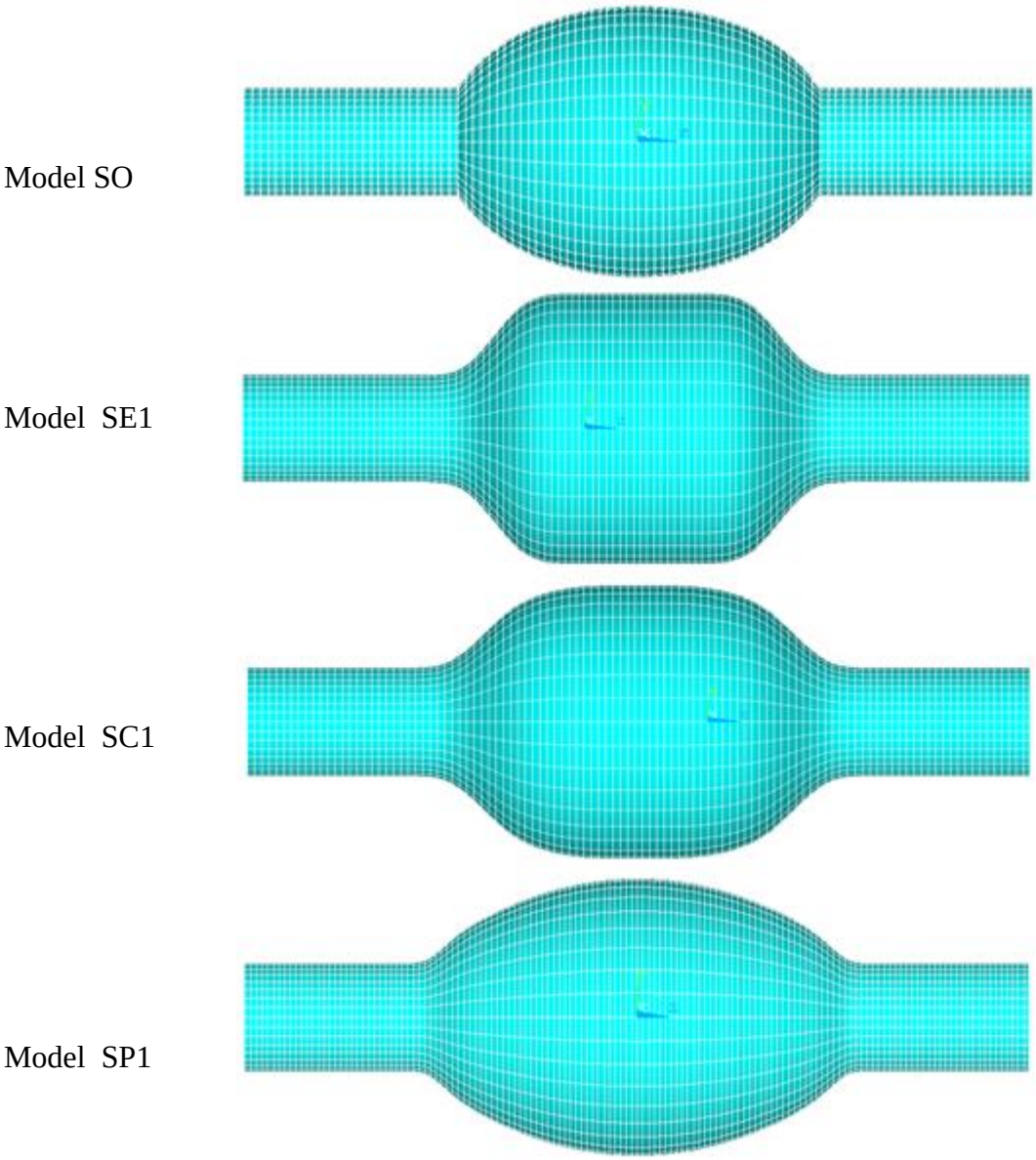

Figure 4-1 Element plots of the four models clearly showing differences in wall curvature.

4.2.2 Results

The stress values are represented as hoop and longitudinal stresses to examine the effect of shape on each one independently. Figure 4-2 illustrates the hoop stress distribution in the walls of the models obtained from static simulations of the peak systolic pressure. It can be seen that the hoop stress distribution around the aneurysm differs from one model to another and the maximum stress occurs at the two ends of the aneurysm in models SO, SE1 and SC1 while for model SP1, the peak stress was found in the middle of the aneurysm.

The maximum hoop stress values are 0.46 MPa, 0.50 MPa, 0.47 MPa and 0.36 MPa for models SO, SE1, SC1 and SP1 respectively as shown in Figure 4-2.

The maximum longitudinal stress values are 0.18 MPa, 0.21 MPa, 0.20 MPa and 0.16 MPa for models SO, SE1, SC1 and SP1 respectively.

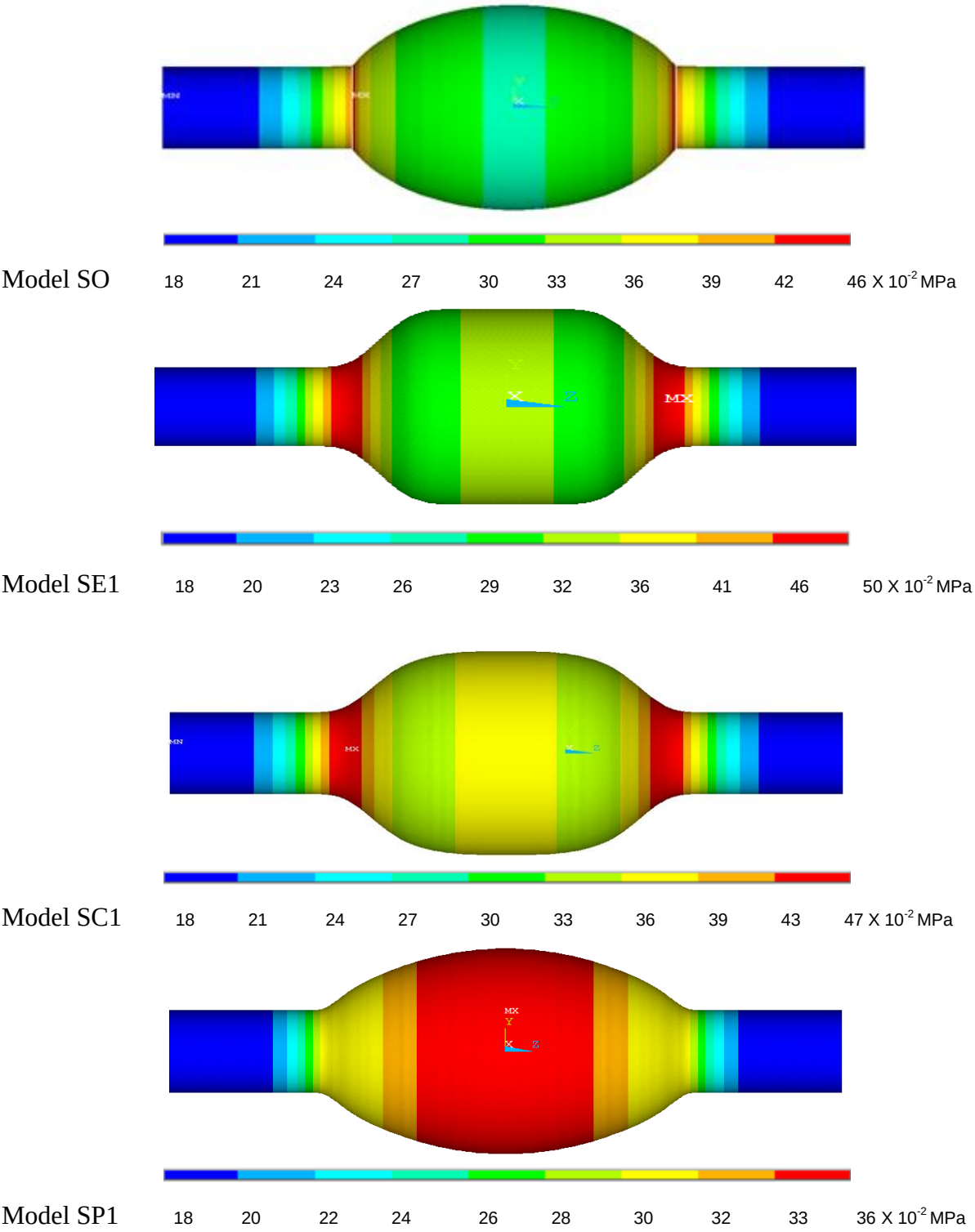

Figure 4-2: Hoop stress distribution of the four models.

4.2.3 Discussion

Based on the four aneurysms studied here as shown in Figure 4-2, it appears that maximum hoop stresses occurs either in the middle or in positions where the geometry tends to have the maximum variation in the curvature, namely where the curve changes rapidly at the beginning and the end of the aneurysm. The hoop stress at the point of maximum diameter is high, but not the highest in all models. The variation in stress distribution according to shape is a clear indicator of the shape effect on the AAA stress distribution.

In Figure 4-3, model SO shows an abrupt change in its profile at the beginning and end of the bulge, which results in a sharp change of the stress curve when compared to other models in which the changes were slow. In vivo, of course, this would not occur and it was only reported here to investigate the effect of wearied shapes.

Model SE1 in Figure 4-3 shows that the maximum stress occurs at the ends of the aneurysm with a value of 0.50 MPa, and then tends to decrease until it reaches the middle of the aneurysm where it starts to increase again. Similarly, Model SC1 shows that the maximum stress occurs also at the ends of the aneurysm with 0.47 MPa and then tends to decrease until it reaches the middle of the aneurysm where it starts to increase again. In model SP1, the maximum stresses of 0.36 MPa occur in the middle of the aneurysm but the stresses at the two ends of the aneurysm are relatively high at 0.31 MPa. These results are similar to Elger et al.'s (1996) findings who reported that the shape of the AAA curvature affects the distribution of the stress on the wall.

Longitudinal stress results show small variation for the four models. It seems that the shape of the aneurysm has a small effect on these stresses. It is noticed that these stresses vary between 0.16 to 0.21 MPa, which is less than half the variation of the hoop stresses. This also agrees with Elger et al.'s study where maximum hoop stress exceeds the maximum longitudinal stress by a factor of 2 to 3.

It is known that aneurysm rupture occurs when the stress on the wall exceeds its strength and this is likely to occur where the maximum stresses occurs. The work in this section clearly indicates that the diameter is not the best predictor of the location of peak stress and that instead, the shape affects the stresses produced in the

aneurysm. Figure 4-4 shows the relationship between aneurysm shape and maximum wall stress value for the same diameter and it clearly shows variation, confirming that the shape of the aneurysm affects the wall stresses.

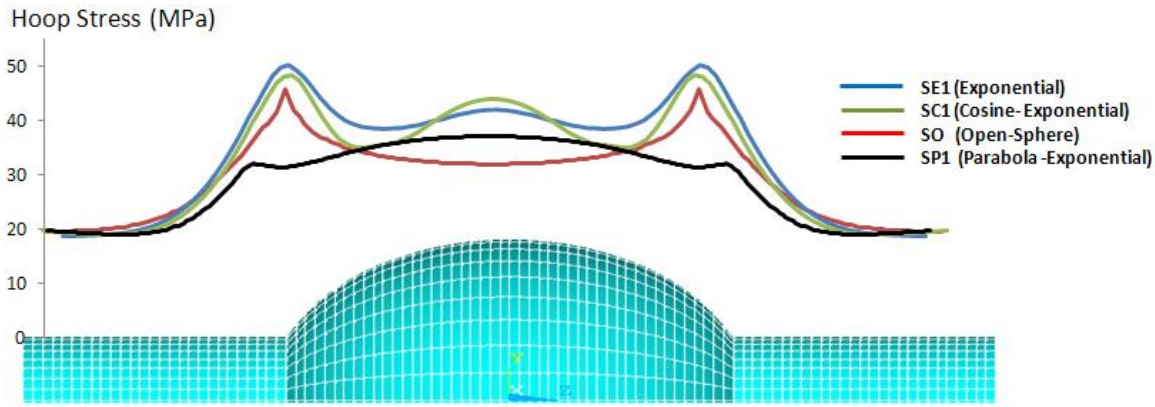

Figure 4-3: Hoop stress profile in X-direction for the four models.

Of the four models examined here, the law of Laplace failed to predict the location of maximum stress in three models (SO, SE1 and SC1). These findings agree with those of Elger et al. (1996) who also concluded that the law of Laplace provided neither qualitative nor quantitative understanding of the stresses on the inner wall of AAA, and that maximum stress does not depend on the maximum diameter, but on AAA shape and curvature.

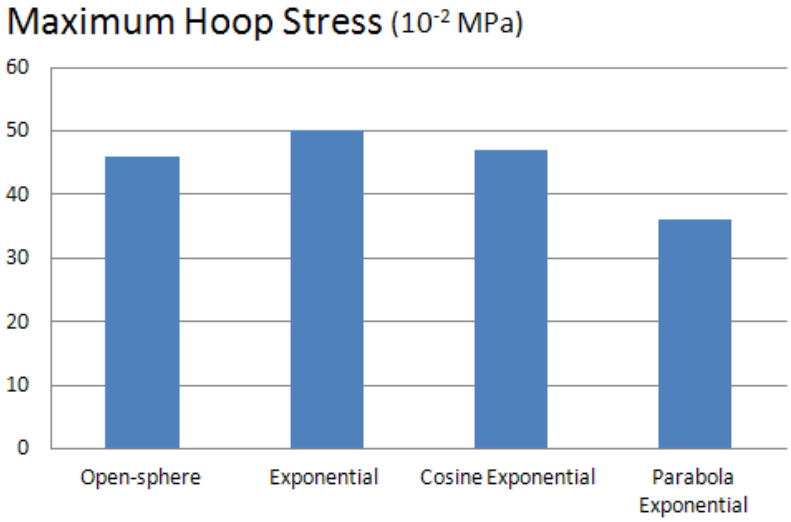

Figure 4-4: Relationship between aneurysm shape and maximum hoop stress of the same diameter (5 cm).

4.3 Blood flow in different aneurysm shapes of AAA

Blood hemodynamics is thought to have a vital role in the mechanical rupture of AAA and therefore needs to be understood. In this section, blood flow inside the aneurysm and the effects of this on the outside wall stresses will be studied.

Most previous simulations have considered simple static stress analysis using finite element analysis (FEA) that does not include the effect of the blood flow and therefore does not give information about what happens inside the aneurysm and how that may affect the risk of rupture of AAA. In applying FEA techniques to analyze the stresses on the internal arterial wall, uniform blood pressure over the whole aneurysm is normally considered and the blood flow effect of varying the distribution of blood pressure are neglected.

In this section, blood flow is added to the models to understand the effect of aneurysm shape and size on blood flow characteristics and to assess the significance of assuming a constant fluid pressure inside the aneurysm compared to the non-uniform pressure resulting from a fluid analysis. The inclusion of blood flow requires the use of computational fluid dynamics (CFD).

Another important reason for performing this analysis is to investigate the controversial recommendations of adding blood flow to the models, which increases the cost and the time of the analysis, compared to using uniform pressure and avoiding the complexity of blood flow analysis.

4.3.1 Method

Six models from Table 3-8 (F1, F2, F3, F4, F5 and F6) with different shapes and diameters were used, but the same boundary conditions were applied to study the blood flow inside the aneurysm. An average steady velocity of 25 cm/s was defined at the inlet, with a pressure of 120 mmHg defined at the outlet. Further details about the numerical models were given in Chapter 3.

4.3.2 Results

Flow streamlines and velocity vectors

Figures 4-5 and 4-6 present the streamlines and velocity vectors. They show that the flow consists of two main parts: high velocity flow in the middle and slow recirculation flow in the aneurysm. In all models there are vortices at the distal end of the aneurysm which, depending on the shape and size of the aneurysm, can be small, sharp, or large. In models of 7 cm diameter, vortices can also be noticed at the proximal end of the aneurysm. It could also be noticed that velocity of the blood increases when flow exits the aneurysm.

Wall pressure distribution

Figure 4-7 presents the pressure gradient in the six models with a very small pressure gradient in all models (less than 1 mm Hg) and higher pressures at the distal end of the aneurysm are noticed.

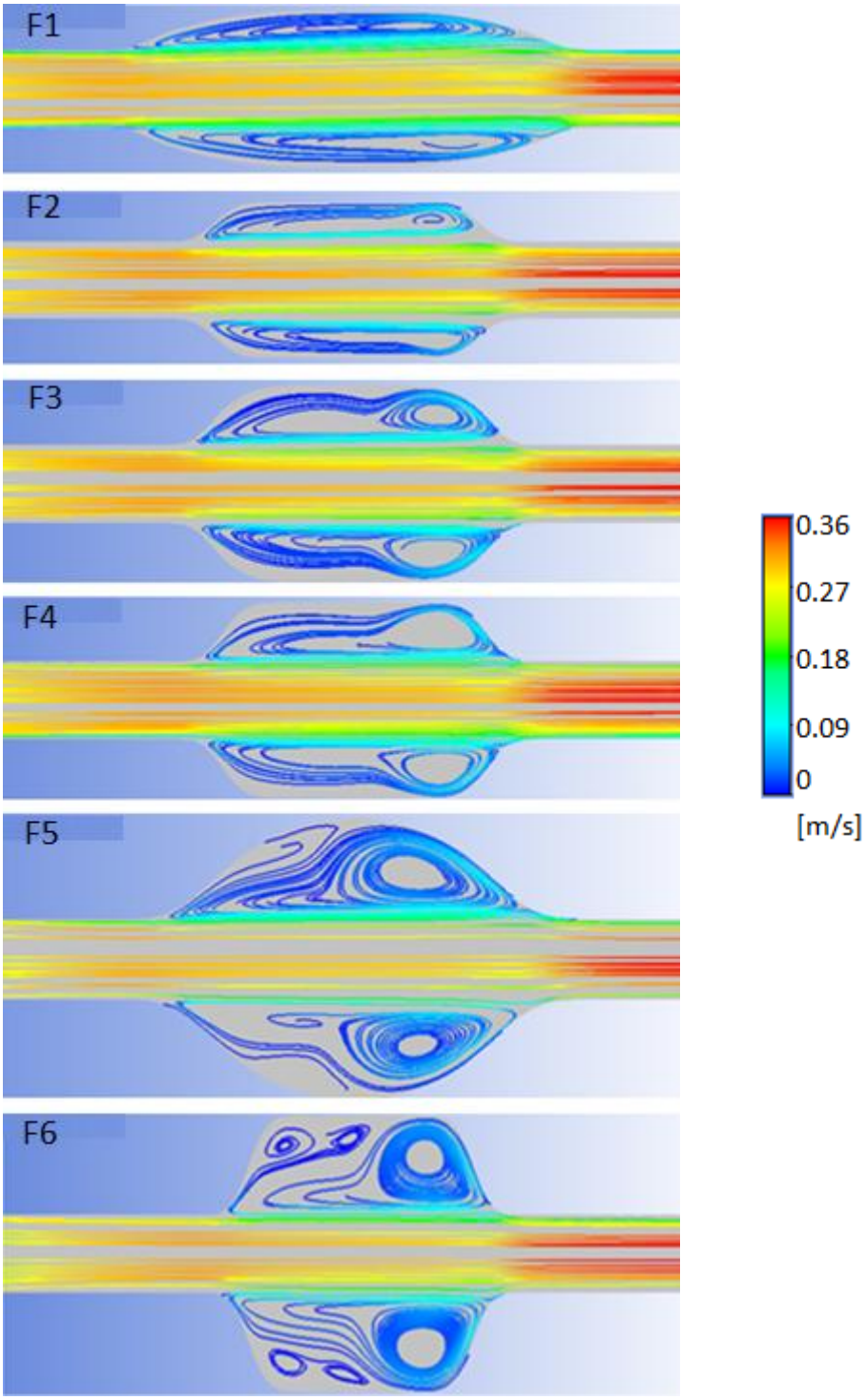

Figure 4-5: Results show that the vortices increase as the aneurysm diameter increases.

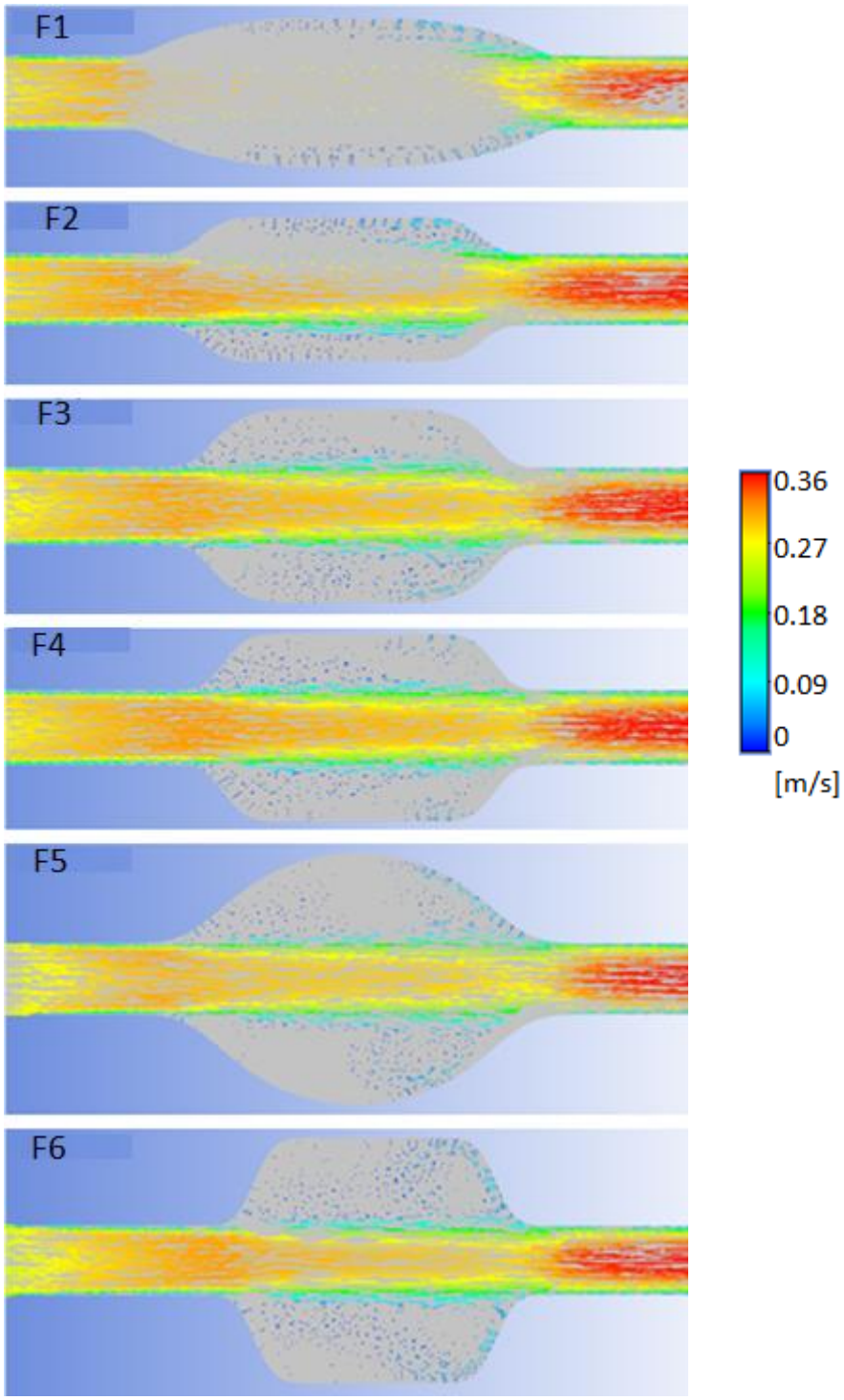

Figure 4-6: Velocity vectors for the six models.

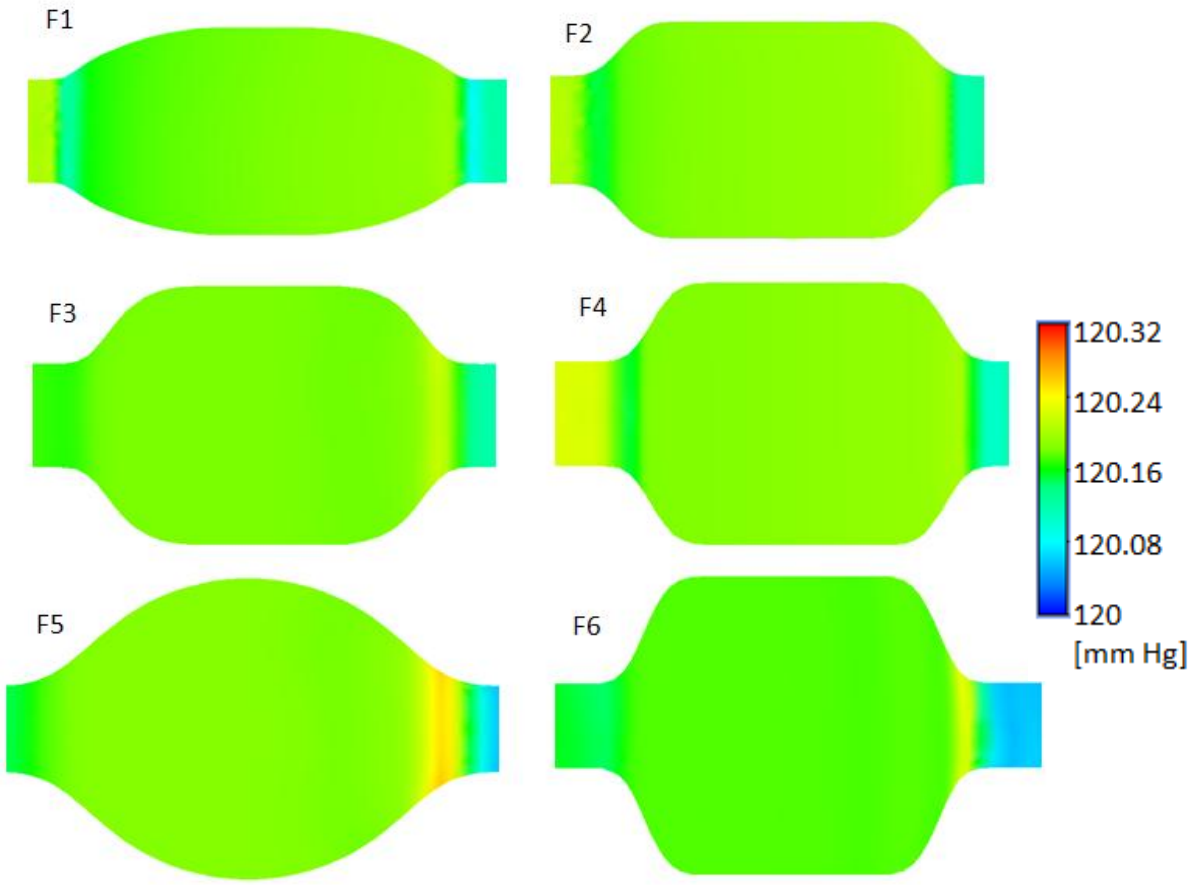

Figure 4-7: Wall pressure distribution for the six models, showing higher wall pressures at the distal ends of all aneurysms.

4.3.3 Discussion

This study shows that flow in an aneurysm consists of two main parts: a high velocity flow in the middle of the geometry with slow recirculation flow on the outside. The high velocity region is similar in all models, but the recirculatory part varies with aneurysm shape and size.

The flow recirculation is a consequence of the adverse pressure gradient imposed by the increase in the cross-sectional area at the aneurysm, and as a result, the larger aneurysms create more vortices than when the diameter is smaller, as can be seen in models F5 and F6 (D= 7 cm). The exponential-shaped aneurysm has sharper vortices due to the sudden change in the diameter compared to the parabolic shapes. Secondary vortices can be noticed also at the proximal end of the large aneurysms and they are stronger in the exponential shape.

Figure 4-8 shows quantitative and qualitative details of the velocity in close-up images of the velocity vectors and velocity map of model F3. The velocity map shows that the flow starts at a constant speed and then changes to a parabolic distribution, with the lowest speed near the wall increasing as the flow moves to the middle, as the aneurysm body starts. It is noticeable that in the middle of the aneurysm, a higher velocity occurs compared to the slow zones in the external body of the aneurysm. It is also noticed that there are some vortices occurring at the distal end of the aneurysm and the flow reverses direction.

The above findings agree with Yu (2000), who reported that a large core existed across the tube before the aneurysm, with very thin boundary layers, formed at the walls with a thickness of about 5% of the diameter as shown in Figure 6-5, which was also noticed in this simulation with a thin boundary layer also with a thickness of 5% of the diameter and could be clearly seen in the velocity map, just before the proximal end when the flow is fully developed, as shown in Figure 4-8.

In this simulation and in the experimental work of Yu (2000), the general flow feature within the aneurysm mainly consisted of a jet of fluid surrounded by weak recirculation vortices on both sides. The flow recirculation was a consequence of the adverse pressure gradient imposed by the increase in cross-sectional area at the aneurysm. The core flow was steady and did not spread noticeably outward as it moved toward the end of the aneurysm. Yu (2000) also reported that the vortex core was located closer to the distal end of the aneurysm and this can also be noticed in the results of this simulation as can be seen in Figure 4-5.

The pressure on the wall shows only a small variation in all models (less than 1 mm Hg) with higher pressures at the distal end of the aneurysm. This was explained by Taylor and Yamaguchi (1994), who have shown that the vortices at the distal end of the AAA models caused regions of high pressure.

A number of experimental and numerical studies have investigated the flow inside AAA to understand the role of blood flow in the risk of rupture of the wall (Budwig et al., 1993; Peattie et al., 1996; Yu, 2000; Finol and Amon, 2001) who all found similar characteristics of blood flow inside the aneurysm. The small variation of blood

pressure inside the aneurysm was also found by Leung et al. (2006) and Kelly et al. (2009), who reported less than 0.1% in the variation of blood pressure along the aneurysm in AAA.

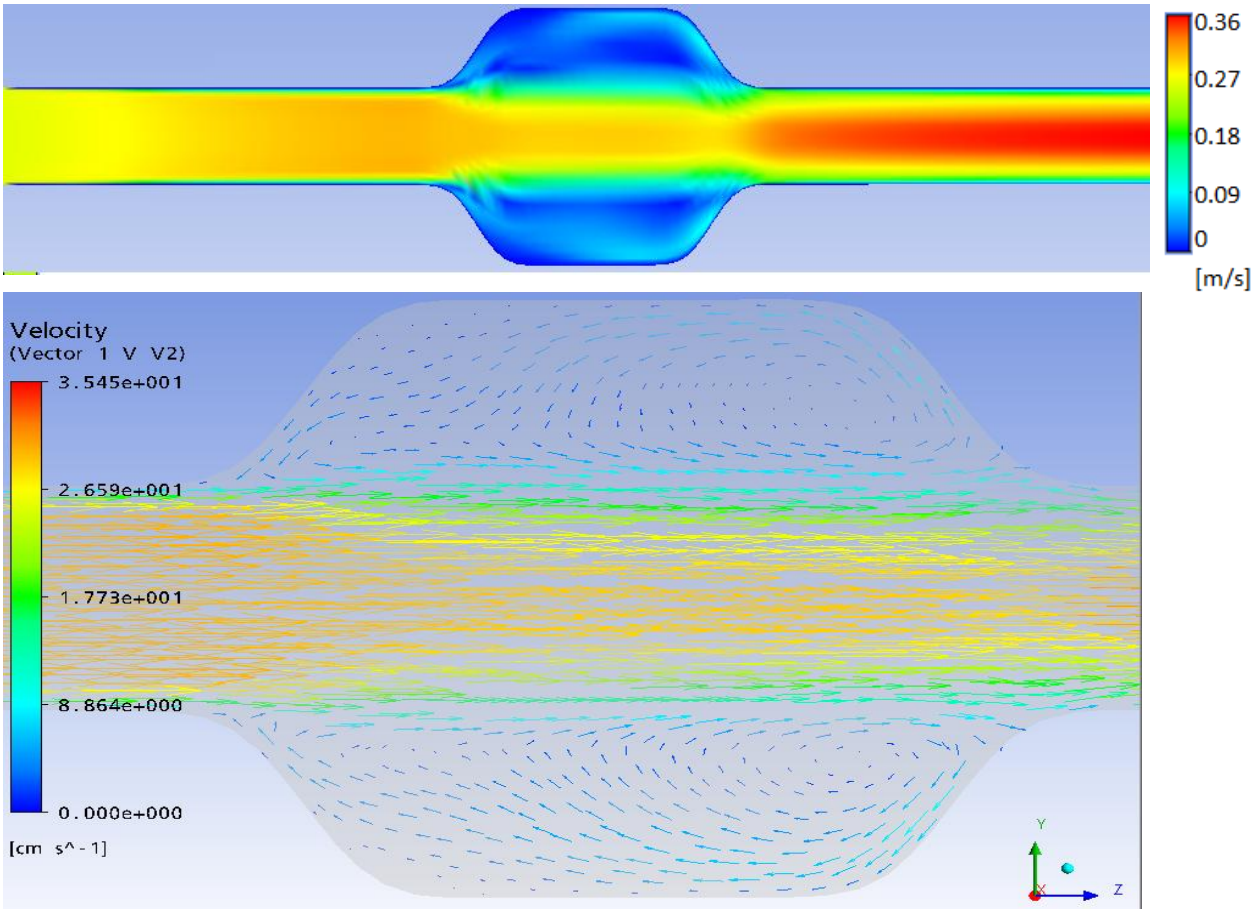

Figure 4-8: Velocity map and zoomed image of velocity vectors showing the quantitative and qualitative details of the velocity for model F3 with diameter 5 cm.

From the above findings, it could be concluded that vortices might play an important role in the formation of ILT and in the pathology of the AAA, which by itself is a factor of the aneurysm shape, meaning that aneurysm shape is a crucial factor in assessing the risk of AAA rupture. It could also be concluded that the variation of the blood pressure caused by blood flow was very small and hence could be neglected if wall stresses are required.

4.4 Effect of the aspect ratio on the stresses on the AAA wall.

Aspect ratio of AAA could refer to the relationship between any two dimensions in the aneurysm, the aspect ratio is defined here as the length of the aneurysm (or bulge) divided by the diameter of the healthy aorta (before the aneurysm starts), and is obtained from basic aneurysm geometry dimensions in Figure 4-9; the aspect ratio is (L/d).

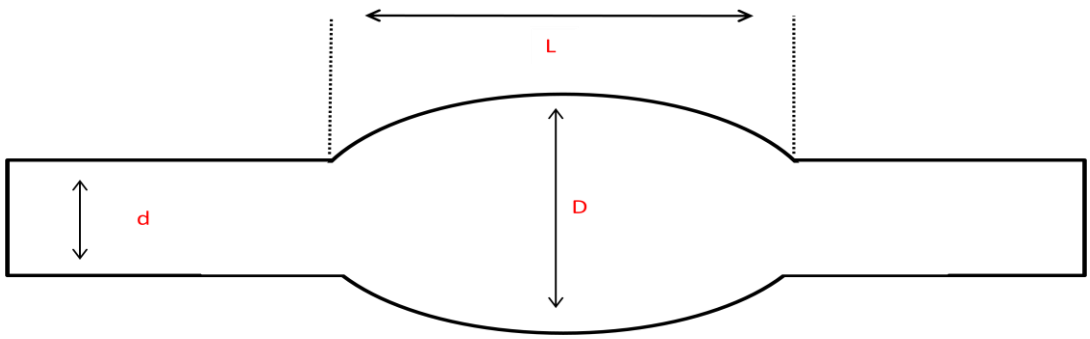

Figure 4-9: Basic aneurysm geometry dimensions.

Relationship between basic dimensions of the aneurysm is likely to have an effect on the wall stresses. There does not appear to be any systematic study in the literature of the effect of aspect ratio on AAA but another form of aspect ratio (relationship between maximum diameter, D and neck diameter, d) is widely used as a reliable indicator for the risk of rupture in cerebral aneurysms[3] (Weir et al.,2003; Ujiie et al., 1999; Ujiie et al., 2001).

In most geometry based studies of AAA, aspect ratio is given an ideal value of 4. This section shows the effect that aspect ratio has on the value, and the location of the wall stresses.

4.4.1 Method

Three models with different maximum diameters and aspect ratios of 3, 4 and 5 were considered to give a total of nine models SE4 (A, B and C), SE5 (A, B and C) and SE7 (A, B and C) from Table 3-1 in Chapter 3. The aneurysm diameter D was also varied between 4, 5, and 7cm to give a better understanding of the aspect ratio effect by examining different aneurysm diameter values. Diameter values were chosen

based on the critical value of 5 cm of the aneurysm; (small = 4 cm; critical = 5 cm; high risk = 7 cm).

Details of the numerical models, methodology and all boundary conditions were described earlier in section 3.1.2 with a wall thickness of 1 mm and internal pressure of 120 mmHg.

4.4.2 Results

The stress values are represented as hoop stresses because it was found to be dramatically affected by the aspect ratio as will be explained at the end of this chapter.

Figure 4-10 shows the hoop stress distribution in model SE4 with diameter = 4 cm but different aspect ratios. It can be noticed that maximum stress value increases as the aspect ratio increases, with peak stress increasing from 29×10^{-2} MPa (with aspect ratio = 3) to 37×10^{-2} MPa and 38×10^{-2} MPa for aspect ratios 4 and 5 respectively. It can also be seen that maximum stress was located at the two ends of the aneurysm at aspect ratio = 3 but the maximum was shifted to the middle of the aneurysm when the aspect ratio was increased to 4. The location of maximum stress at aspect ratio 5 is also in the middle with a small increase of the value.

Figure 4-11 illustrates the hoop stresses in model SE5 with a diameter of 5 cm, showing that maximum hoop stress increased from 0.35 MPa to 0.44 MPa when the aspect ratio increased from 3 to 4, then to 0.48 when the aspect ratio increased to 5. The location of maximum stress is shifted from the aneurysm ends, to the middle, by increasing the aspect ratio from 3 to 4. When the aspect ratio was increased to 5, maximum stress increased and the location was still in the middle.

Model SE7 in Figure 4-12 with a diameter 7 cm has a maximum hoop stress of 0.47 MPa with an aspect ratio of 3 increasing to 0.50 MPa, with an aspect ratio of 4 then increasing to 0.60 when the aspect ratio increased to 5. The maximum stress was located at the ends of the aneurysm at an aspect ratio of 3, then moved to two locations, in the middle and at the ends of the aneurysm at an aspect ratio of 4; maximum stress was then concentrated in the middle at aspect ratio 5.

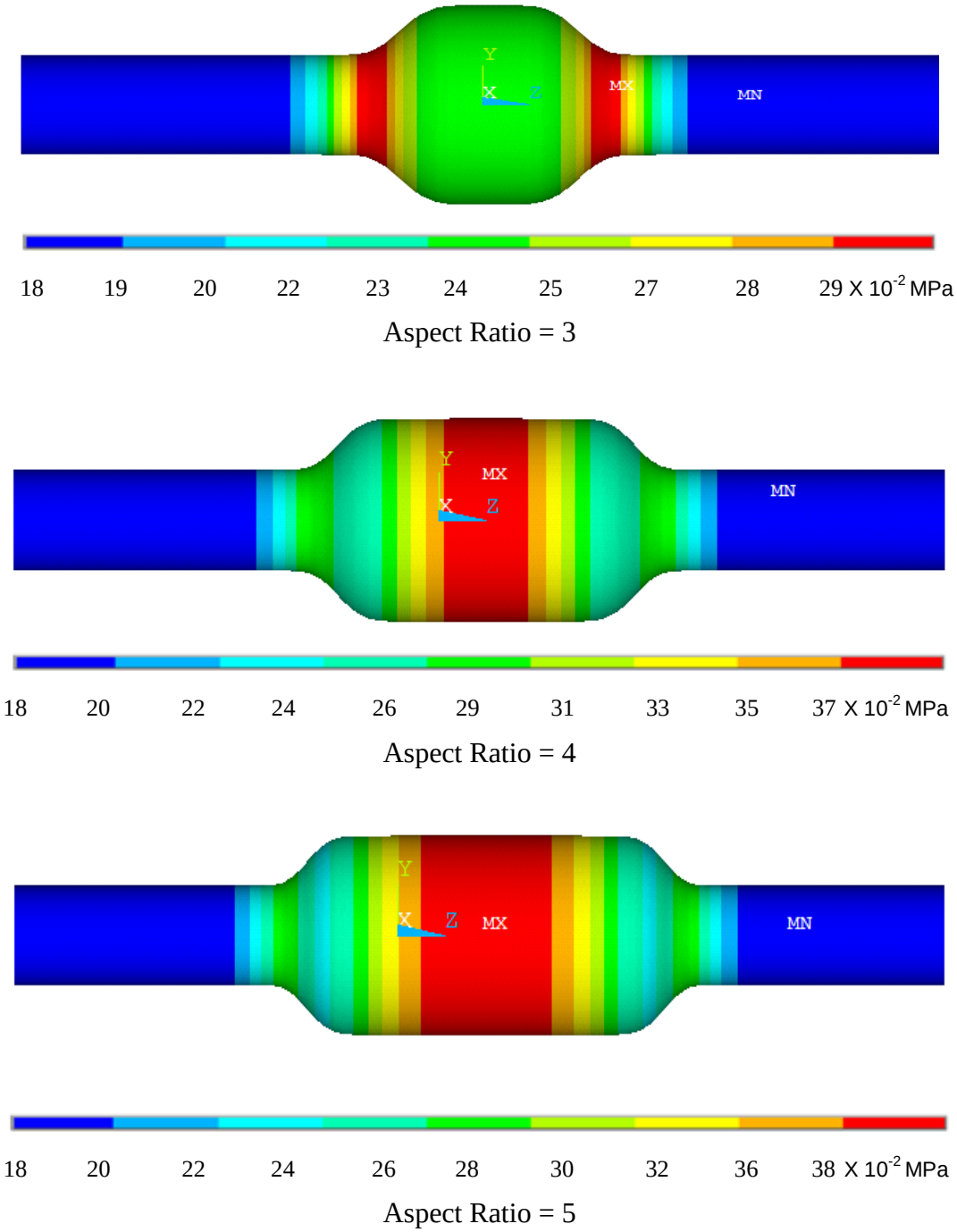

Figure 10-4: Hoop stress distribution for models SE4 A, B and C (D= 4cm) with aspect ratios 3, 4, and 5

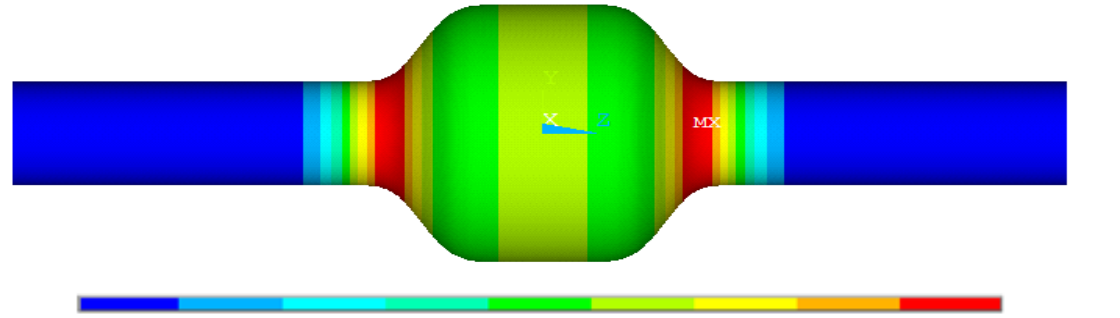

Aspect Ratio = 3

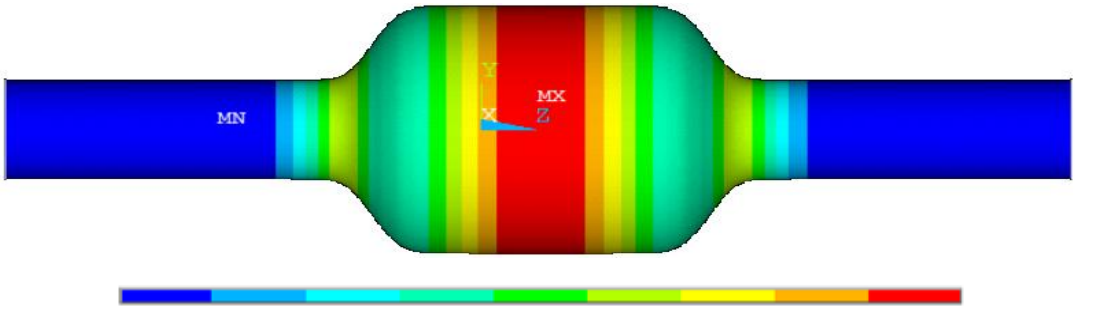

Aspect Ratio = 4

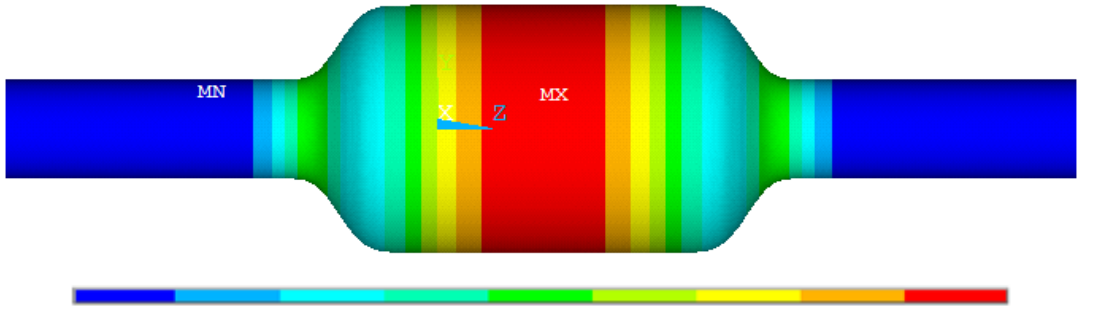

Aspect Ratio = 5

Figure 11-4: Hoop stress distribution for models SE5 A, B and C (D= 5cm) with aspect ratios 3, 4, and 5

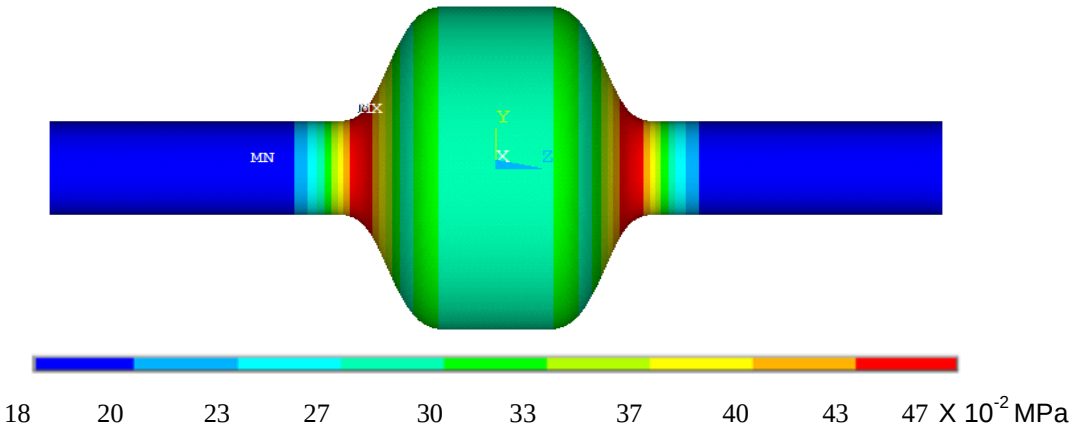

18 20 23 27 30 33 37 40 43 47 X 10^{-2} MPa

Aspect Ratio = 3

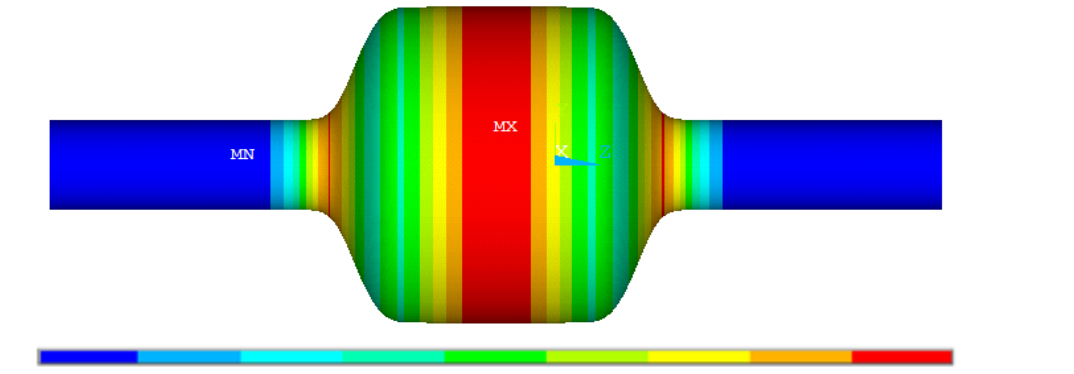

18 21 24 28 32 35 39 43 46 50 X 10^{-2} MPa

Aspect Ratio = 4

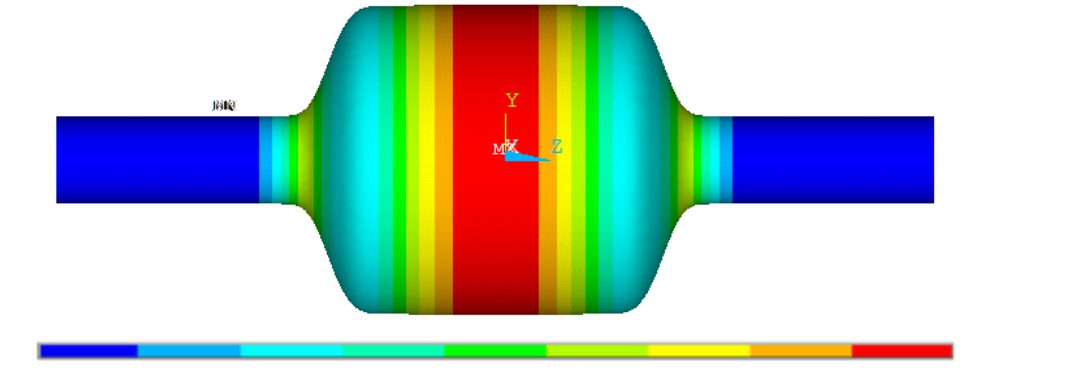

18 23 26 31 37 42 48 54 58 60 X 10^{-2} MPa

Aspect Ratio = 5

Figure 4-12: Hoop stress distribution for models SE7 A, B and C (D= 7cm) with aspect ratios 3, 4, and 5

4.4.3 Discussion

Based on the hoop stress distribution in the walls of the models with increasing aspect ratios shown in Figures 4-10, 4-11 and 4-12, with aneurysm diameters of 4, 5, and 7 cm respectively, two important changes can be observed. Firstly, the value of maximum stress in the aneurysm wall increases with the increase in aspect ratio, and secondly the location of the maximum stress moves from the aneurysm ends, towards the middle of the aneurysm as the aspect ratio increases.

In models with diameters of 4 and 5 cm, the peak stress locations shifted from the sides to the middle of the aneurysm, between aspect ratio 3 to 4, while for model SE7-B, with a diameter of 7 cm and aspect ratio of 4, the peak stress was found in both the sides and the middle; it was only concentrated in the middle at an aspect ratio of 5. These findings suggest that there is an aspect ratio threshold when the maximum hoop stress shifts from the two sides to the middle and this threshold depends on diameter.

To identify the location of the critical aspect ratio with respect to the position of maximum hoop stress, further investigation has been carried out by generating extra models with aspect ratios of 3.25, 3.5 and 3.75. These values were chosen as they have more data points between the two critical values found from Figures 4-10, 4-11 and 4-12.

The variation of maximum hoop stress is plotted for different diameters and aspect ratios in Figure 4-13. The figure shows that the maximum stress value increases by 25% between aspect ratios 3 and 4 in models with diameters of 4 and 5 cm, while for the same models it increased by less than 10% when the aspect ratio changed from 4 to 5. In models of 7 cm diameter, the largest change occurred between aspect ratio 4 to 5 (20%), rather than between aspect ratio 3 to 4, similarly to the other two models, where the change was found to be less than 10%.

The location of maximum hoop stress occurs at the two sides for smaller aspect ratio models and then shifts to the middle. In Figure 4-13 it is identified by the sign (⬭) when it shifts from the sides to the middle.

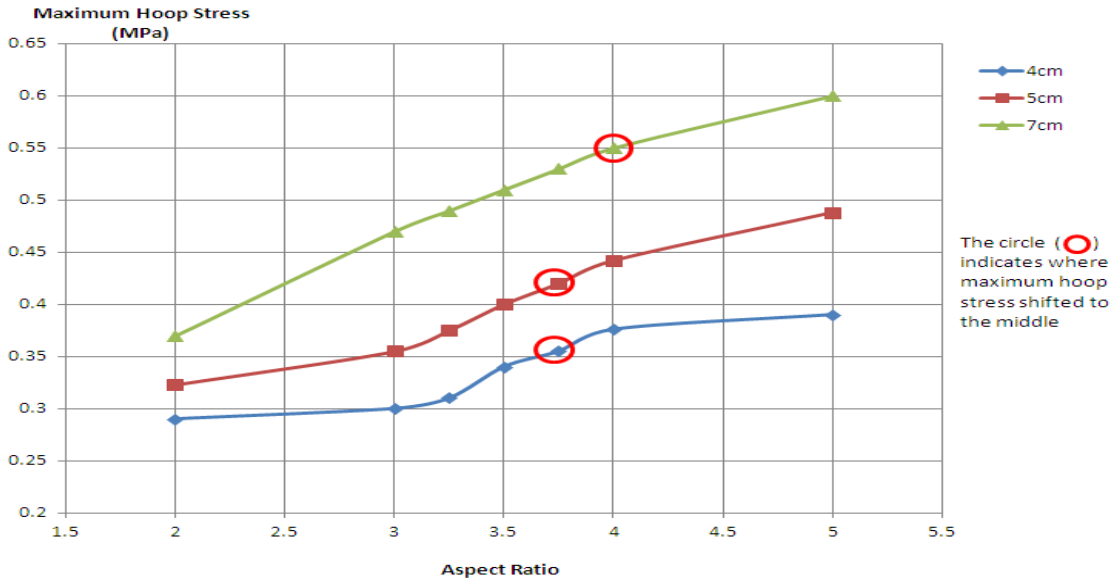

Figure 4-13a: Graph showing the relationship between aspect ratios from 2 – 5 and maximum hoop stress on the wall for the three diameters of 4, 5 and 7 cm.

In Figure 4-13a it is noted that the maximum hoop stress increases when the aspect ratio increases, but the relationship is not linear. The relationship between the maximum hoop stress and aspect ratio that can be described as follows:

$$\sigma = a + b\,(AR) + c\,(AR)^2 \qquad \text{Eq. (4.1)}$$

where:σ = maximum hoop stress for specific shape and diameter, AR = aspect ratio for the specific aneurysm, and a, b and c are the parameters that can be calculated from each curve in Figure 4-13a, so that the equations are found to be:

for diameter 4 cm: $\sigma = 2.22 \times 10^{-1} + 2.59 \times 10^{-2}\,AR + 1.84 \times 10^{-3}\,AR^2$

for diameter 5 cm: $\sigma = 2.32 \times 10^{-1} + 3.58 \times 10^{-2}\,AR + 3.30 \times 10^{-3}\,AR^2$

for diameter 7 cm: $\sigma = 9.87 \times 10^{-2} + 1.58 \times 10^{-1}\,AR - 1.16 \times 10^{-2}\,AR^2$

Solving for the variation of each parameter as a function of diameter, D, then provides the following equations:

$$a = -3.52 \times 10^{-1} + 2.47 \times 10^{-1}\,D - 2.62 \times 10^{-2}\,D^2 \qquad \text{Eq. (4.2)}$$

$$b = 3.32 \times 10^{-1} - 1.46 \times 10^{-1}\,D + 1.73 \times 10^{-2}\,D^2 \qquad \text{Eq. (4.3)}$$

$$c = -6.38 \times 10^{-2} + 2.83 \times 10^{-2}\,D - 2.98 \times 10^{-3}\,D^2 \qquad \text{Eq. (4.4)}$$

Using equations (4.1 - 4.4) it is then possible to predict the value for maximum stress at any given aspect ratio within the curve. Figure 4-13a is reproduced using the above

equations for any diameter with exponential shape as shown in Figure 4-13b. This could be used in clinical practice to provide an indicator of maximum stress value for specific shape.

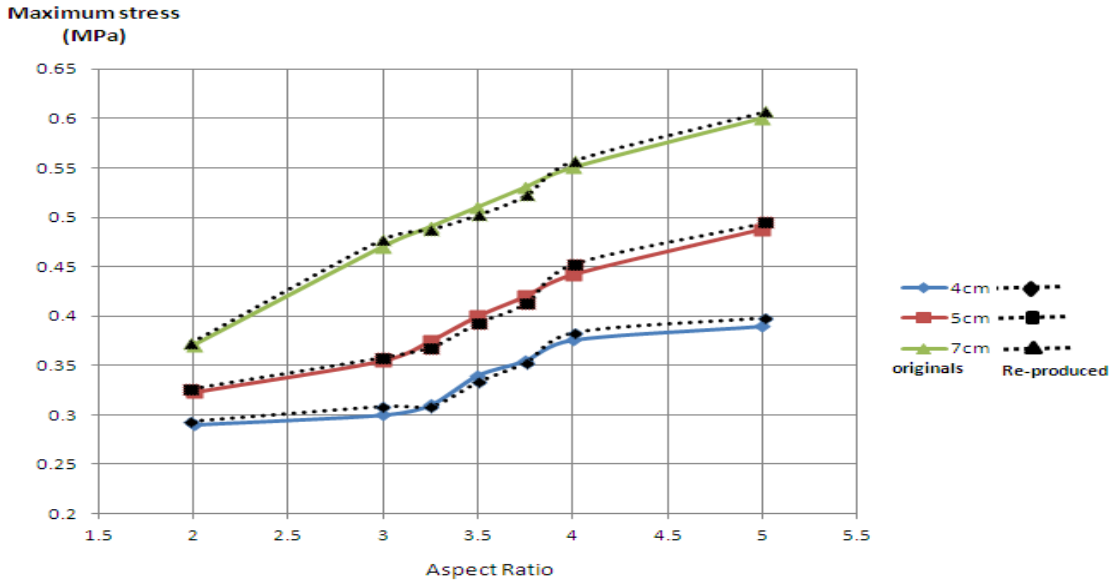

Figure 4-13b: Data points are showing the expected stress for any diameter using equations (4.1 - 4.4) reproduced from figure 4-13a.

It is also noted from Figure 4-13a that maximum hoop stress shifted from the two sides to the middle for models with 4 cm diameter at an aspect ratio of 3.5, while for models with 5 cm diameter the shift occurs at 3.75 and for models with 7 cm diameter the shift occurs at aspect ratio of 4.25; hence it could be concluded that there is a threshold at which the maximum hoop stress shifted and this threshold could be calculated with the combination of aspect ratio and diameter plus the expected effect of wall curvature. This could also be used in clinical practice to provide an indicator of maximum stress location for specific shape.

Of course, aneurysm shape and hence the slope and curvature of the aneurysm may affect the relationship between aspect ratio, diameter, and maximum hoop stress location. In the next section, studies of different aneurysm shapes have been carried out for more understanding of this effect.

4.4.4 Verifying the effect of the aspect ratio using different shapes.

In this section, further investigation on the effect of aspect ratio is carried out by studying other aneurysm shapes.

4.4.4.1 Cosine-exponential aneurysm shape.

Cosine-exponential aneurysm shape is another popular shape for investigating AAA and has been used in a number of studies (Elger et al., 1996; Scotti et al.,2005).

4.4.4.1.1 Method

Three models with different maximum diameters and aspect ratios of 3, 4 and 5 were used to give a total of nine models, SC4 (A, B and C), SC5 (A, B and C) and SC7 (A, B and C) from Table 3-1 in Chapter 3. The aneurysm diameter D was varied between 4, 5, and 7cm. The methodology and all boundary conditions were the same as those described earlier in section 3.1.2 with wall thickness of 1 mm and internal pressure of 120 mmHg.

4.4.4.1.2 Results

Figure 4-14 shows the hoop stress distribution in model SC4 with a diameter of 4 cm but with different aspect ratios. The maximum hoop stress value increases as the aspect ratio increases, with peak stress increasing from 26×10^{-2} MPa (with aspect ratio = 3) to 34×10^{-2} MPa and 35×10^{-2} MPa for aspect ratios 4 and 5 respectively. It can also be seen that maximum hoop stress was distributed between the two ends of the aneurysm and along the curvature but not exactly in the middle at the aspect ratio of 3; the maximum hoop stress then shifted to the middle of the aneurysm when the aspect ratio was increased to 4. The location of maximum stress at aspect ratio 5 is also in the middle of the aneurysm with a small increase in the value.

Figure 4-15 illustrates the hoop stresses in models SC5, showing that maximum hoop stress increased from 0.32 MPa to 0.40 MPa when the aspect ratio increased from 3 to 4 then to 0.45 MPa when the aspect ratio increased to 5. The maximum hoop stress is located at the two sides for aspect ratios 3 and 4. The location of maximum stress shifts from the aneurysm ends to the middle by increasing the aspect ratio from 4 to 5.

Model SC7 in Figure 4-16 with a 7 cm diameter has a maximum hoop stress of 0.43 MPa with an aspect ratio of 3, increasing to 0.46 MPa with an aspect ratio 4, then to 0.56 when the aspect ratio increased to 5. The location of maximum stress was at the ends of the aneurysm at aspect ratio 3 and was then located in two positions, at the middle and at the ends of the aneurysm at an aspect ratio of 4; it was then concentrated in the middle at aspect ratio 5.

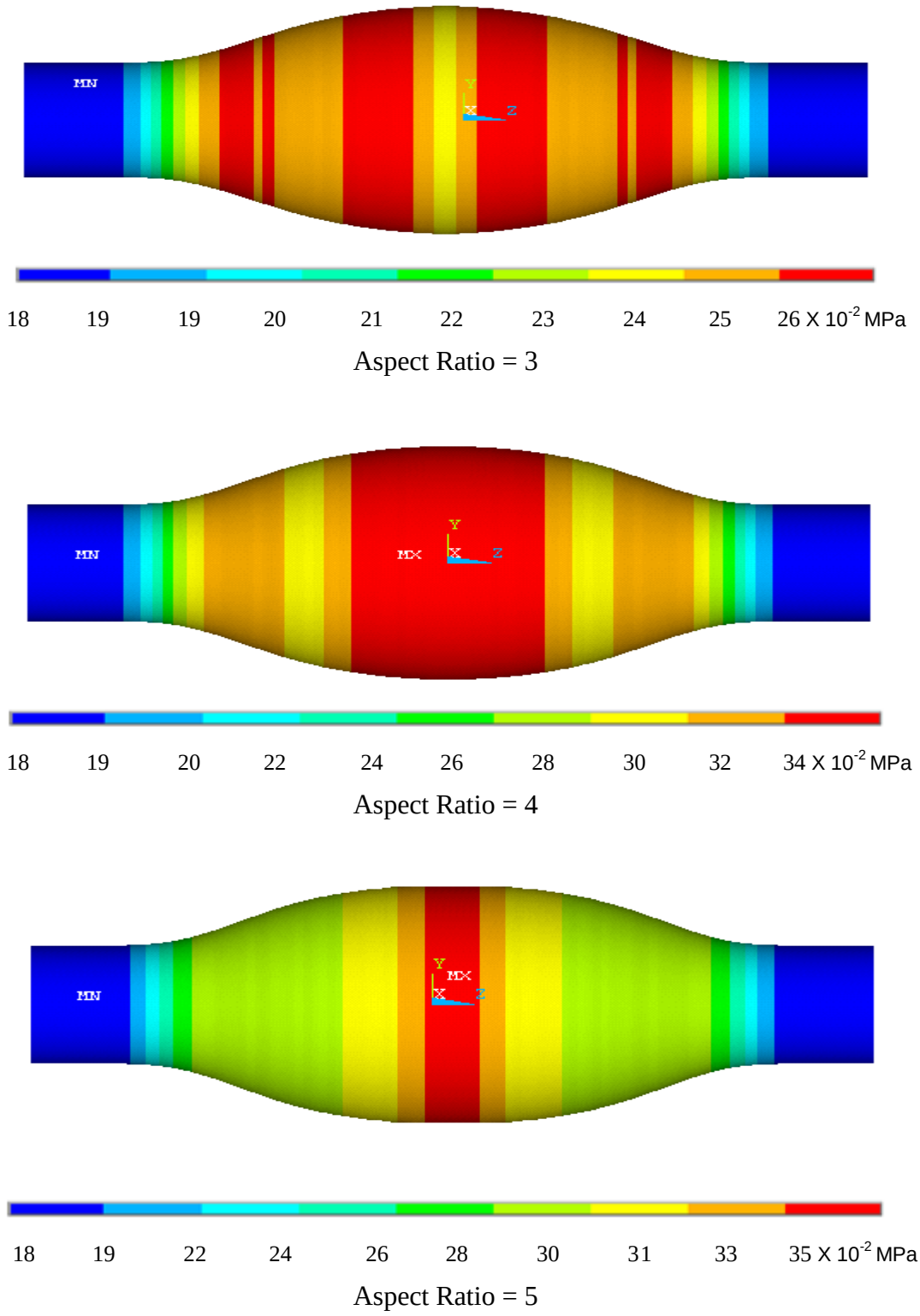

Figure 4-14: Hoop stress distribution for models SC4 A, B and C (D= 4cm) with aspect ratios 3, 4, and 5

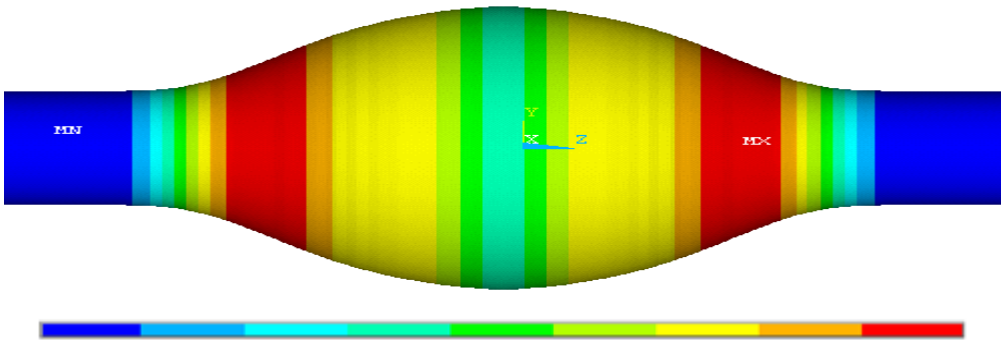

Aspect Ratio = 3

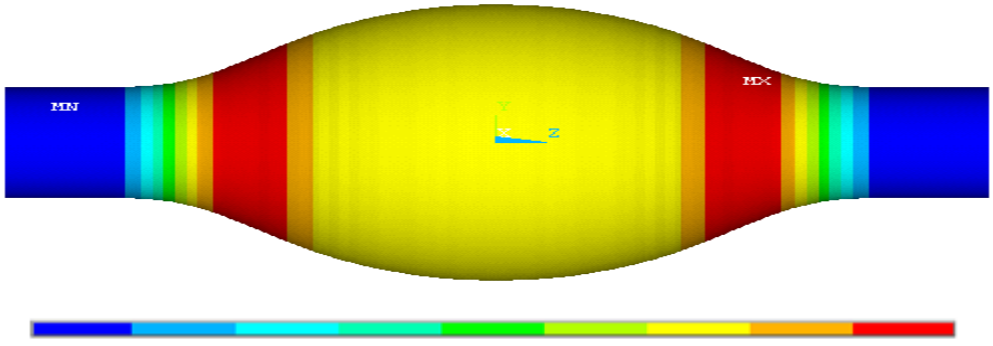

Aspect Ratio = 4

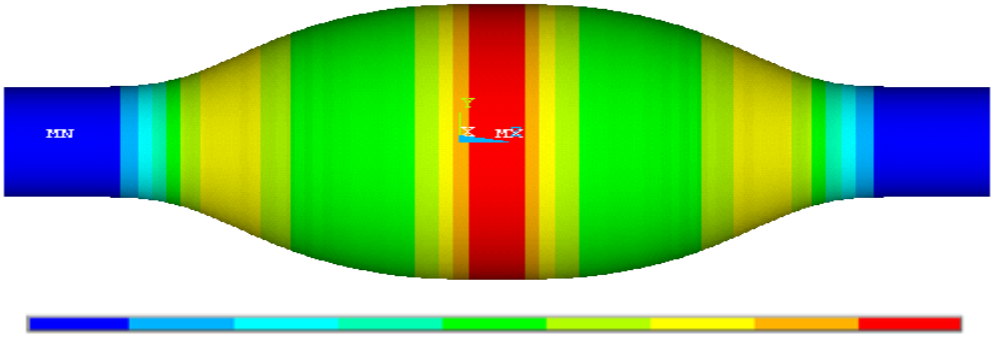

Aspect Ratio = 5

Figure 15-4: Hoop stress distribution for models SC5 A, B and C (D= 5cm) with aspect ratios 3, 4, and 5

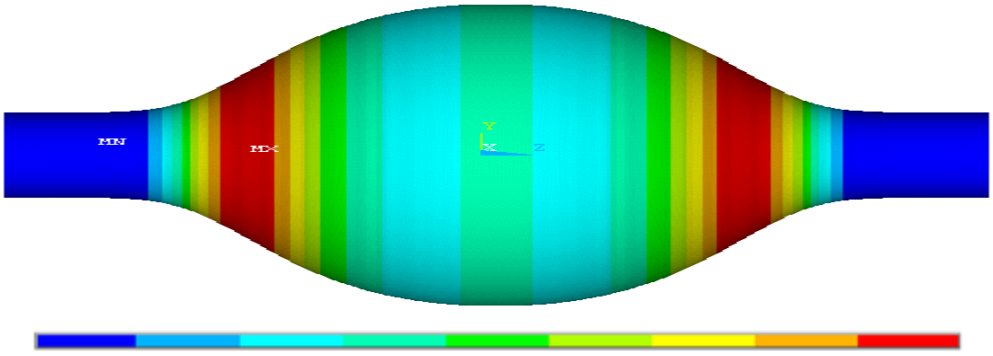

18 20 23 27 30 33 37 39 41 43 X 10^{-2} MPa

Aspect Ratio = 3

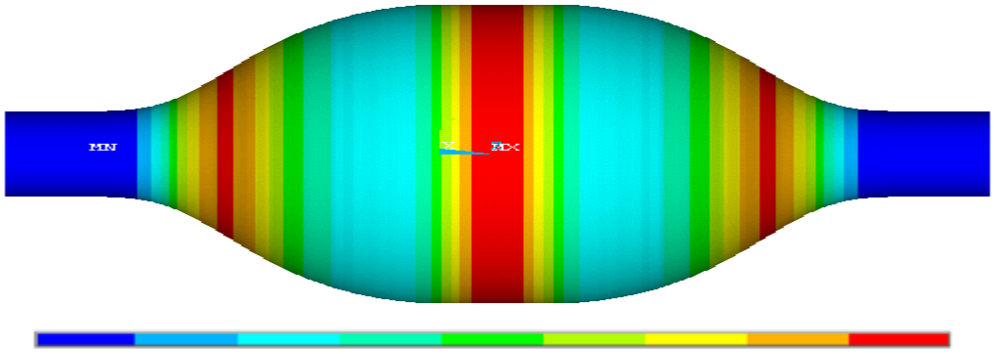

18 21 24 28 32 35 39 41 44 46 X 10^{-2} MPa

Aspect Ratio = 4

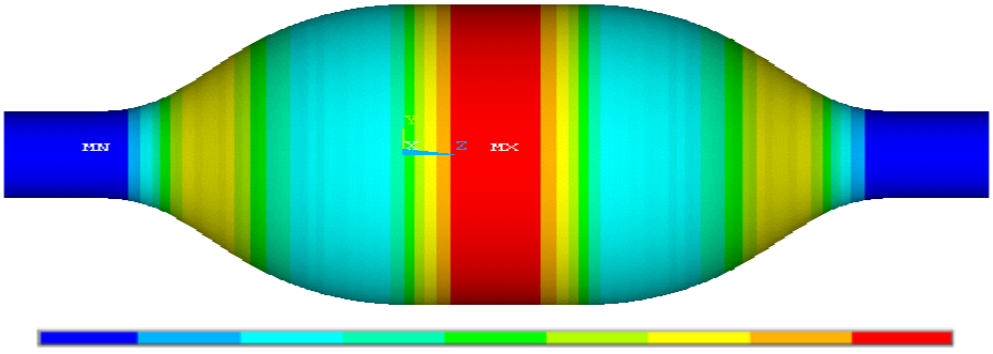

18 23 26 31 37 42 48 51 54 56 X 10^{-2} MPa

Aspect Ratio = 5

Figure 4-16: Hoop stress distribution for models SC7 A, B and C (D= 7cm) with aspect ratios 3, 4, and 5

4.4.4.2 Parabola-exponential aneurysm shape.

The parabola-exponential aneurysm shape is another popular shape for investigating AAA and has been taken from Elger et al, (1996).

Method.

Three models with different maximum diameters and aspect ratios of 3, 4 and 5 were used to give a total of nine models SP4 (A, B and C), SP5 (A, B and C) and SP7 (A, B and C) from Table 3-1 in Chapter 3. The aneurysm diameter D was varied between 4, 5, and 7cm. The methodology and all boundary conditions were the same as described earlier in section 3.1.2 with a wall thickness of 1 mm and internal pressure of 120 mmHg.

Results

Figure 4-17 shows the hoop stress distribution in model SP4 with a diameter of 4 cm with different aspect ratios. It can be noticed that maximum stress value increases as the aspect ratio increases, with peak stress increasing from 26×10^{-2} MPa (with aspect ratio of 3) to 30×10^{-2} MPa and 33×10^{-2} MPa for aspect ratios of 4 and 5 respectively. It can also be seen that maximum hoop stress was distributed between the two ends of the aneurysm and along the curvature but not exactly in the middle at an aspect ratio of 3 and the maximum then shifted to the middle of the aneurysm when the aspect ratio was increased to 4. The location of maximum stress at aspect ratio 5 is also in the middle with a small increase in value.

Figure 4-18 illustrates the hoop stresses in model SP5, showing that maximum hoop stress increased from 0.32 MPa to 0.33 MPa when the aspect ratio increased from 3 to 4 then to 0.38 when the aspect ratio increased to 5. At an aspect ratio of 3 the location of maximum hoop stress is found at the two ends of the aneurysm and was then distributed between the two ends and the middle at an aspect ratio 4. Maximum hoop stress then shifts to the middle by increasing the aspect ratio from 4 to 5.

Model SP7 in Figure 4-19 with a diameter of 7 cm have a maximum hoop stress of 0.45 MPa with an aspect ratio of 3 increasing to 0.49 MPa with an aspect ratio of 4 then to 0.59 when the aspect ratio increased to 5. The location of maximum stress was at the ends of the aneurysm at an aspect ratio 3, and was then located in two positions

at the middle and the ends of the aneurysm at an aspect ratio of 4; it was then concentrated in the middle at an aspect ratio of 5.

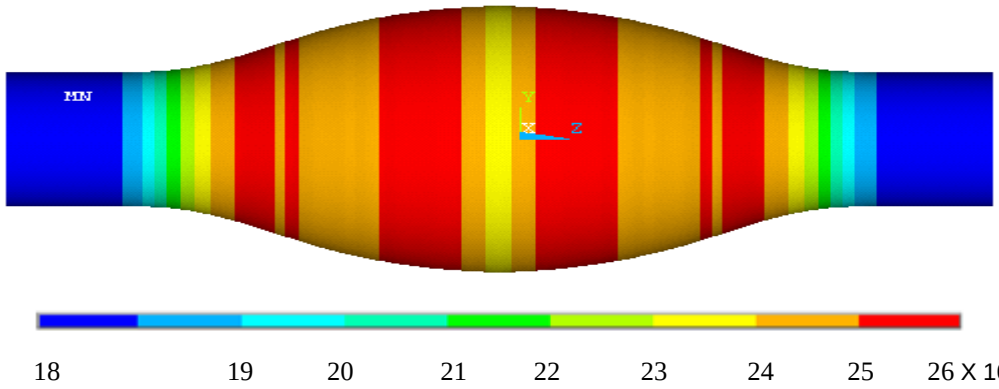

18 19 20 21 22 23 24 25 26 X 10^{-2} MPa

Aspect Ratio = 3

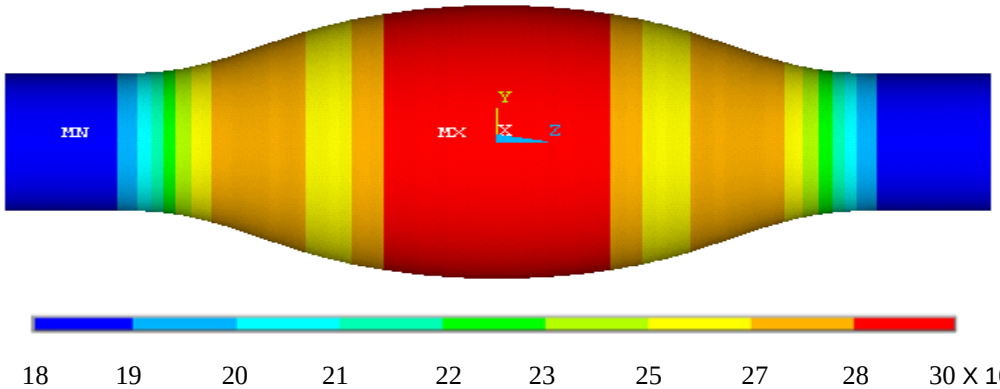

18 19 20 21 22 23 25 27 28 30 X 10^{-2} MPa

Aspect Ratio = 4

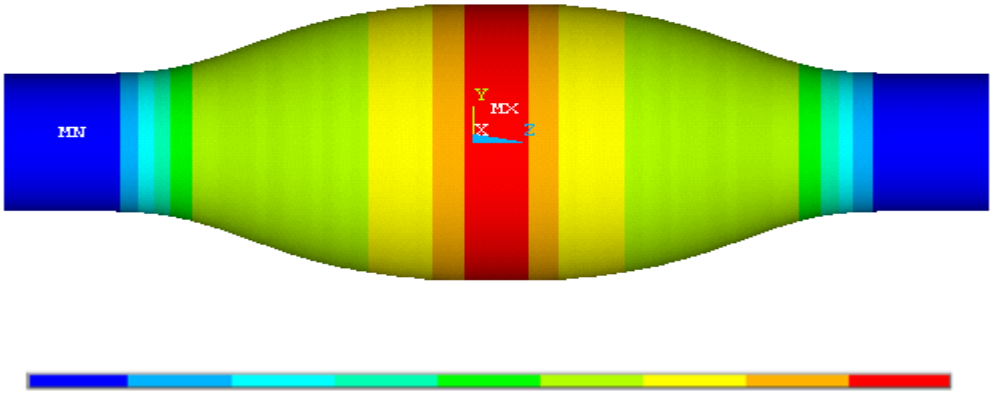

18 20 22 23 24 25 27 29 31 33 X 10^{-2} MPa

Aspect Ratio = 5

Figure 4-17: Hoop stress distribution for models SP4 A, B and C (D= 4cm) with aspect ratios 3, 4, and 5

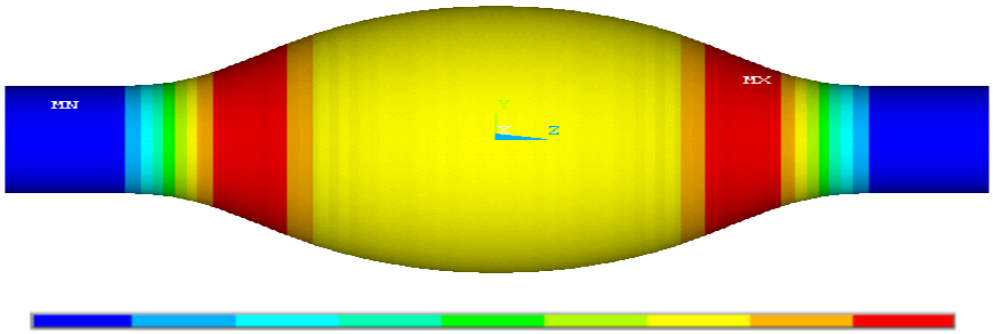

Aspect Ratio = 3

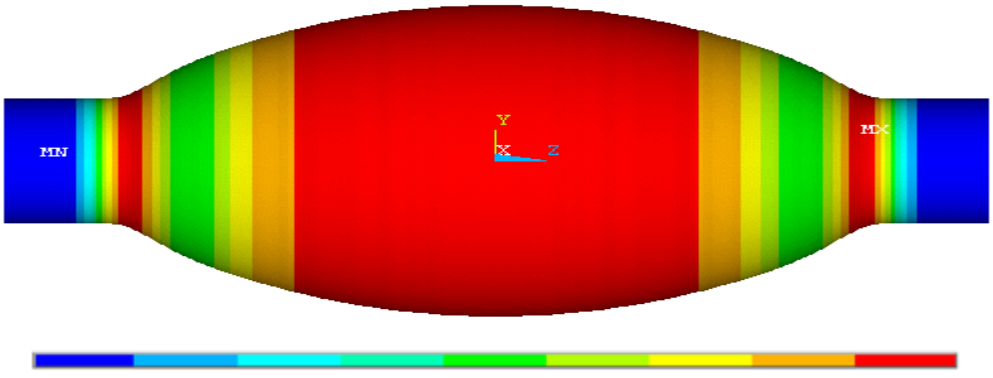

Aspect Ratio = 4

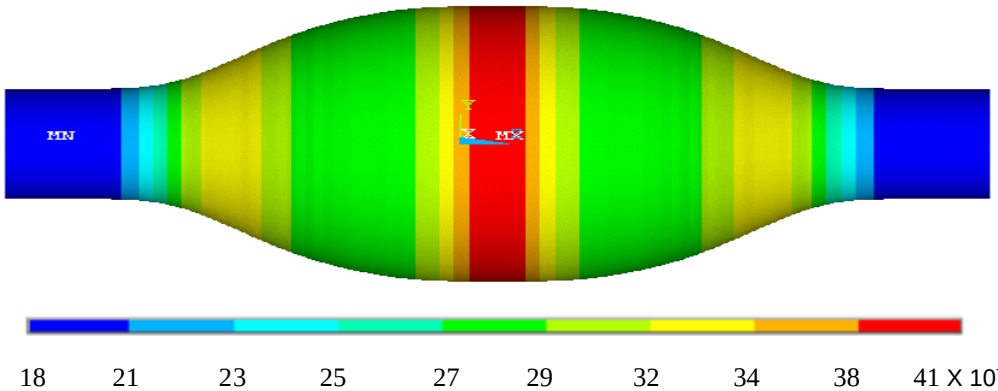

Aspect Ratio = 5

Figure 18-4: Hoop stress distribution for models SP5 A, B and C (D= 5cm) with aspect ratios 3, 4, and 5

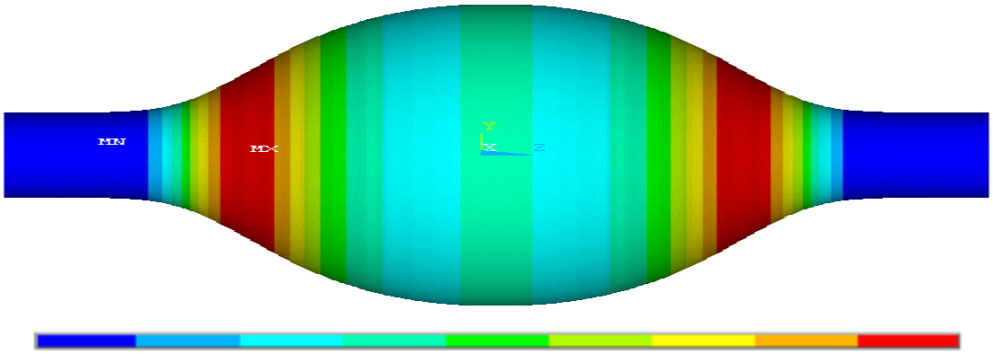

18 20 23 27 30 33 37 40 43 45 X 10^{-2} MPa

Aspect Ratio = 3

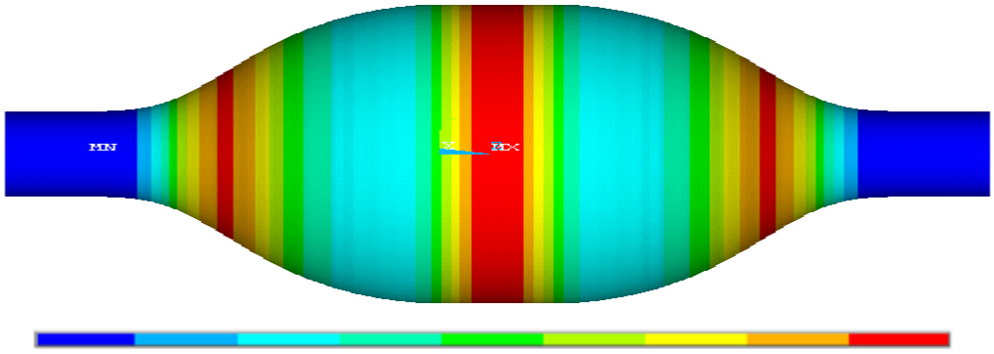

18 21 24 28 32 35 39 43 46 49 X 10^{-2} MPa

Aspect Ratio = 4

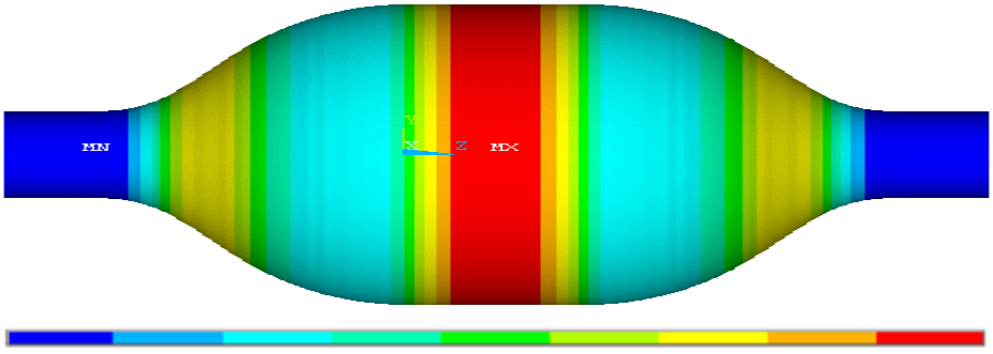

18 23 26 31 37 42 48 54 57 59 X 10^{-2} MPa

Aspect Ratio = 5

Figure 4-19: Hoop stress distribution for models SP7 A, B and C (D= 7cm) with aspect ratios 3, 4, and 5

4.4.4.3 Discussion.

Based on the six models with the three different aspect ratios studied here, Figures 4-14 to 4-19 appear to show that the maximum hoop stress increases with the increase in aspect ratio and the location of the maximum stress moves towards the middle of the aneurysm as the aspect ratio increases. Both the cosine-exponential and parabola-exponential shapes behaved similarly to the exponential shape studied earlier and this supports that the findings discussed earlier is applied on other shapes of aneurysm.

To identify the location of the critical aspect ratio with respect to the position of maximum hoop stress, further investigation has been carried out by generating extra models with aspect ratios of 3.5 and 4.5. The variation of maximum hoop stress is plotted in Figure 4-20 for different diameters and aspect ratios.

In the four models of SC5, SP5, SC7 and SP7, the maximum hoop stress was located at the two sides of the aneurysm at an aspect ratio of 3 and it then shifted to the middle as the aspect ratio increased. For models SC4 and SP4 the maximum hoop stress was not concentrated at the two ends at aspect ratio of 3 but was rather distributed between the two ends and along the curvature of the aneurysm but not in the middle. The obvious justification of this observation is that for a small aneurysm with these shapes, there is no quick variation of the aneurysm curve compared to those with larger diameters.

Figure 4-20 shows that the maximum hoop stress increases when the aspect ratio increases but the relationship is not linear and the empirical relationship between maximum hoop stress and aspect ratio suggested in Eq. (4-1) could also be applied here.

In models with a diameter of 4 cm, the peak stress locations were concentrated in the middle of the aneurysm at an aspect ratio of 3.5, while for models with a diameter of 5 cm, the maximum hoop stress shifted from the two sides to the middle at an aspect ratio of 4.5 and for models with a diameter of 7 cm, the shift occurs at an aspect ratio of 5.

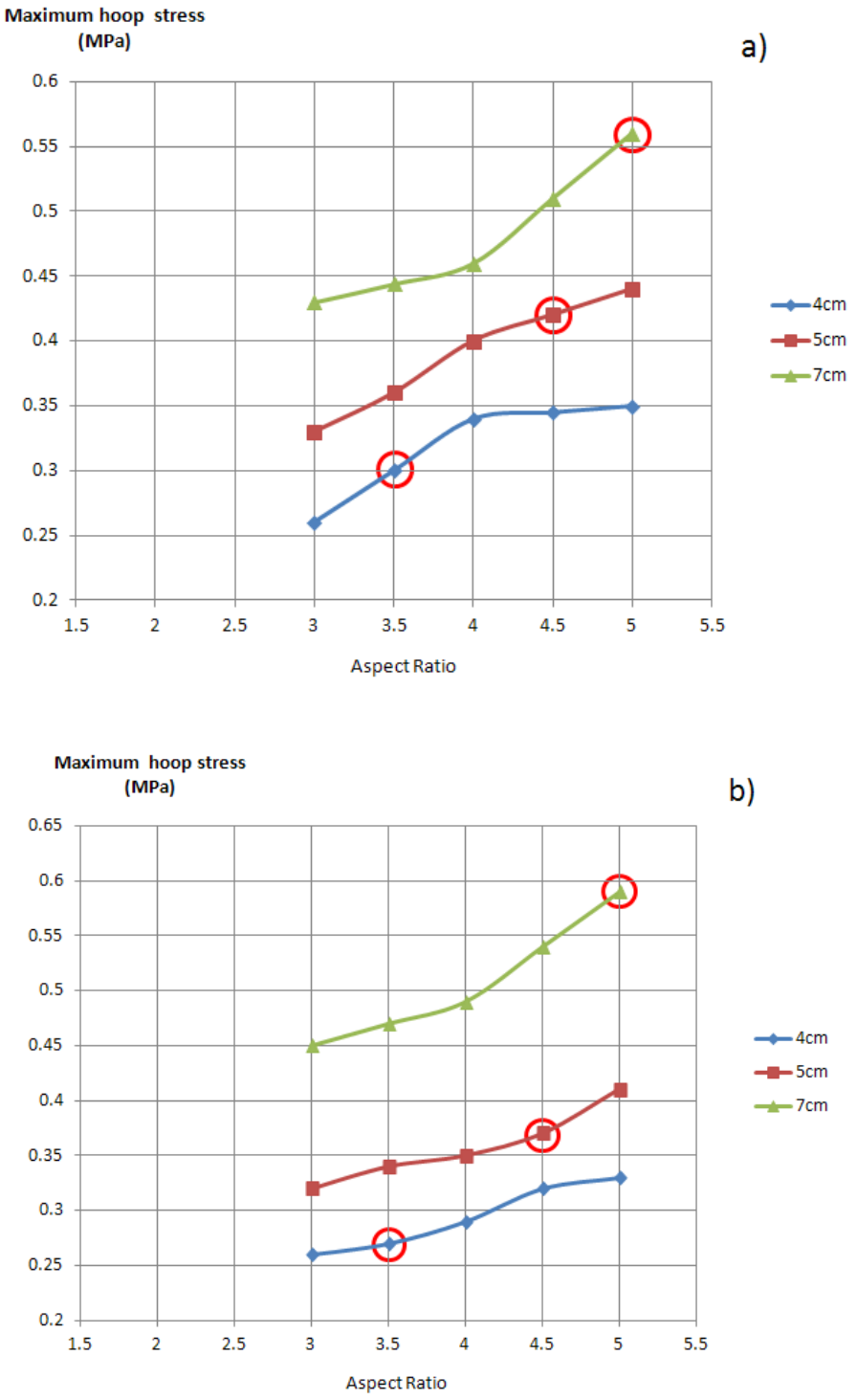

Figure 4-20: Graph showing the relationship between aspect ratio (from 3 – 5) and maximum hoop stress on the wall for a) Cosine-exponential shapes and b) Parabola-exponential shapes.

(The circle ( ) indicates where the maximum hoop stress has shifted to the middle)

This confirms the hypothesis that there is an aspect ratio threshold when the maximum hoop stress shifts from the two sides to the middle and this threshold depends on diameter.

Aspect ratio threshold was reported by Salsac et al. (2004) who carried out an experimental study using tomographic digital particle image velocimetry to examine the changes occurring during the progressive enlargement of AAA and a critical aneurysm aspect ratio was found, for which the flow change from laminar state to a turbulent state. This indicates that aspect ratio does not only change the wall stresses but also the blood flow behaviour inside aneurysm.

4.4.5 Engineering justifies aspect ratio effect

From an engineering point of view, the reason for this shift from the ends to the middle is that an aneurysm with a small aspect ratio becomes a spherical-like vessel, while with a large aspect ratio the aneurysm is more cylindrical in shape as shown in Figure 4-21. It is known that the stress in spherical vessels of thin walls is:

$$\sigma = pr/2t \qquad \text{(Eq 4.2)}$$

Where σ is the hoop and longitudinal stress, p is pressure, r is inner radius, t is wall thickness, for thin walled pressure vessels when $r/t \geq 10$ (Hibbeler, 2004).

On the other hand, the hoop stress in cylindrical vessels is:

$$\sigma = pr/t \qquad \text{(Eq 4.3)}$$

While the longitudinal stress remains the same in both shapes

$$\sigma = pr/2t \qquad \text{(Eq 4.4)}$$

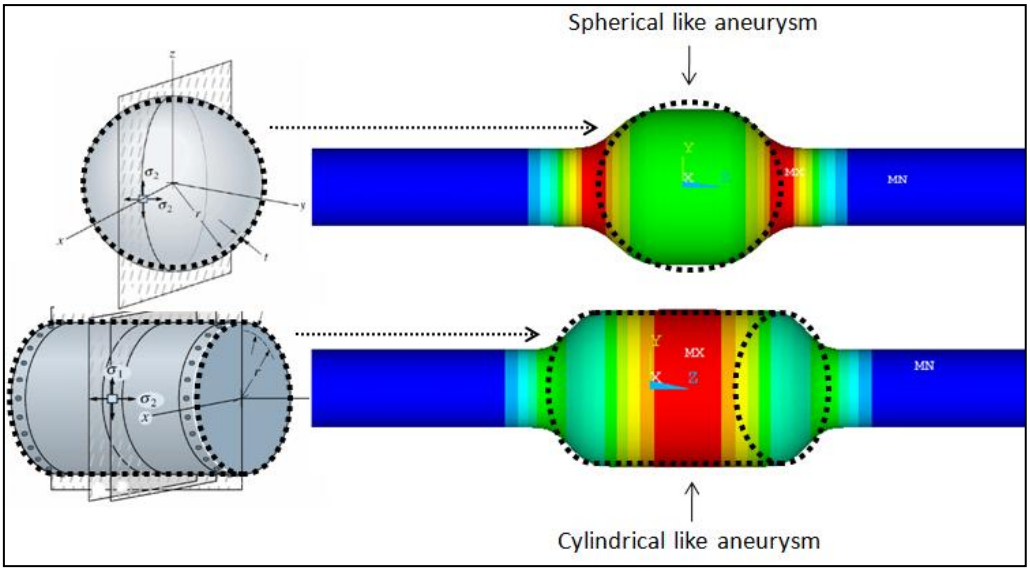

Figure 4-21: Aneurism shape changing from is spherical-like to cylindrical-like vessel which explains the reason for the changing position of the peak wall stress.

Thus, when the aneurysm changes from a spherical to a cylindrical shape, the hoop stress in the centre of the aneurysm body increase to nearly the double of its magnitude. For example; if the hoop stress at the two ends is 0.35 MPa and at the middle is 0.30 MPa when the aneurysm is spherical like shape (maximum hoop stress is located at the two ends), then when it change to cylindrical like shape, the hoop stress at the two ends will not change but the hoop stress in the middle may increase up to 0.6 MPa (maximum hoop stress is located in the middle).

4.4.6 Clinical application for these findings

Findings of this work can be used as a valuable indicator that aspect ratio adds to the value and location of the maximum wall stresses.

Figures 4-13 and 4-20 could be used to predict the value of maximum wall stresses contributed by the aspect ratio. This needs to be examined on patient specified models and it will be clinically valuable if the common shapes can be studied and a curve similar to those in Figures 4-13 and 4-20 needs to be plotted.

Figure 4-22 could be used to predict the location of maximum wall stresses based on the aspect ratio measured. This also needs to be examined on patient specified models

and it will be clinically valuable if the common shapes can be studied and a curve similar to those in Figure 4-22 can be plotted.

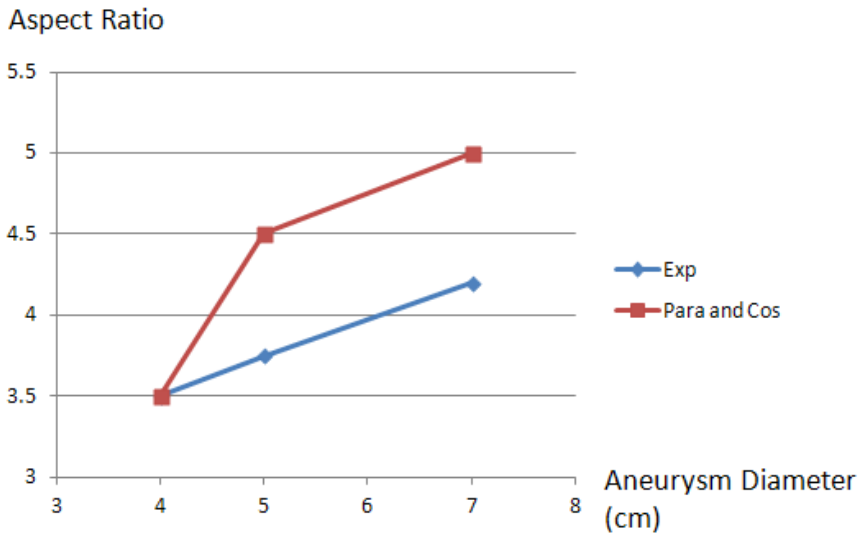

Figure 4-22: Relationship between critical aspect ratio and diameter (in cm) for different aneurysm shapes.

4.5 Summary

In this chapter, the effect of aneurysm shape was examined using four different shapes and it was found that even with the same diameter, the maximum wall stress differed. There was about a 40% difference between the shape with maximum wall stress and the shape with minimum wall stress, clearly indicating that aneurysm shape has a significant impact on wall stresses. It also showed that using the law of Laplace for AAA assessment is not accurate since only one of the four models followed the Laplace law.

The blood flow inside the different shapes and sizes of aneurysm was examined and two important results were found; first, the variation of blood pressure within the aneurysm caused by blood flow is very small and this variation will not affect results if wall stresses are required. Second, the blood dynamics inside the aneurysm, specifically the vortices, might play an important role in the formation of ILT and in the pathology of the AAA.

The aspect ratio of the aneurysm was extensively studied using 42 models (variety of shapes, diameters and aspect ratios) and it was found that the aspect ratio of the

aneurysm affects the value and the location of the maximum wall stress. It was suggested that a general clinical assessment scale be applied to enhance the assessment of AAA maximum wall stress value and location.

To the author's knowledge, this study is the first to examine the effect of the aspect ratio in the location and the magnitude of maximum stress in aneurysm wall and the findings are valuable and justified through engineering analysis. The effect of the aspect ratio could dramatically impact any future studies or clinical assessment of the aneurysm.

Chapter 5
The role of intraluminal thrombus

5.1 Introduction

As previously discussed in Chapter 2, the understanding of the role of the intraluminal thrombus (ILT) in AAA rupture is controversial. Some studies suggest that ILT increases the risk of rupture as it weakens the wall (Vorp et al., 2001) while other studies suggest that the presence of ILT may work as a cushion to the wall and decrease the risk of rupture (Wang et al., 2002). Other studies also suggest that it plays two roles of weakening the wall and decreasing stress on the wall, which results in no effect. In this chapter, the role of ILT presence will be investigated using different thicknesses, structure, and material properties to examine the hypothesis that the presence of ILT affects AAA wall stress magnitude and distribution. Non-complex shape models of AAA were analysed with thin and thick ILT compared to the same model without ILT to provide a clear understanding of the ILT in isolation of any other effects.

In the literature, the role of ILT within AAA has been examined using ILT with solid material; however, in reality ILT is a highly porous material with an average porosity of 80% (Ashton et al., 2009). It was assumed as a solid material simply for simplification purposes.

Only two recent numerical studies have examined the porosity of ILT using finite element models (Avinash et al., 2010; Polzer and Bursa, 2010) and provided useful information about the impact of thrombus porosity on AAA biomechanics. However, these two studies neglected the effect of blood being transmitted from the blood lumen to the porous material of ILT and the role this may play in AAA rupture.

In this chapter, the porosity of ILT will be examined using two models. Firstly, the finite element model is used to examine the pressure reduction by porous ILT and how this may affect the wall stresses and the computational fluid dynamics model which investigates how blood flows from the blood lumen to, and within, the

thrombus. This chapter will also examine how the information gained can be used to aid in AAA diagnosis and to determine the possible reasons for its growth.

This work is the first to examine the flow of blood in the 'blood lumen - thrombus interface- using porous media for the thrombus inside the aneurysm; the results may therefore contribute vital knowledge to the field.

5.2 Effect of ILT using different thicknesses

ILT with variable thicknesses will be used here to examine the effect of ILT on wall stresses compared with AAA without ILT.

5.2.1 Method

Five models from Table 3-1 were used (SENLT, SLT2.5, SLT5, SLT15 and SLTV). The dimensions of the models were the same but the thrombus thickness inside the aneurysm was varied. One of the models had no ILT (SENLT), while three of the models (SLT2.5, SLT5 and SLT15) had ILT with thicknesses of 2.5, 5, and 15 mm, respectively as shown in Figure 5-1. ILT thickness was uniform along the axial axis of these three models and non-uniform in one model (SLTV) to provide further understanding of the variation of the thickness within the same aneurysm. In model SLT15, the thickness was modelled to fill all aneurysm bulges, allowing only a blood lumen to be similar to the non-aneurysmal aorta.

The ILT was modelled as an incompressible, isotropic, homogeneous, linear elastic material with a Young's modulus E = 0.11 MPa and a Poisson's ratio $\mu = 0.45$. These values of E and U represent the population mean values obtained from uniaxial loading tests performed on ILT specimens harvested during AAA surgery by Di Martino et al. (1998). The effect of varying the material properties is examined later in this Chapter.

A homogeneous pressure of 145 mmHg was applied to the internal surface of the models, representing the peak systolic pressure of a 'normal' patient.

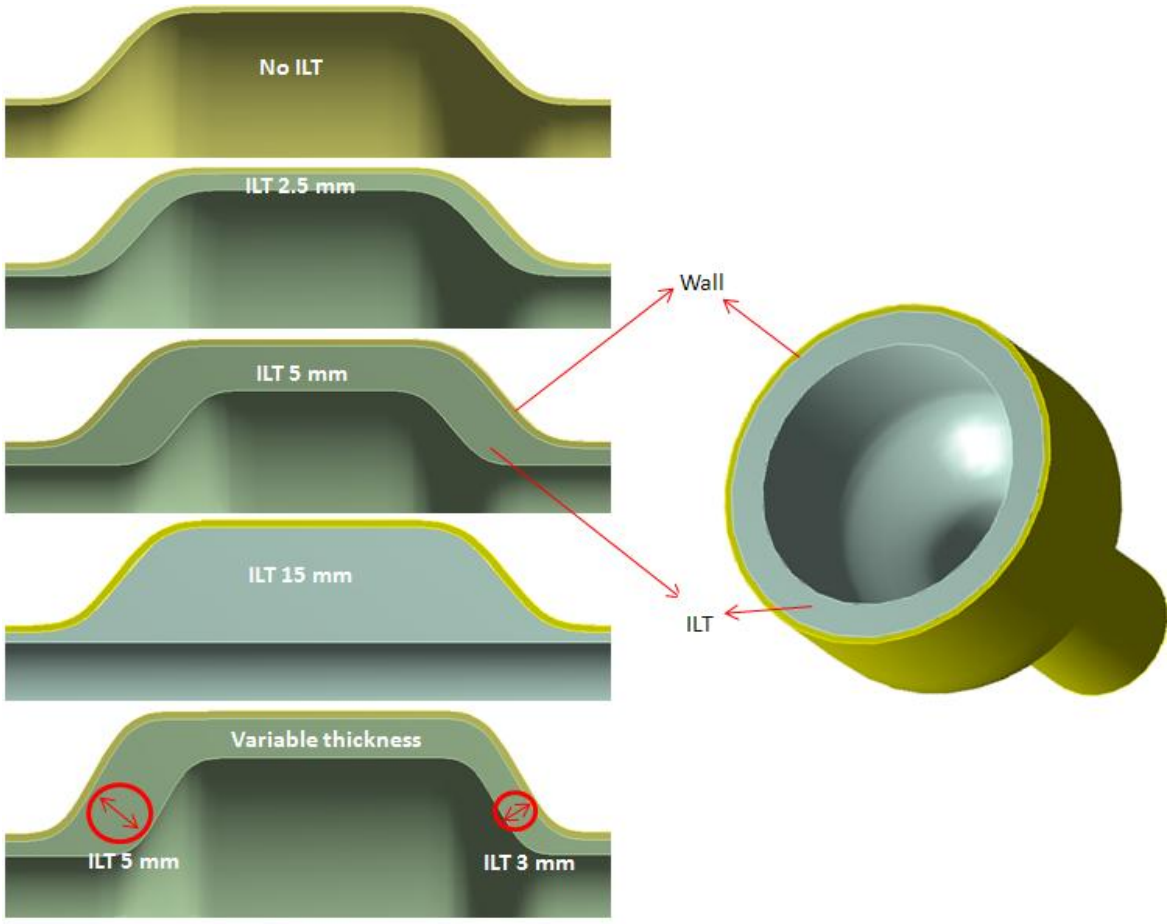

Figure 5-1: Models with different ILT thicknesses.

5.2.2 Results

The stress value is represented as Von Mises stress, which is a method used to combine the stresses in three-dimensions to calculate the failure criteria. Von Mises stress is widely used in the assessment of AAA stresses for most FEA studies to calculate the failure of the AAA wall.

Figure 5-2 illustrates the Von Mises stress distribution in the wall of the five models (with and without thrombus) obtained from static simulations of the peak systolic pressure. The most obvious detail is that stress is inversely proportional to the thickness. Model SENLT with no thrombus has a maximum stress value of 54×10^{-2} MPa, then peak stress decreases to 38×10^{-2} MPa, 31×10^{-2} MPa, and 22×10^{-2} MPa, with thicknesses of 2.5, 5 and 15 mm, respectively. Model SLTV with non-uniform ILT thickness shows higher stresses in the region with thinner thicknesses with a maximum value of 35×10^{-2} MPa.

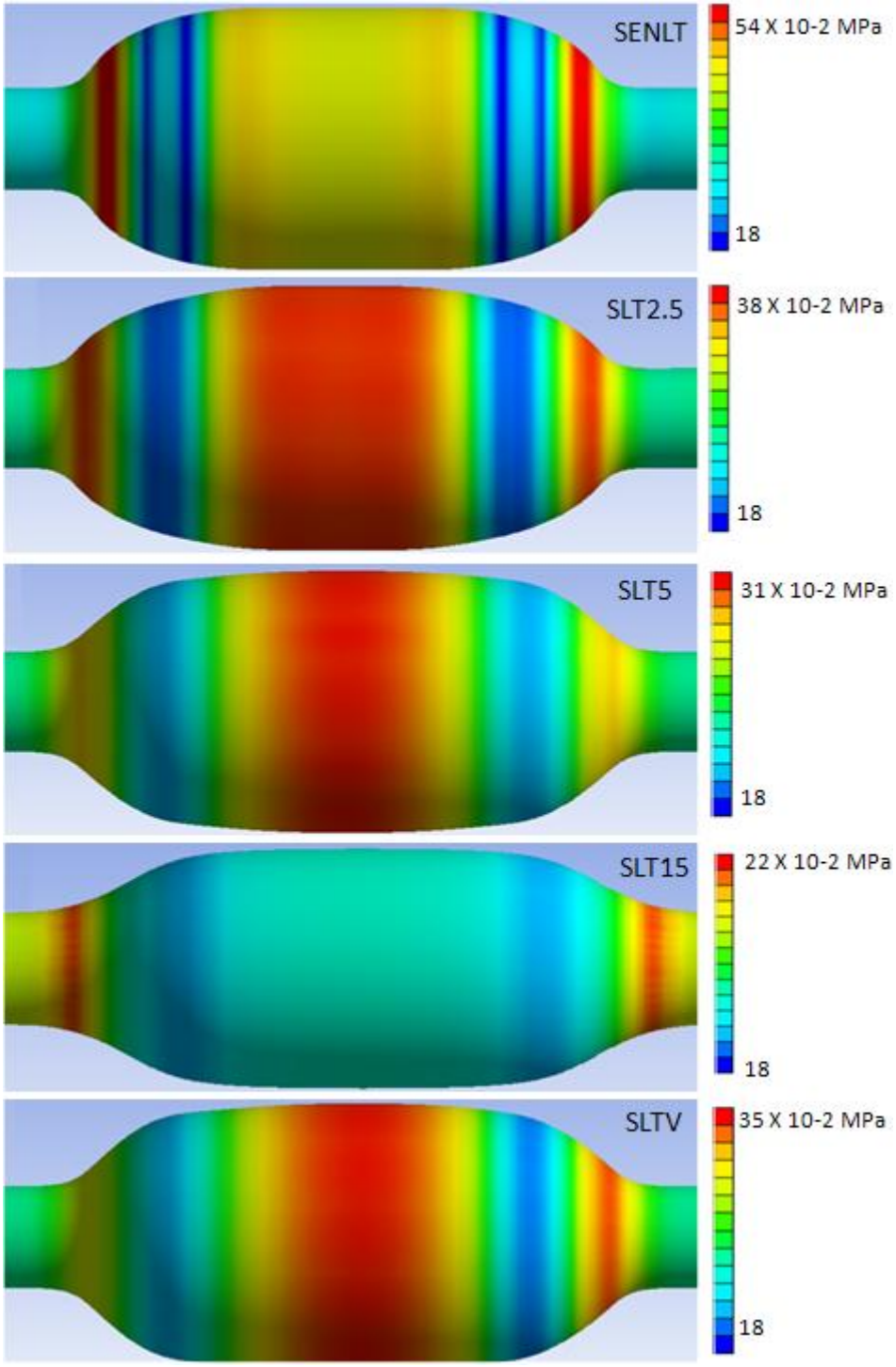

Figure 5-2: Von Mises stress distribution of the models (SENLT) without thrombus, SLT2.5 with 2.5 mm thickness thrombus, SLT5 with 5 mm thickness thrombus, SLT15 with 15 mm thickness thrombus and SLTV with non-uniform thickness thrombus.

5.2.3 Discussion

Based on the five models studied here, it appears from Figure 5-2 that the stresses drop by 30% in the presence of a 2.5 mm thrombus and by almost half in the presence of a 5.0 mm thrombus, then to 60% with a thrombus thickness of 15 mm, which demonstrates how the thrombus could act to lower stresses in the arterial wall. The results show there is an inverse relationship between thrombus thickness and maximum stress on the wall as can be seen in Figure 5-3. The results also show that the presence of thrombus changes the distribution of maximum stresses as shown in Figure 5-2. In the model in which ILT thickness was not uniform, the stress was found to be higher in regions with a thin layer of thrombus compared to regions with thick layers of thrombus.

Thus, these findings support the results of Wang et al. (2002) and Polzer and Bursa (2010) that suggest that thrombus reduces AAA wall stress and as a result play a positive role in supporting the wall and decreasing the chance of AAA rupture, while the effect is linearly related to the relative thrombus volume. However, this contradicts the clinical observation of Schurink et al. (2000) who concluded that the thrombus may increase the chance of AAA rupture.

The conclusion of the work undertaken here is that from a mechanical point of view, the thrombus clearly works as a cushion to protect the AAA wall. However, no information here about the biological role of ILT on the pathology of the wall and more research is required that examines the links between the mechanical and biological factors to understand the role of the thrombus within AAA. Later in this chapter, attempts will be made to understand how blood moves inside the ILT using porous ILT material has been carried out to provide more understanding of the possible mechanical and biological role of ILT within AAA.

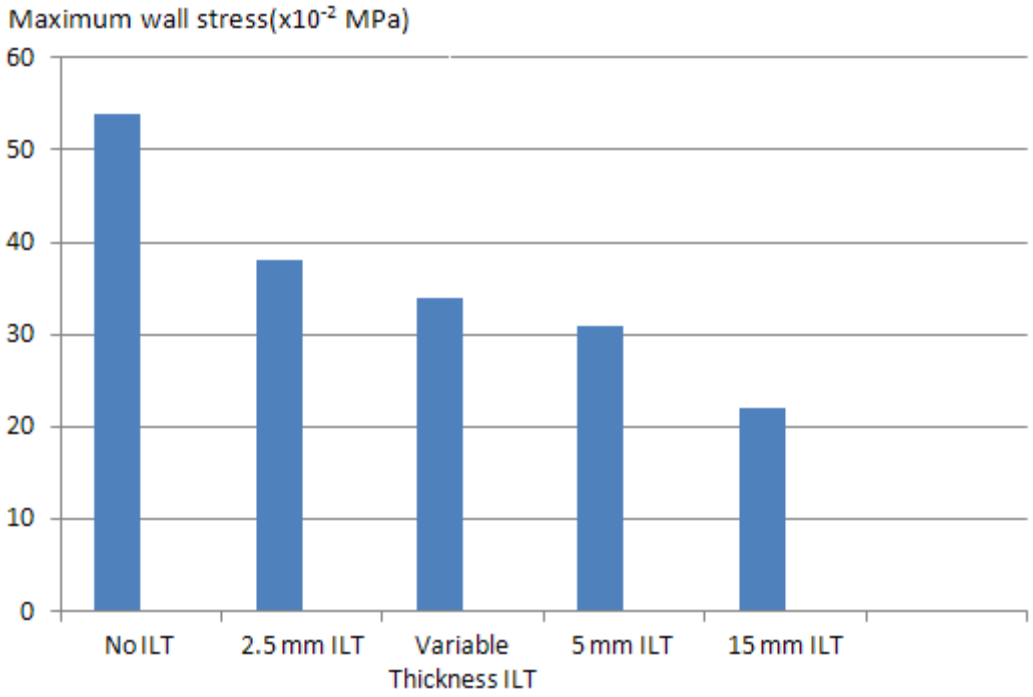

Figure 5-3: Maximum wall stress showing inverse relationship to ILT thickness.

5.3 More realistic ILT with three layers of different material properties

In the work carried out thus far, ILT was modelled as one homogenous material; however, in reality ILT consists of three layers, as discussed in Chapter 2 and each layer has different material properties.

In a recent numerical study of ILT, Meyar et al. (2010) recommended that modelling ILT could be improved if the three layers of ILT differed in luminal versus medial versus abluminal thrombus.

In this section, the advantages of using three layers with different material properties for each layer of ILT will be examined to measure the effect of ILT on wall stresses.

5.3.1 Method

The two models, SLT7 and SLT15, shown in Table 3-1 were used to model the inhomogeneous ILT using three deferent layers of ILT (abluminal, medial and luminal) as shown in Figure 5-4 in order to be able to assign different material properties for each layer. The thickness of the first, second and third layers on the SLT7 model are 2.5, 2.25 and 2.25 mm respectively (total thickness of ILT = 7 mm).

The first, second and third layers on the SLT15 model are all 5 mm thick (total thickness of ILT = 15 mm).

The values of Young's modulus of each layer were taken from Ashton et al.'s (2009) experimental measurements, in which it was reported that the abluminal layer (Young's modulus = 0.193 MPa) is stiffer than the medial (Young's modulus = 0.0249 MPa) and luminal (Young's modulus = 0.0154 MPa) layers. The Poisson's ratio (μ) for the three layers was 0.45.

To enable the comparison with homogenous ILT, two other models with equivalent ILT thicknesses (7 and 15 mm) were used, but the material properties of ILT did not vary. ILT here was modelled as an incompressible, isotropic, homogeneous, linear elastic material with an average Young's modulus E of 0.0777 MPa and a Poisson's ratio (μ) of 0.45.

A homogeneous pressure of 145 mmHg was applied to the internal surface of the four models, representing the peak systolic pressure of a 'normal' patient.

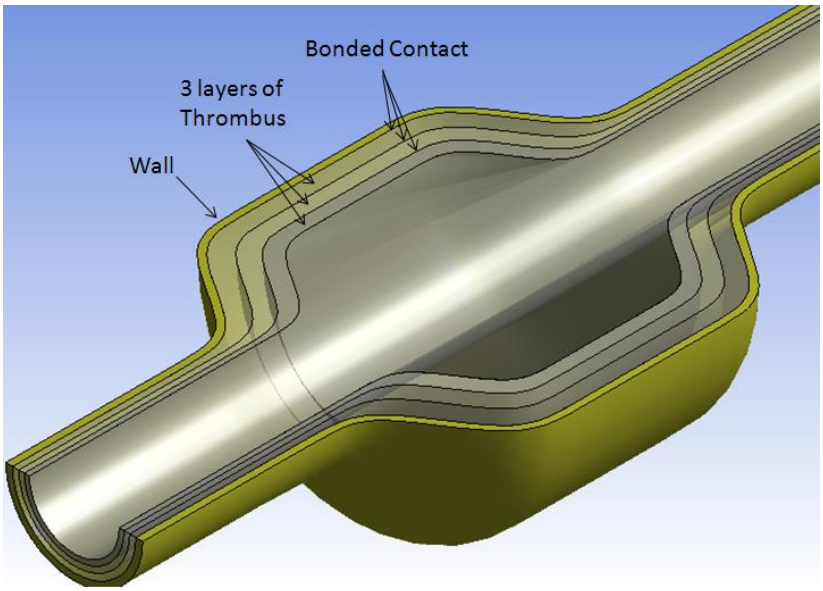

Figure **Error! No text of specified style in document.**5-4: Three layer thrombus model.

5.3.2 Results

Figure 5-5 illustrates the Von Mises stress distribution in the wall of the two 7 mm ILT thickness models (homogeneous and inhomogeneous ILT) obtained from static

simulations of the peak systolic pressure. The maximum wall stress in the homogeneous and inhomogeneous ILT models are 30×10^{-2} MPa and 28×10^{-2} MPa respectively. The maximum wall stress location and the stress variation along the wall are similar in the two models.

Figure 5-6 illustrates the Von Mises stress distribution in the wall of the two 15 mm ILT thickness models (homogeneous and inhomogeneous ILT) obtained from static simulations of the peak systolic pressure. The maximum wall stress in the homogeneous and inhomogeneous ILT models are 25×10^{-2} MPa and 22×10^{-2} MPa respectively. The maximum wall stress location and the stress variation along the wall are similar in the two models.

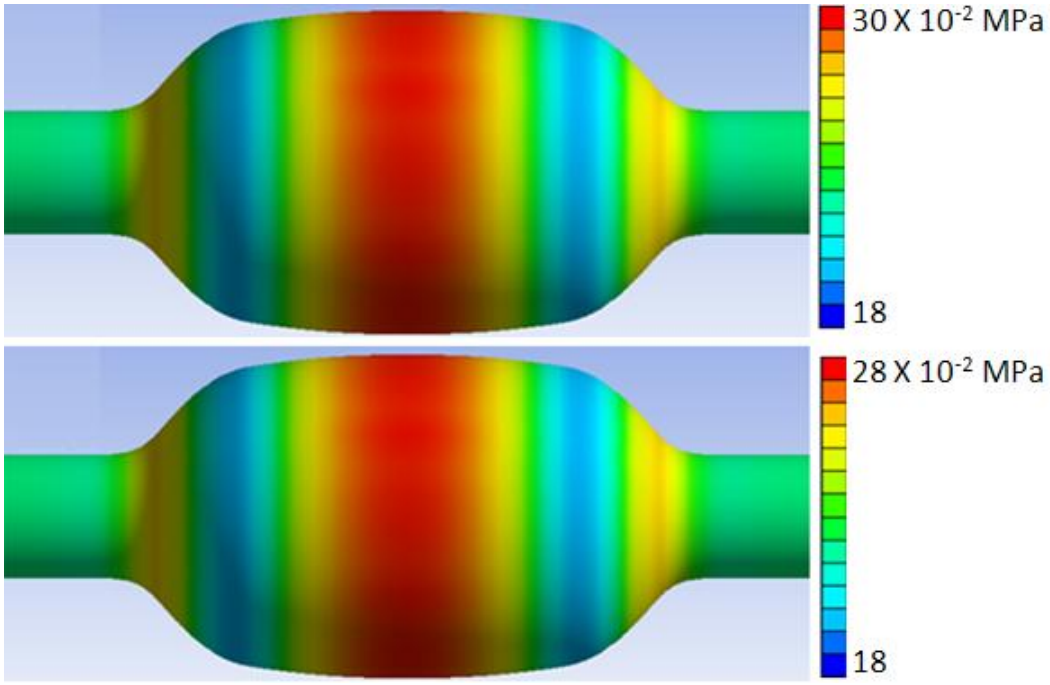

Figure 5-5: Von Mises stress distribution of homogeneous (bottom) and inhomogeneous ILT (top) for model SLT7 with 7 mm ILT thickness.

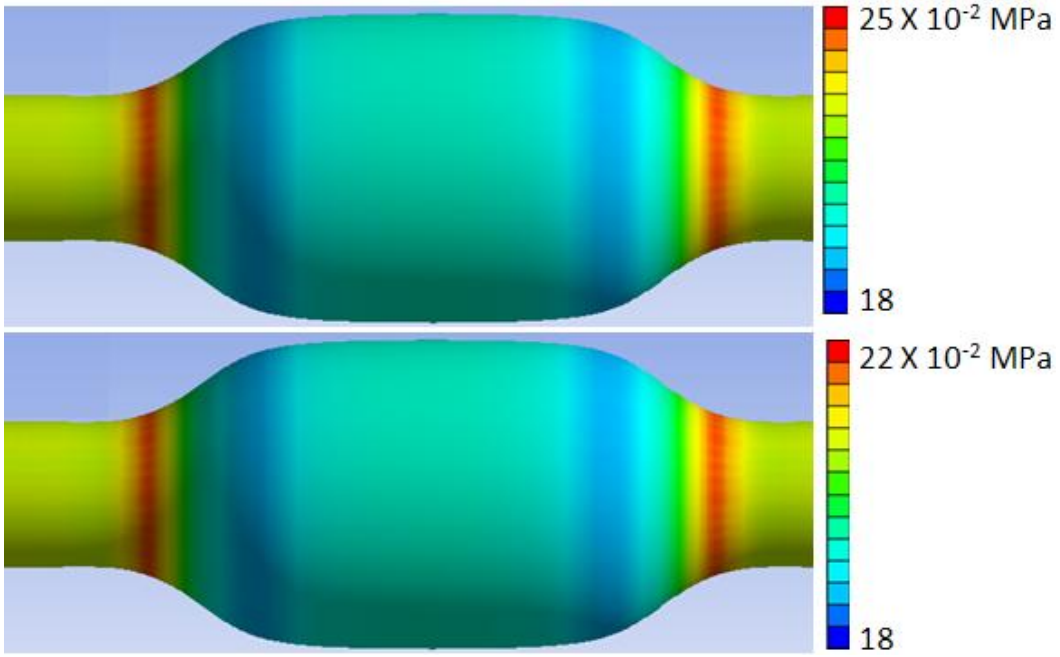

Figure 5-6: Von Mises stress distribution of homogeneous (bottom) and inhomogeneous ILT (top) for model SLT15 with 15 mm ILT thickness.

5.3.3 Discussion

Based on the four models studied here, it appears that Figures 5-5 and 5-6 show that for ILT with a 7 mm thickness the maximum wall stress is about 06% less when the ILT was modelled as inhomogeneous with three layers compared to the model with homogeneous ILT; for 15 mm ILT thickness the difference is about 12%. These differences are shown in Figure 5-7.

It could be concluded from the above figures that using homogeneous material properties for ILT when modelling AAA could lead to overestimation of the wall stresses and may affect the accuracy of the results. However, the location of maximum wall stress was not affected.

These finding are not surprising in terms of a biomechanical perspective, because using an average value for ILT can underestimate the protective role of the abluminal layer which is connected directly to the wall; it is reported by Ashton et al. (2009) that the stiffness of the abluminal layer is about 10 times higher than that of the other two layers.

Findings from this work support the recommendations of Meyar et al. (2010) who recommended that modelling ILT could be improved if within the three layers of ILT, there were differences in the luminal, medial and abluminal thrombus.

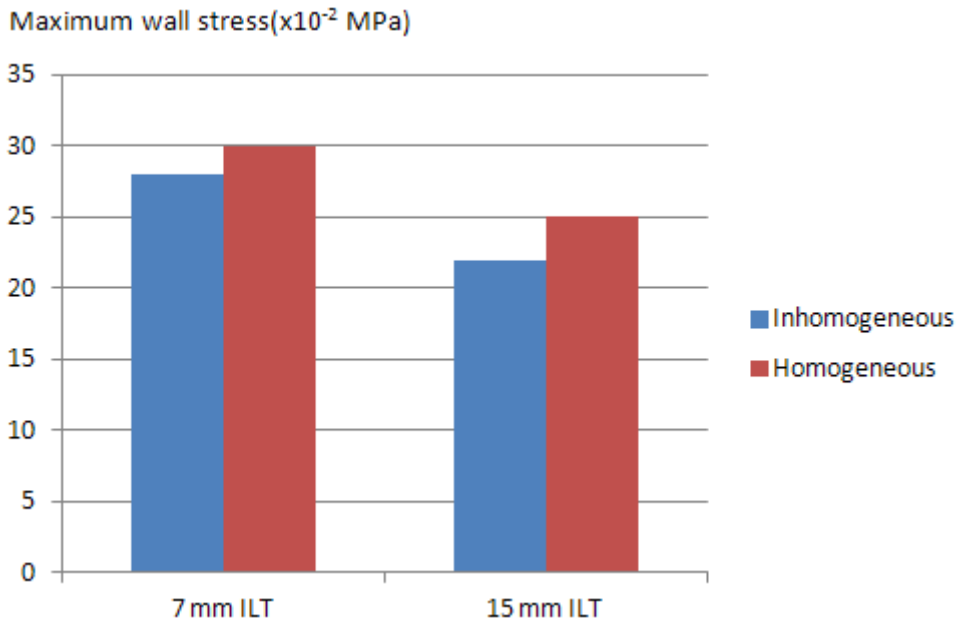

Figure 5-7: Von Mises stress distribution of homogeneous and inhomogeneous ILT of the two models.

5.4 Sensitivity studies of the material properties of the ILT

While the mechanical properties of the ILT have been investigated in a number of previous experiments, most have only investigated the tensile behaviour of the ILT (Wang et al., 2001; Van Dam et al., 2006; Gasser,et al., 2008). Sufficient information about ILT is important in identifying how stress distributions are distributed within the ILT and aneurysm wall and to help in future studies on ILT mechanobiology and its accurate role (Ashton et al., 2009).

In this section the effect of varying the material properties of ILT will be investigated using both linear and non-linear material properties.

5.4.1 Effect of Young's Modulus

In this sensitivity study, Model SLT5 (ILT thickness 5 mm) was used with Young's modulus values from 0.01 to 1.0 MPa, with a constant Poisson's ratio of 0.45. The peak stress produced with these values is indicated in Table 5-1 and a graph of this relationship is shown in Figure 5-8.

From the results it can be seen that maximum stress varies inversely with Young's modulus, but the location of maximum stress in all simulations remained the same. By changing the value from 0.01 to 1.0 MPa, maximum stress was decreased from 0.43 to 0.11 MPa. This could decrease the chance of rupture from high to low as proposed by Hall et al. (2000), who report that the AAA failure stress is 0.28MPa. This may explain why some researchers believe that the presence of ILT will reduce the chance of AAA failure, while others believe it increases it. Thus, the chance of rupture may depend on the stiffness and the thickness of the ILT.

Young's Modulus (MPa)	Maximum Stress (MPa)
0.01	0.433
0.1	0.323
0.2	0.267
0.3	0.229
0.4	0.201
0.5	0.179
0.6	0.162
0.7	0.148
0.8	0.136
0.9	0.126
1	0.118

Table 5-1: Maximum stress decreases as the value of Young's Modulus increases.

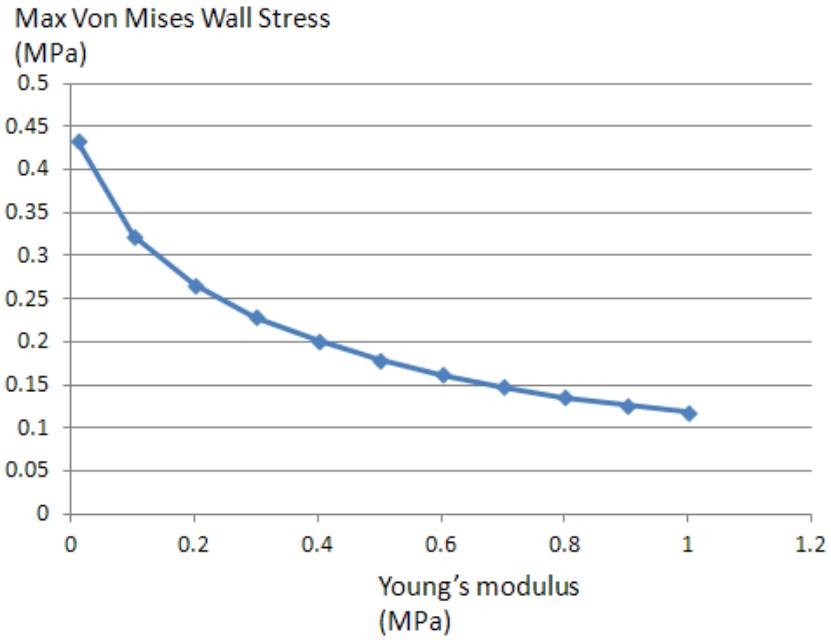

Figure 5-8: Graph showing how the value of the ILT Young's modulus affects the peak wall stress.

5.4.2 Effect of varying Poisson's Ratio

Poisson's ratio is the ratio of transverse to longitudinal strains. In this section the effect of varying Poisson's ratio on the maximum stress on the AAA wall is investigated. The same model, as above, was used but the Young's Modulus value was fixed at 0.11 MPa and the Poisson's ratio values varied between 0.3 and 0.499 (incompressible).

Poisson's Ratio	Maximum Stress (MPa)
0.3	0.29
0.4	0.30
0.499	0.32

Table 5-2: Maximum stress slightly increases as the value of Poisson's ratio increases. (Young's Modulus = 0.11 MPa in all cases)

Clearly, Poisson's ratio has only a limited effect on the peak wall stress value and therefore does not need to be known to any great degree of accuracy.

5.4.3 Non-linearity effect

In this section, the nonlinearity effect of the ILT will be examined to provide further understanding of the effects of material properties. The ILT was assumed to have hyperelastic, homogenous, incompressible and isotropic materials. The ILT constitutive model was the same as that derived by Wang et al., (2001) - Mooney Rivlin model- having a functional form for the strain energy density (W) of:

$$W = C_1 (I_{II}-3) + C_2 (I_{II}-3)^2 \qquad \text{(Eq. 5-1)}$$

Where C_1 and C_2 are the material parameters and I_{II} is the second invariant of the left, Cauchy–Green stretch tensor, $C_1 = C_2 = 2.6$ N/cm$^{2:}$

Figure 5-9 shows that the stress is higher in all models when the ILT is modelled with hyperelastic material properties and it can be concluded therefore that non-linear material properties can lead to higher stresses. The difference here is small but with a thicker ILT and maybe with patient specific models, the effect could be greater.

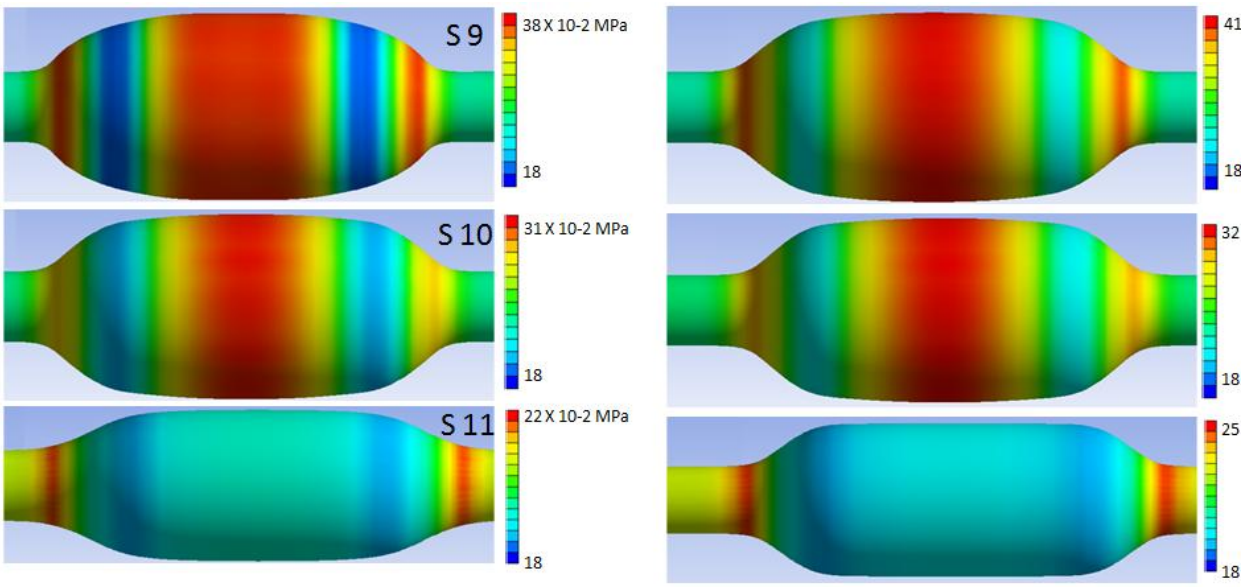

Figure 5-9: Comparison of the stresses predicted by the three models (S9, S10, S11) using elastic and hyperelastic material properties.

5.5 Effect of using ILT porous media

The role of the ILT within AAA was examined using variable thickness and material properties of the thrombus. For simplification purposes, it is assumed that ILT is a solid material, as sourced from previous studies, even though in reality ILT is a highly porous material with an average porosity of 80% (Ashton et al., 2009). The porosity of the ILT has been experimentally examined in number of studies (Adolph et al.,1997; Di Martino and Vorp, 2003; Gasser et al., 2010).

As mentioned earlier, only two recent numerical studies have examined the porosity of ILT using finite element models (Avinash et al., 2010; Polzer and Bursa, 2010) which have provided useful information about the impact of thrombus porosity on AAA biomechanics. In addition, Meyer et al., (2010) used trans-thrombus blood pressure to mimic porosity; considering that ILT has no reduction effect on blood pressure, they applied the pressure directly on the wall underneath the ILT but they did not actually model the porous ILT material.

In their studies, Meyer et al., (2010) and Polzer and Bursa (2010) neglected the actual dynamics of blood flow while Avinash et al., (2010) used the fluid phase of a porohyperelastic model to provide some information about blood flow within ILT.

A lack of knowledge remains on how modelling the porosity of the ILT may contribute to the understanding and the assessment of AAA.

In this section, the porosity of ILT will be examined using two models. Firstly, the finite element model is used to examine the pressure reduction by porous ILT and how this may affect the wall stresses and secondly, a computational fluid dynamics model is used to investigate how blood flows within the thrombus. This section also examines how the information gained can be used to aid in AAA diagnosis and possible reasons for its growth.

5.5.1 Effect of porosity on ILT using finite element model

In this section, porosity will be examined using two approaches. The first approach involves using porous media for ILT while the second approach uses the trans-thrombus pressure theory used by Meyer et al., (2010). Results from these two approaches will be compared with results gained by using solid ILT material.

5.5.1.1 Method.

Two models (SLT5 and SLT15 as shown in Table 3-1) were used and three cases were examined for each model; the first case was examined using poroelastic material for ILT and a homogeneous pressure of 145 mmHg was applied on the blood lumen acting on the ILT as shown in Figure 5-10 (a), while the second case involved using solid material for ILT, but the pressure is applied directly on the internal wall (underneath the ILT) acting on the wall and in the blood lumen acting on the ILT as shown in Figure 5-10(b). The third case was examined using solid material for ILT and the pressure was applied only on the blood lumen acting on the ILT as can be seen in Figure 5-10 (b).

In the first case, ILT was modelled as porous using poroelastic elements based on Biot's theory (ANSYS help). The governing equations for Biot's consolidation problems are:

$$\begin{cases} \nabla \cdot (\sigma' - \alpha\rho I) + f = 0 \\ \alpha\varepsilon' V + \frac{1}{k_m}\rho' + \nabla \cdot q = s \end{cases} \qquad \text{(Eq. 5-2)}$$

Where:

$\nabla \cdot$ = Divergence operator of a vector or second order tensor

σ' = Biot effective stress tensor

α = Biot coefficient = 1

ρ = Pore pressure

I = Second-order identity tensor

f = Body force of the porous media

$\varepsilon' V$ = Elastic volumetric strain of the solid skeleton

Km = Biot modulus

q = Flow flux vector

s = Flow source

The relationship between the Biot effective stress and the elastic strain of solid skeletons is given b:

$$\sigma' = \mathrm{D}:\varepsilon^e \qquad \text{(Eq. 5-3)}$$

Where ε^e is the second-order elastic strain tensor and D is the fourth order elasticity tensor.

The relationship between the fluid flow flux and the pore pressure is described by Darcy's Law:

$$q = -k\,\nabla p \qquad \text{(Eq. 5-4)}$$

Where k is the second-order permeability tensor and ∇ is the gradient operator.

The permeability value of the ILT was taken from Adolph et al., (1997) who reported an ILT of 0.91 $\pm$0.54 $mm^4/N \cdot s$ and for this work the average value of 0.91 $mm^4/N \cdot s$ is used.

The solid phase of the ILT in the first case and the solid ILT for the second and third cases were modelled as linear elastic with Young's modulus E= 0.11 MPa and Poisson's ratio u = 0.45.

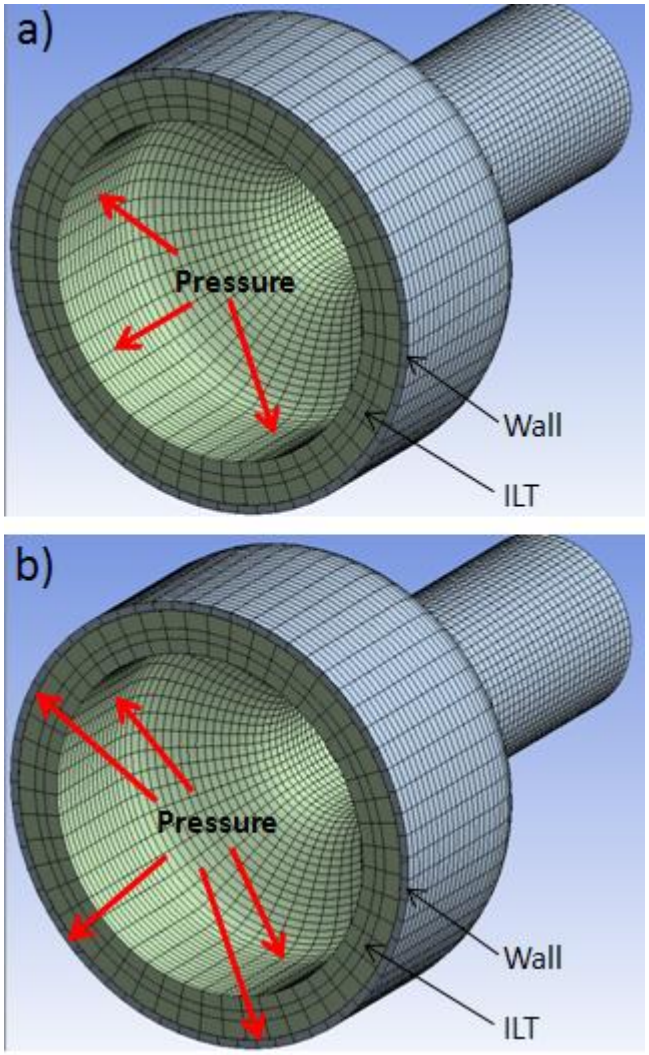

Figure 5-10: Methods of applying the pressure in each case, a) First and third cases where pressure is applied on the ILT and, b) Second case where the pressure was applied on both the ILT and the wall.

5.5.1.2 Results

Figures 5-11 and 5-12 illustrate the Von Mises stress distribution in the wall of the two models for each of the three cases (Porous ILT and two solid ILT) obtained from static simulations of the peak systolic pressure.

Figure 5-11 shows that maximum wall stresses for model SILT5 are 0.315 MPa, 0.315 MPa and 0.31 MPa for case 1, 2 and 3 respectively. Figure 5-12 shows that maximum wall stresses for model SILT15 are 0.223 MPa, 0.223 MPa and 0.22 MPa for cases 1, 2 and 3 respectively.

Stress distribution and maximum stress location are the same for the three cases in each model.

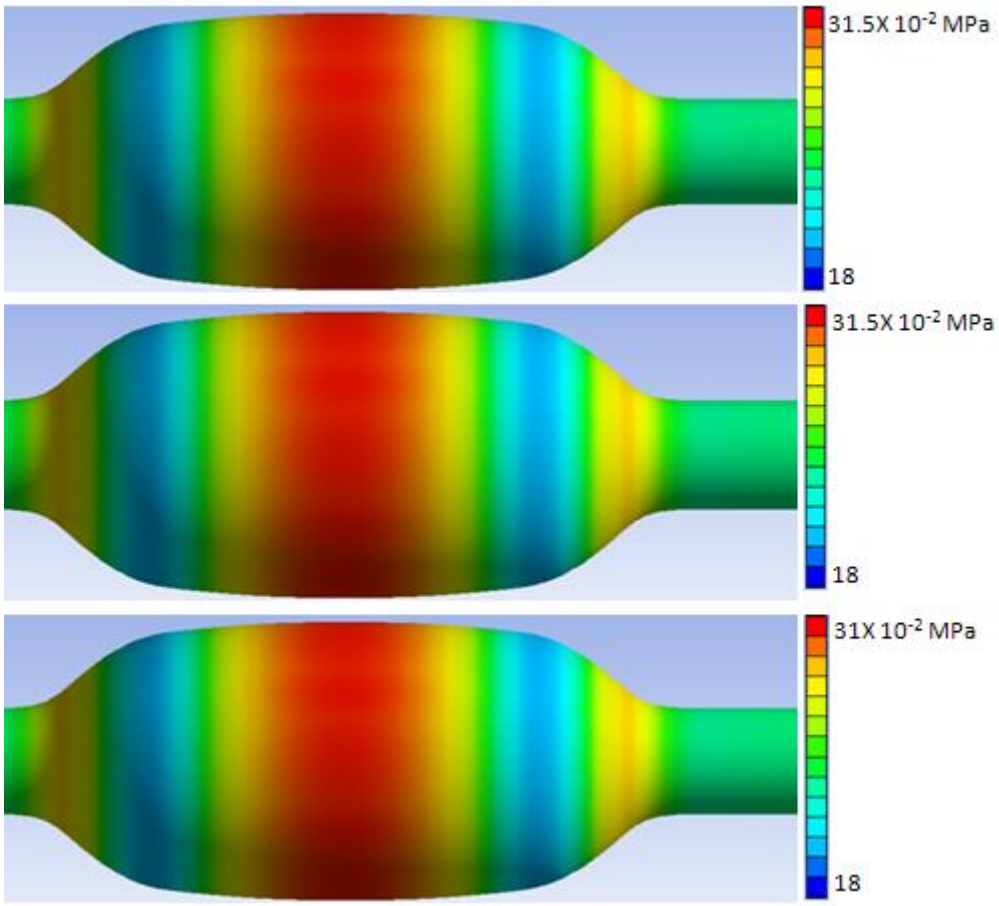

Figure 5-11: Von Misses stress distribution on AAA wall for cases 1, 2 and 3 (Model SLT5).

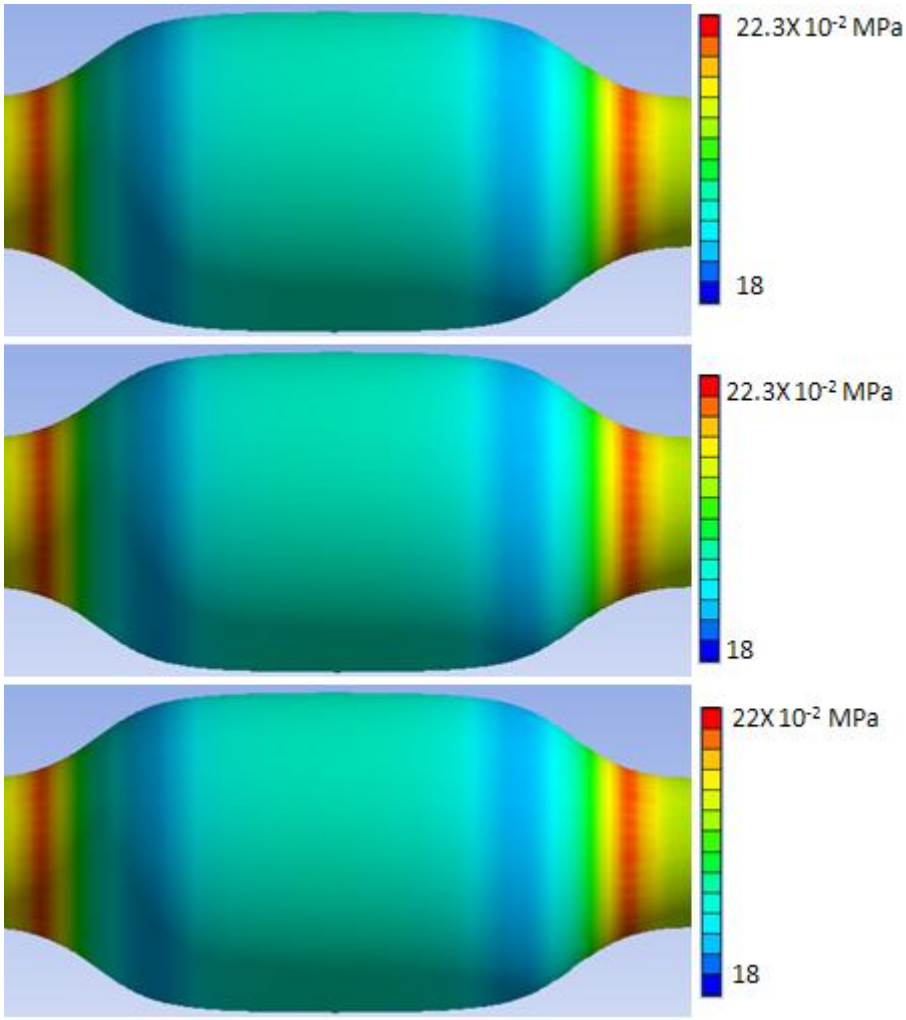

Figure 5-12: Von Misses stress distribution on AAA wall for cases 1, 2 and 3 (Model SLT15).

5.5.1.3 Discussion

Based on the two models studied here and the three cases for each model, Figures 5-11 and 5-12 show that the difference in wall stresses gained from the three cases is very small (about 1.6%). There is no change in the location of maximum stress or in the distribution of wall stress. It seems that the ILT plays a supportive role in the wall even in cases where the pressure is acting directly on the wall. The wall stresses were expected to increase when the pressure is applied directly on the inner wall (case three) compared to applying the pressure on the solid ILT (case one) due to the fact that solid ILT will reduce the pressure at the wall to ILT interface and stress was expected to be equivalent to the stresses gained when no ILT is used; interestingly though, the results here show very small difference in the two cases. The biomechanical explanation of this is that ILT reduced the deformation on the wall which led to a reduction in the stress on the wall.

These findings are in agreement with results gained by Polzer and Bursa (2010) who used solid and porous models for ILT; by comparing the results of the two models they reported that the poroelasticity of ILT did not alter the wall stress and concluded that ILT porosity can be neglected when wall stress distribution is required. The findings are also in good agreement with Polzer and Bursa (2010) Meyer et al. (2010) who used trans-thrombus theory and found that applying the pressure directly underneath the ILT has only a small effect (about .03% difference) on wall stresses compared to applying the pressure on the ILT.

In contrast, the results from Ayyalasomayajula et al. (2010), who utilize porohyperelastic FEA models for both the ILT and aneurysm wall, show that the porosity of the ILT increased the wall stresses compared with a non-porous ILT. They reported an increase of up to 81.0% in peak maximum principal wall stresses in comparison of a porous ILT to non-porous ILT.

This seems very high; indeed, it is even higher than the stresses recorded if the ILT was completely removed (between 20% - 60% in this work, and 55% in Polzer and Bursa's (2010) work). From the mechanical point of view, the ILT was found to have a protective role, while porosity may decrease the protective role but not have a negative effect.

Ayyalasomayajula et al. (2010) recorded the pressure drop caused by the ILT as small, therefore the possible reason for the high stresses that they reported is the use of a porous material (with very low permeability) for the aneurysm wall, which may cause larger deformation of the wall compared to a solid wall and thus result in the higher stresses recorded.

In the work carried out here, and in the work of Polzer and Bursa (2010) and Meyer et al. (2010), the permeability of the wall was neglected because the scope of these studies was limited to the ILT role. It can be concluded that the effect of using porous media for the ILT on the wall stress maximum value and distribution is very small; hence, if maximum wall stresses are needed, the porosity of the ILT could be neglected.

5.5.2 Effect of porosity for the ILT using blood flow

In this section porous media in the ILT will be used to examine the blood flow behaviour at the interface of blood-ILT mediums, and blood flow within the ILT itself. This work will involve implementing mass transport of the blood into the model, which includes two mediums, blood lumen and ILT mediums. This will involve the use of computational fluid dynamics (CFD).

To the author's knowledge, this is the first study which introduces the mass transport of blood flow at the interface of blood-ILT mediums, and blood flow within the ILT itself.

5.5.2.1 Method

Due to the large computational resources of this analysis, only one quarter of the aneurysm was constructed, as shown in Figure 5-13 (Model F7 from Table 3-8), which will not underestimate any calculation due do the axisymmetric nature of the aneurysm. The model here consists of two mediums: the fluid medium and porous medium, and they are attached with a "porous-fluid" interface.

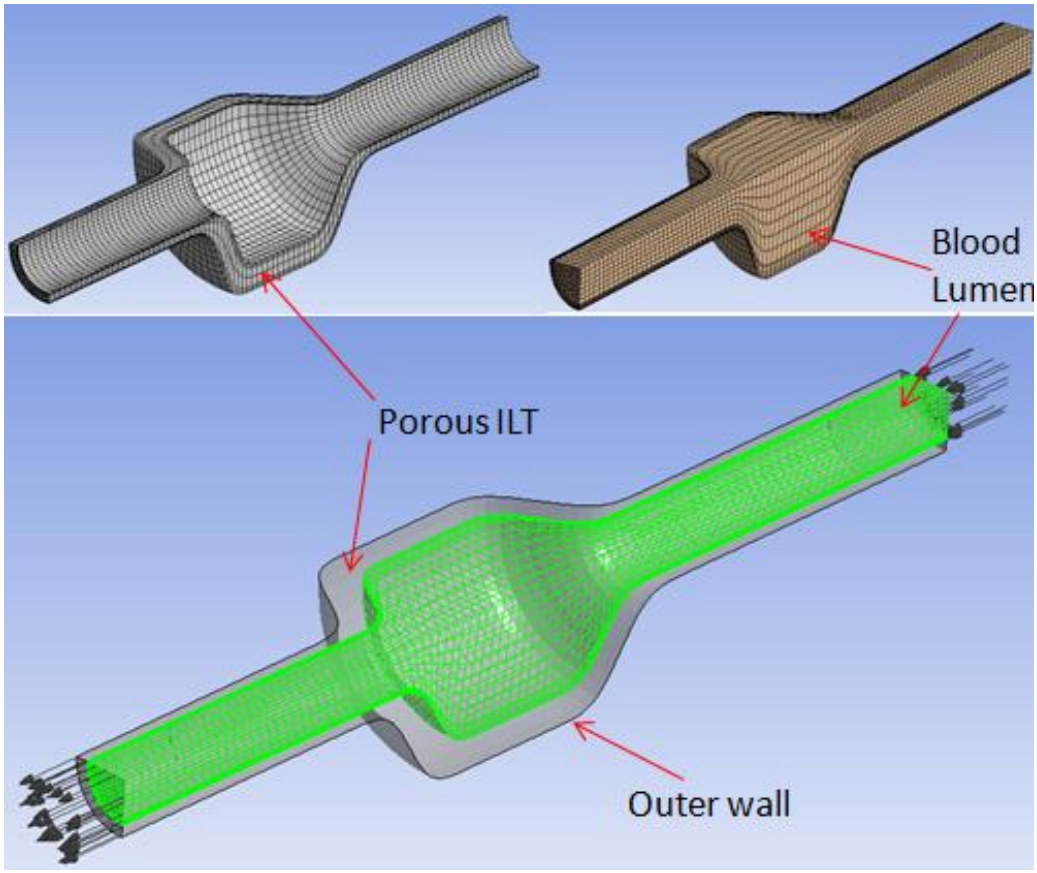

Figure 5-13: The porous ILT in grey and blood lumen domain in green mesh.

In CFD, modelling porous material numerically involves applying Darcy's law that describes the flow of a fluid through a porous medium in the following form:

$$Q = \frac{kA}{\mu} \left(\frac{\partial P}{\partial L}\right) \quad \text{(Eq. 5-4)'}$$

Where Q is the flow rate of the blood.
k is the permeability of the ILT.
A is the cross-sectional area of the aorta.
μ is the viscosity of the blood.
L is the length of the porous media the fluid will flow through.
$\left(\frac{\partial P}{\partial L}\right)$ represents the pressure change per unit length of the blood.

The interface between the blood lumen and the porous ILT material allows blood to flow inside the ILT. The permeability value of the ILT was taken from Adolph et al. (1997), who reported that ILT of 0.91 $\pm$0.54 $mm^4/N \cdot s$. The three values of permeability will be examined to understand its effect.

For the fluid medium, all boundary conditions used in 3.2.2 were applied here, with a steady flow at a constant velocity of 25cm/s at the inlet and blood pressure of 120 mmHg at the outlet used with a blood density of 1121 kg/m3 and blood dynamic viscosity of 0.0035 Poiseuille (Pa.s) (Yu, 2000).

5.5.2.2 Results

Figure 5-14 shows longitudinal pressure gradients on the interface between blood-ILT varying between 119.9 to 120 mmHg.

Figure 5-15 shows longitudinal pressure gradients on the internal wall varying between 119.5 to 120 mmHg.

Figure 5-16 shows the pressure gradients of the cross sectional view of the ILT in the middle of the aneurysm varying between 119 to 120 mmHg.

Figure 5-17 shows the blood velocity and direction of the blood and blood lumen at four positions in the aneurysm.

Figure 5-18 shows the velocity map on a cross sectional views for blood flow on the whole aneurysm and only in the ILT varying between 0 to 22 cm/s .

Figure 5-19 shows the velocity in X-direction of blood flow in three positions of ILT using three values of permeability.

Figure 5-20 shows the flow in the blood lumen and inside the ILT. It is noticed that fluid is transmitted from blood lumen (grey background) to the ILT (white background) at the distal end of the aneurysm.

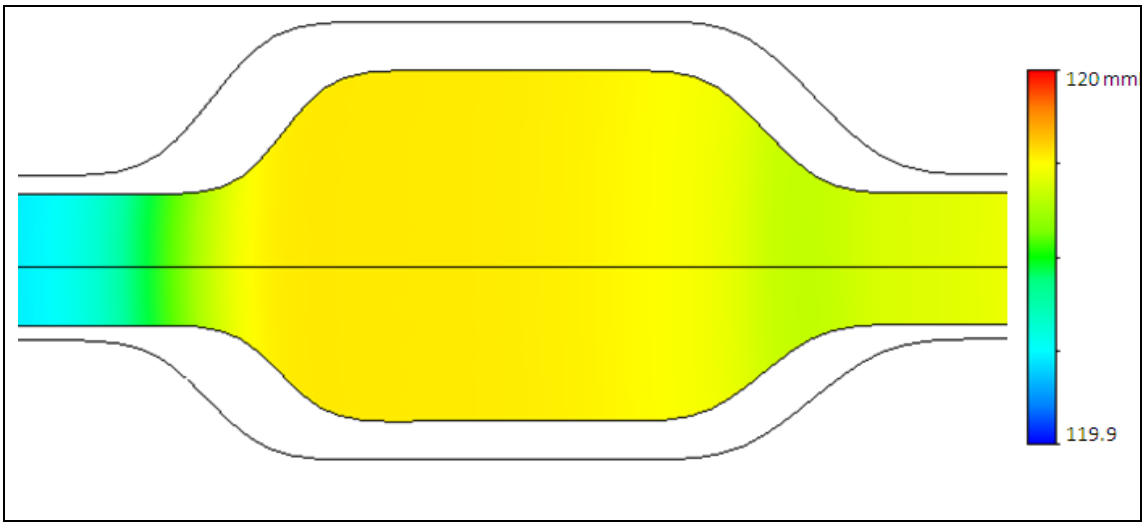

Figure 5-14: Pressure gradients on the interface between blood-ILT mediums.

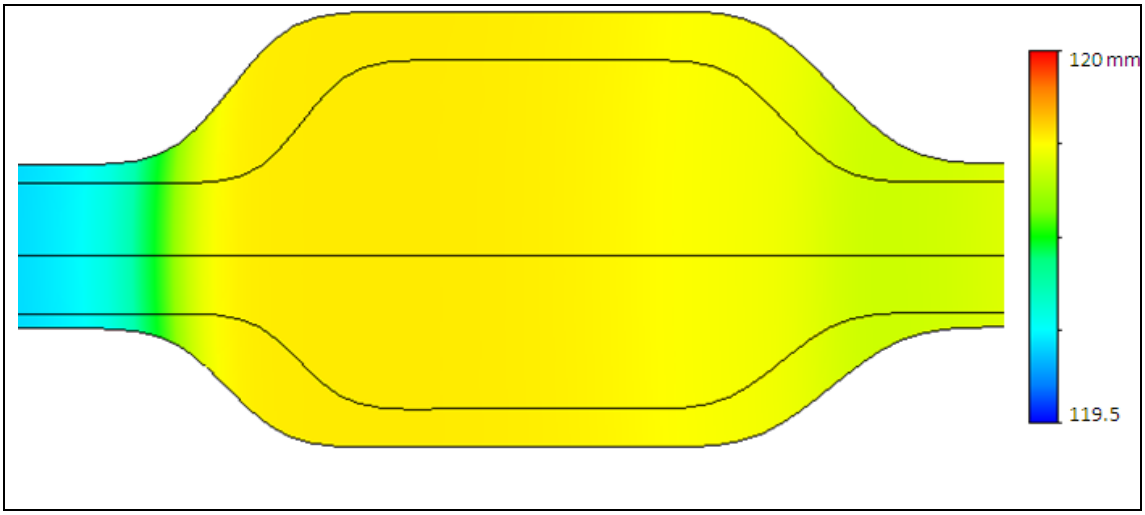

Figure 5-15: Pressure gradients on the internal wall.

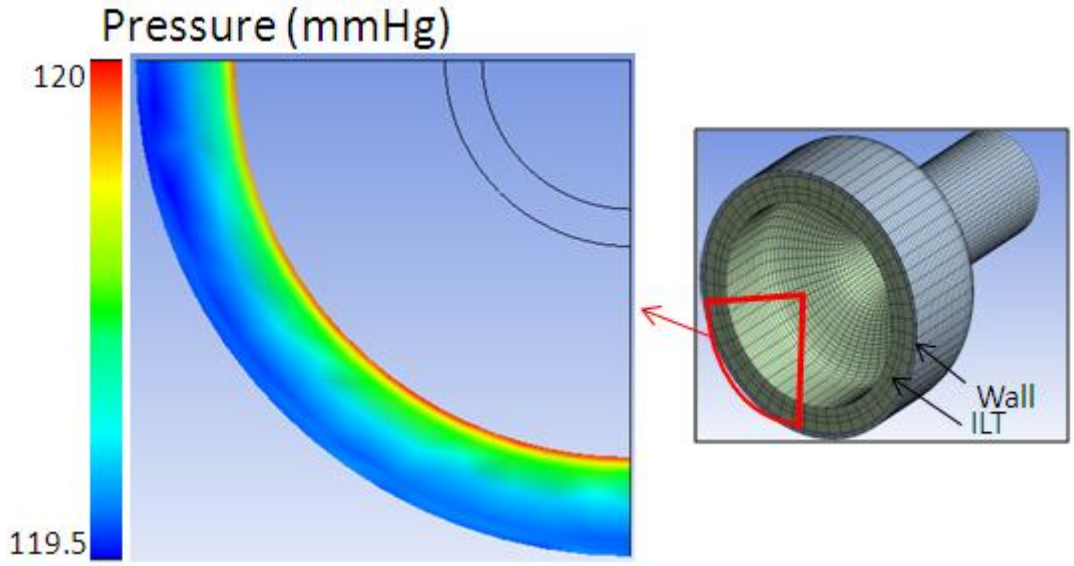

Figure 5-16: Pressure gradients of the cross sectional view of the ILT in the middle of the aneurysm.

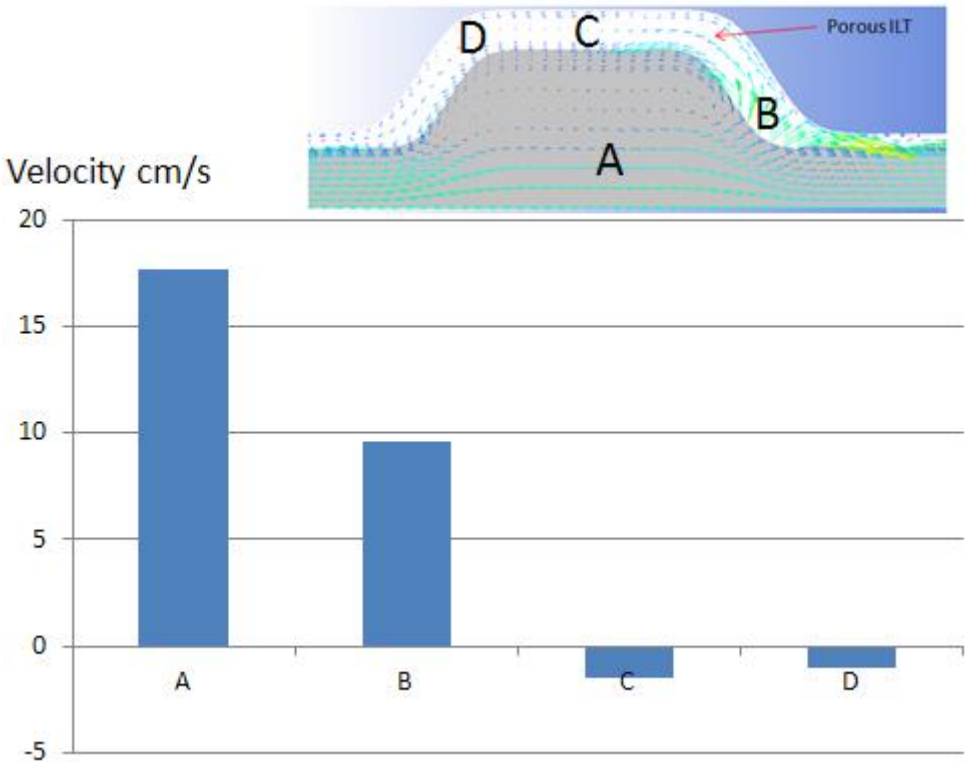

Figure 5-17: Velocity in X-direction of blood flow in four positions of the aneurysm.

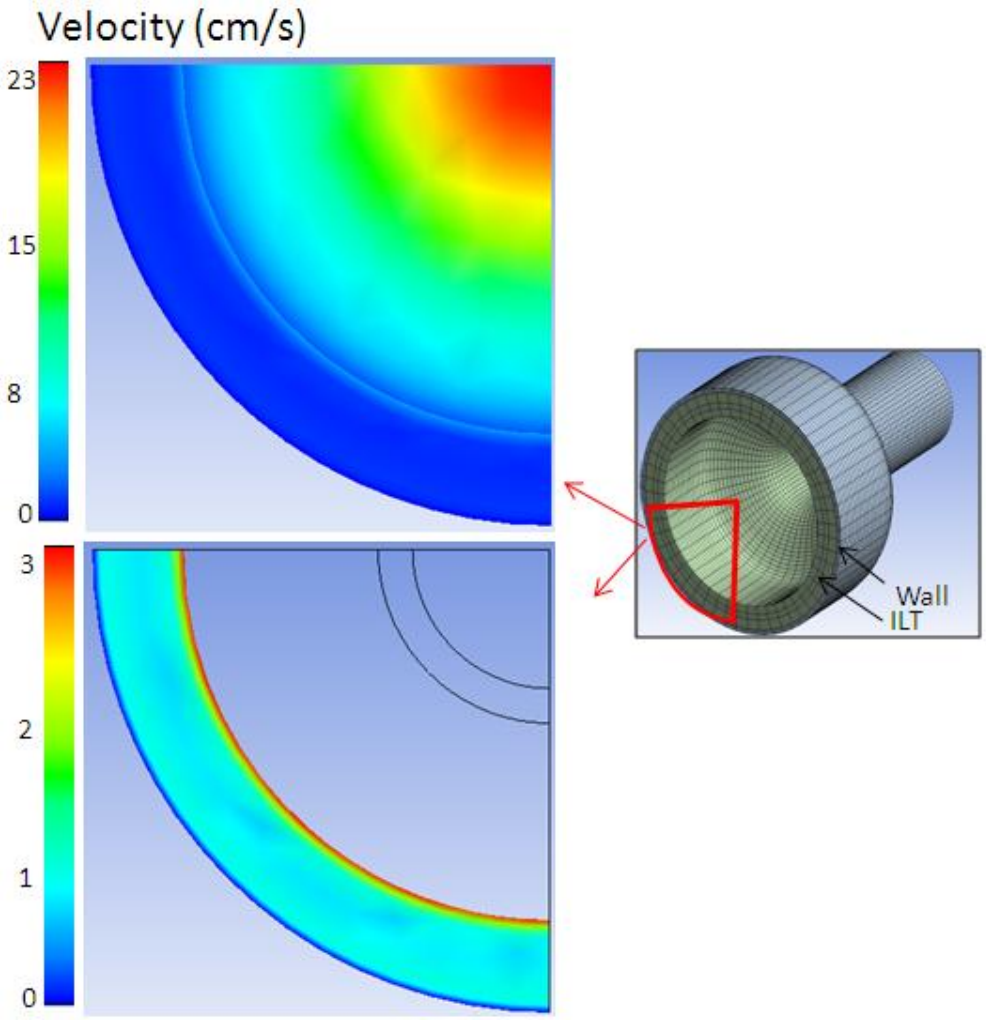

Figure 5-18: Velocity map on a cross sectional view for blood flow on whole aneurysm (top) and only in the ILT (bottom).

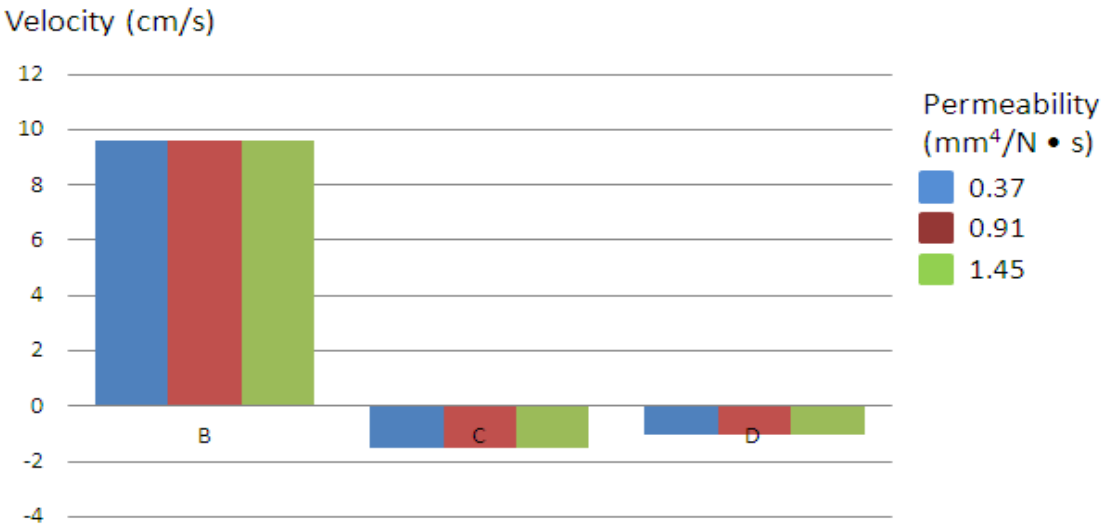

Figure 5-19: Velocity in X-direction of blood flow in three positions of the ILT using three values of permeability.

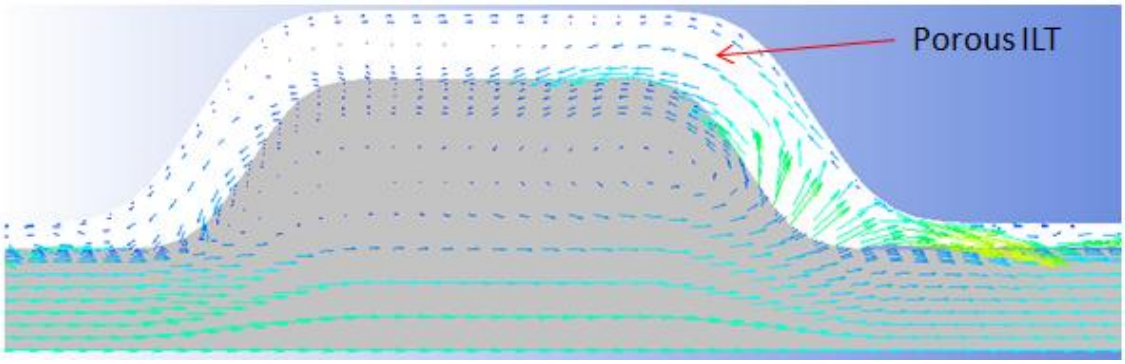

Figure 5-20: Velocity vectors of blood flow in the blood lumen (grey background) and the ILT (white background).

5.5.2.3 Discussion

The results from these analyses, illustrated in Figure 5-14 and 5-15, show that there was a very small pressure drop between the blood lumen and the internal wall; this means that the presence of the ILT has a very small effect (less than 0.5 %) on the pressure transmitted to the internal wall. Figure 5-16 illustrates the pressure drop within the ILT, where it can be seen that the pressure decreases with ILT depth but that the total drop is very small (less than 0.5%). This is not a surprising observation because the ILT was modelled with high porosity (80%) and it will be expected that the pressure drop will be minimal. This is in strong agreement with the results reported by Schurink et al. (2000), who found no reduction in blood pressure under the ILT. In their clinical study, Schurink et al. (2000) investigated nine patients who underwent operations for an AAA at the level of the thickest thrombus lining; the pressure within the aneurysmal thrombus (just inside the aneurysmal wall) was measured and compared with the systemic pressure and no deference were found. Similar results reported by Takagi et al.(2005) who conclude that the thrombus of an aneurysm does not significantly decrease the pressure on the aneurysmal wall. It is also in agreement with the recent blood pressure measurements of Polzer and Bursa (2010), who numerically used poroelastic material for the ILT and reported no reduction of pressure between the blood lumen and underneath the ILT.

Velocity value and direction of blood flow in several positions are shown in Figure 5-17, where it can be noted that velocity decreased when transmitted from blood lumen to the ILT. The ILT decreases the velocity of the blood, so it can be seen from figure 5-18 that maximum velocities occur in the middle of the blood lumen and the velocity

decrease towards the wall. It could be thought from this figure that there seems to be a slow region at the interface between blood and the ILT lumens and this may seem to be slower than the first layer of the ILT, however this is not accurate. This apparent phenomenon is because this is an average velocity map of all the velocities in a specific region, and because at the interface of the lumen-ILT any velocity component that hits the solid part of the porous interface will record a velocity of zero (in flow, the velocity at wall equals zero).

The second part of Figure 5-19 shows the velocity map of blood only within the ILT; it can be noticed that higher velocities are recorded at the first layers of the ILT (near lumen) and that the flow tended to have uniform slow velocity inside the ILT and was very slow near the wall. The velocity variation seems to follow a decay pattern. These finings are in agreement with Ayyalasomayajula et al.'s (2010) work, who used FEA models to investigate the convective transport within the ILT and reported that the interstitial fluid velocities decreased continuously across the thickness of the ILT with the maximum on the luminal side and the minimum occurring at the outer wall.

Inside the ILT the velocity of the blood is relatively slow (between 0 and 3 cm/s) in most positions and was recorded at higher rates in specific positions which will be discussed in the next paragraph. Varying the permeability of the ILT between 0.37, 0.91 and 1.45 $mm^4/N \bullet s$ did not alter the velocity of flow inside the ILT, as shown in Figure 5-19, which is also in agreement with Ayyalasomayajula et al. (2010), who reported that interstitial fluid velocities were not affected by varying the permeability of the ILT.

Figure 5-20 shows that the flow can actually move from blood lumen to the ILT and noticeable blood movement could be seen within the ILT, which agrees with the conclusion of Adolph et al. (1997), who experimentally carried out a histologic analysis for the ILT and suggested that fluid and smaller molecules may pass freely through the thrombus via the canaliculi network. Another very interesting observation can be also seen at the distal end of the aneurysm, in that the flow is more able to transmit through the ILT in this region (recorded velocity in this region is the highest in ILT = 9.6 cm/s) compared to other locations of the ILT. This could be as a result of

the perpendicular force of the flow and the continuous vortices' formation in this location, and could have implications for the rupture in these regions. This observation needs to be investigated clinically as it may explain why the aneurysm grows at the distal region of the aneurysm. That could be a result of the continuos movement of the blood and its smaller molecules in this region. Specifically, it could explain why the Matrix metalloproteinases (MMPs) - which is highly linked with AAA pathology and discussed in details in chapter 2 - are concentrated in a region of AAA which is at high risk of rupture, as concluded by Wilson et al. (2006) in their clinical study, who reported that there was a localized increase in MMP-8 and MMP-9 concentrations at the site of aortic rupture.

Another possible advantages of such modelling is that modelling blood flow within the ILT will be important in future work investigating drug delivery solutions in AAA, which is a significant potential new AAA treatment methodology as reported by Ayyalasomayajula et al. (2010).

5.6 Summary

This chapter has examined the role of ILT in AAA using different factors. The effect of the ILT presence on wall stresses was examined using a variety of thicknesses, by comparing these to each other, and by comparing them to an aneurysm with no ILT. It was shown that the presence of the ILT decreases the stresses on the wall and this is found to be proportional to the thickness of the ILT. The ILT was also modelled as non-homogenous using different properties for the three layers of the ILT making the adjacent layer to the wall stiffer than the other two (as seen in-vivo) and by comparing the results of wall stresses from models with three layers of ILT to other models with average value of stiffness. It was found that modelling the ILT as three layers provided a more protective role to the wall and it was suggested that this is a result of the stiff layer decreasing the deformation (strain) of the wall and leading to a decrease in wall stresses.

In the sensitivity study of ILT material properties, the stiffness of the ILT was found to decrease the wall stresses on the aneurysm. However, the non-linearity of the material properties of a homogenous ILT do not have a significant impact on the wall stresses, while using linear values can provide acceptable results.

The porosity of the ILT was examined using FEA and CFD and it was found that aneurysm wall stresses were not affected when a porous ILT was used. It was found also that the pressure drop caused by the ILT was very small and concluded that the supportive role of the ILT is not a result of reducing the pressure on the wall, instead it eliminates the deformation (strain) of the wall which results in reducing wall stress.

It was concluded that if wall stresses are required, ILT porosity can be neglected. However, valuable information about blood behaviour inside the ILT was observed which may help in understanding the aneurysm growth and rupture mechanism in addition to its possible contribution to the significant potential new AAA treatment methodology of drug delivery solutions in AAA.

Chapter 6
Discussion

6.1 Introduction

An accurate and reliable stress analysis of AAA requires clear understanding of the role of every parameter that may directly or indirectly affect the stresses on the wall. Various studies attempt to contribute to the understanding of how each parameter can affect the stresses. The shape of the aneurysm was investigated by number of researchers and they found useful information about the influence of aneurysm shape on stresses on the wall (Elgers et al., 1996; Vorp et al., 1998; Scotti et al., 2005; Doyle et al., 2009).

In this thesis, a number of factors that have influence on wall stress have been investigated. Aneurysm shape was investigated by using four different models with different shapes but all having the same diameter in order to understand the effect of shape on wall stresses. Following this, blood flow was implemented in the models to examine its effect on the internal wall pressure and resulting wall stresses using a variety of shapes and sizes. Blood flow was also used to understand what is happening inside the aneurysm and how this may affect the stresses on the wall or how it may contribute to the pathology of AAA.

The effect of aspect ratio effect on the AAA wall stresses is examined for the first time in this thesis. Extensive study has been carried out using a variety of shapes and diameters which has lead to novel and valuable results that can contribute to the understanding of the aneurysm shape effect on the magnitude and distribution of the stresses on the wall, and could have clinical use to enhance the assessment of AAA.

The presence of thrombus on the AAA site was also intensively investigated to understand its role within the aneurysm. Different ILT thicknesses, material properties and structures were examined and a clear understanding for the role of each factor was gained. The thrombus porosity was examined with and without the inclusion of

blood flow, and new outcomes have been reported on the effect of porosity on wall stresses as well as in the blood flow from lumen to the ILT and within the ILT.

6.2 The effect of aneurysm shape on wall stresses and on blood flow

It is known that aneurysm rupture occurs when the stress on the wall exceeds its strength and this is likely to occur where the maximum stresses occur. The current practice of using the maximum diameter as an indicator of maximum stress (based on Laplace's law) is not accurate. In this work, four FEA models with the same diameter but different shapes were used to understand how shape can alter wall stresses. Uniform blood pressure was applied on the internal wall of the four models and it was found that wall hoop stresses values and distribution were not the same in the four models that have the same diameter; this means that it is not only the diameter but also aneurysm shape that can alter the magnitude and the distribution of wall hoop stresses. There was an approximate 40% difference between the shape with maximum wall hoop stress and the shape with minimum wall hoop stress, clearly indicating that aneurysm shape has an accountable impact on wall hoop stresses. It also showed that using Laplace's law for AAA assessment is not accurate since only one of the four models followed the Laplace law here; in the other three models applying Laplace's law lead to wrong estimations on wall hoop stresses. Moreover, wall hoop stresses were higher at the two ends (not in the middle where maximum diameter is found) in three models, which clearly means that maximum wall hoop stress did not occur on the maximum diameter region, but, depending on the shape, maximums hoop stress could occur either in the middle or on the aneurysm ends. It was concluded that maximum stress occurred either in the middle or where the geometry tends to have the maximum variation in the curvature, namely where the curve changes rapidly at the beginning and the end of the aneurysm.

These findings are in agreement with the results of Elger et al. (1996), who examined the effect of aneurysm shape using analytical models, and found that maximum stress depended on AAA shape and curvature. The results are also in agreement with reports from Vorp et al. (1998), Scotti et al. (2005), and Doyle et al. (2010), who have proven using different approaches that the shape of aneurysm, independently from its diameter, has a vital effect on the distribution and magnitude of stresses on AAA wall. The results are also in line with Rodrguez et al.'s (2007) findings who found that in

AAAs with the same diameter, the peak wall stress can increase significantly as the aneurysm becomes more asymmetric (sharper wall curvatures).

The above work used uniform blood pressure. It was necessary to examine the accuracy of using uniform blood pressure and neglect the variation of the blood pressure along the aneurysm that could be caused by blood flow. Hence, mass blood flow was implemented in six models of different shapes and sizes to examine its effect on blood pressure and to understand how the shape and the size of the aneurysm may affect its pathology.

CFD analysis of the blood flow inside the aneurysm for all models found that it consisted of two main parts. There was a high velocity flow in the middle of the aneurysm and a slow recirculation flow in the aneurysm body. These recirculations (or vortices) could be affected by the shape and size of the aneurysm, while the pressure on the AAA wall has only a small variation (less than 1 mm Hg) in all of the eight models for different shapes and sizes with higher pressures at the distal end of the aneurysm.

A number of experimental and numerical studies have investigated the flow inside AAA to understand the role of blood flow in the risk of rupture of the wall (Budwig et al., 1993; Peattie et al., 1996; Yu, 2000; Finol and Amon, 2001) who all found similar characteristics of blood flow inside the aneurysm. The small variation of blood pressure inside the aneurysm was also found by Leung et al. (2006) and Kelly et al. (2009), who reported less than 0.1% in the variation of blood pressure along the aneurysm in AAA.

From the above it was concluded that the variation of the blood pressure caused by blood flow was very small and hence could be neglected if wall stresses are required. It could be also concluded that vortices inside AAA might play an important role in the formation of the ILT and in the pathology of the AAA, which by itself is a factor of the aneurysm shape, which means that aneurysm shape is a vitally important factor in assessing the risk of AAA rupture.

The importance of the above findings is that they can provide valuable information in understanding what effect could be expected from the assessment of different shapes of aneurysm, and that applying the law of Laplace in the assessment of AAA does not provide accurate results in all aneurysm shapes. The above findings also show how the shape and size of an aneurysm may alter blood dynamics inside AAA.

6.3 Effect of aspect ratio on the stresses on the AAA wall

The aspect ratio of an aneurysm in AAA is the relationship between its length and diameter of its neck (normal aorta). 42 models (27 for the basic study and 15 to produce more data points on graphs) with a variety of shapes and diameters were used to investigate the effect of aspect ratio on wall stresses. Aspect ratio was found to change the magnitude and distribution of the wall hoop stresses for the same shape with the same diameter when the length of the aneurysm body was varied, and this was verified using three deferent shapes and three different diameters for each shape.

It was found from this work that for aneurysms with a small aspect ratio (short aneurysm), maximum wall hoop stress is expected to be concentrated at the two ends of the aneurysm, but for a similar aneurysm with a larger aspect ratio (longer aneurysm) it was found that the maximum wall hoop stress is concentrated in the middle with higher magnitude. Aspect ratio was found to shift the magnitude and the location of the maximum hoop stress from the proximal and distal ends of the aneurysm to the middle at critical value. This critical value can help to predict the location of maximum wall stress and the possible region of rupture or growth. An empirical relationship between maximum hoop stress and aspect ratio was plotted, which could be used as an additional indicator for the assessment of an aneurysm by predicting the magnitude and the location of the maximum wall stresses. It was suggested that a general clinical assessment scale be applied to enhance the assessment of AAA maximum wall stress value and location.

Aspect ratio threshold was reported by Salsac et al. (2004) who carried out an experimental study using tomographic digital particle image velocimetry to examine the changes occurring during the progressive enlargement of AAA and a critical aneurysm aspect ratio was found, for which the flow change from laminar state to a

turbulent state. This indicates that aspect ratio does not only change the wall stresses but also the blood flow behaviour inside aneurysm.

These findings are important to the field as they introduce the aspect ratio of the aneurysm as an important indicator of the assessment of the disease in terms of predicted location for maximum wall stresses that may lead to the location of a rupture, and in terms of the predicted magnitude caused by this factor.

To the author's knowledge, this study is the first to examine the effect of the aspect ratio on the location and the magnitude of maximum stress in the aneurysm wall. Furthermore, the findings are valuable and justified through engineering analysis. The effect of the aspect ratio could dramatically impact any future studies or clinical assessment of the aneurysm.

6.4 The role of intraluminal thrombus

The role of thrombosis inside AAA on rupture risk is not clearly understood, and is controversial because some researchers believe that its presence increases the risk of rupture while others suggest it supports the wall and decreases the risk of rupture.

To investigate this, four models with different ILT thicknesses have been used to compare the effect of the ILT thickness on the wall stresses and to compare this with an aneurysm with no ILT. The results showed that the presence of an ILT markedly reduces peak wall stress and alters wall stress distribution. Wall stresses were decreased 30% in the presence of thin thrombus and 60% in the presence of thick thrombus. These findings support the results of Wang et al., (2002), Speelman et al., (2007), and Polzer and Bursa (2010), who reported that thrombus reduces AAA wall stress and as a result plays a positive role in supporting the wall and decreasing the chance of AAA rupture.

Some realistic and sensitivities studies have been carried out to measure the effect of different factors on the role of the ILT. The ILT was modelled as non-homogenous with three layers, each with different material properties to mimic the realistic ILT that has three layers with different material properties for each layer.

The results showed that maximum wall stress varies inversely with ILT stiffness. By varying the stiffness factor from 0.01 to 1.0 MPa, maximum stress was decreased from 0.43 to 0.11 MPa. This could decrease the chance of rupture from high to low as proposed by Hall et al. (2000), who reported that the AAA failure stress is 0.28MPa which may explain why some researchers believe that the presence of an ILT will reduce the chance of AAA failure, while others believe it will increases it. Thus, the chance of rupture may depend on the stiffness of the ILT.

The non-linearity of the material properties of a homogenous ILT does not have a significant impact on the wall stresses, and using linear values can provide acceptable results. Using a non-homogenous ILT showed a noticeable effect on wall stresses compared to a homogenous ILT.

Early numerical studies of the ILT have considered it to be a solid material (including the first ILT results in this thesis), but in reality, it is not a solid material, it is actually porous. Many researchers raise the consideration of the ILT as being solid as a modelling limitation and have suggested that porosity be included in future studies. In this work the consideration of the ILT as a porous material is applied.

The porosity of the ILT was examined using FEA and CFD and it was found that aneurysm wall stresses were not affected when a porous ILT was used. It was found also found that there is no pressure drop between blood lumen and the internal wall caused by the ILT, thus it was concluded that the supportive role of the ILT is not a result of reducing the pressure on the wall, but it eliminates the deformation (strain) of the wall which results in reducing the wall stress.

These findings are in agreement with the results gained by Polzer and Bursa (2010) who used solid and porous models for the ILT; by comparing the results of the two models they reported that the poroelasticity of the ILT did not alter the wall stress and concluded that ILT porosity can be neglected when wall stress distribution is required. The findings are also in strong agreement with Polzer and Bursa (2010) and Meyer et al. (2010), who used trans-thrombus theory and found that applying pressure directly underneath the ILT has only a small effect (about .03% difference) on wall stresses compared to applying the pressure on the ILT. In contrast, results from Avinash

Ayyalasomayajula et al. (2010), who utilize porohyperelastic FEA models for both the ILT and wall, showed that the porosity of the ILT increased the wall stresses compared with non-porous ILT. They reported an increase of up to 81.0% in peak maximum principal wall stresses in a comparison of a porous ILT to a non-porous ILT. This seems to be very high, and is even higher than the stresses recorded if the ILT was completely removed (between 20% - 60% in this work, and 55% of Polzer and Bursa's (2010) work). From the mechanical point of view, the ILT was found to have a protective role, while it was thought that porosity may decrease the protective role it did not have a negative effect. Ayyalasomayajula et al. (2010) recorded the pressure drop caused by the ILT as small, therefore the possible reason for the high stresses that they reported was the use of a porous material (with very low permeability) for the wall, which may cause a larger deformation of the wall compared to a solid wall and result in higher stresses recorded. In the work carried out here, and in the work of Polzer and Bursa (2010) and Meyer et al. (2010), the permeability of the wall was neglected because the scope of these studies was limited to the ILT role.

The results of blood velocity within the ILT show higher velocities are recorded at the first layers of the ILT (near lumen) and that the flow tended to have uniform slow velocity inside the ILT and was very slow near the wall. The velocity variation seems to follow a decay pattern. These finings are in agreement with Ayyalasomayajula et al. (2010), who used FEA models to investigate convective transport within the ILT and reported that interstitial fluid velocities decreased continuously across the thickness of the ILT with the maximum on the luminal side and the minimum occurring at the outer wall. ILT permeability variation did not alter the results of this work nor the results reported by Ayyalasomayajula et al. (2010).

The results showed that the flow can actually transmit from blood lumen to the ILT and that noticeable blood movement could be seen within the ILT, which is in agreement with the conclusion of Adolph et al. (1997), who experimentally carried out a histologic analysis for the ILT and suggested that fluid and smaller molecules may pass freely through the thrombus via the canaliculi network. It was found that the flow is more able to transmit through the ILT in the distal end of the aneurysm compared to other locations of the ILT which could be as a result of the perpendicular

force of the flow and the continuous vortices' formation in this location; this could have implications for the rupture in these regions.

The importance of these findings to the field is found in their introduction of a porous model that it could be used to mimic the ILT in AAA, and the display of the effect of such modelling to the wall stresses. This study also introduced the first numerical simulation which introduced the mass transport of blood flow at the interface of blood-ILT mediums, and blood flow within the ILT itself.

The key result of this thesis, and the results gained, is that it was able to explain the basic roles of different aspects in relation to stress variation. A number of studies in the literature have contributed very good results, but, when compared to others in the literature, gave conflicting conclusions. Modelling a patient-specific aneurysm may give good results about that specific patient but not necessarily lead to more understanding of the basic role for the criteria that are intended to be used to assess the rupture in AAA. This thesis tried to understand, and conclude, the basic effect of each parameter in isolation of the effects of other factors, which can lead to a better understanding of the general effect of the whole shape.

Chapter 7
Conclusions and future work

7.1 Conclusions

The conclusions that could be taken from this work are listed here:

- **Maximum diameter is not the best parameter to predict aneurysm risk of rupture.**

It was clearly proven that maximum stress is not always located in the maximum diameter because the rupture is a mechanical event which occurs when stress on the wall exceeds its strength. Hence, maximum diameter is not the best predictor of maximum stress.

- **Aneurysm aspect ratio can affect the magnitude and locations of maximum stresses.**

Aneurysms with small aspect ratios generally have lower maximum stress, compared to ones with large aspect ratios. Also the location of maximum stress in aneurysms with small aspect ratios is likely to be at the aneurysm ends, while for large aspect ratios aneurysms the maximum stress is expected to be in the middle. Aspect ratio assessment can enhance the prediction of the location and the magnitude of maximum wall stress.

- **Mechanically, the presence of the ILT reduces the stresses on the wall.**

From a mechanical point of view, the ILT will work as a cushion and decrease the stresses on the wall. This role is inversely proportional to the thrombus thickness.

- **The stiffness of the ILT will affect its role on the rupture mechanism.**

The ILT has a harmful role on the AAA wall but its stiffness can determine if its presence will be favourable or not to the AAA. A stiff ILT will overcome its harmful role and result in it supporting the wall, while a non-stiff ILT will have a harmful role.

- **The porosity of the ILT does not increase or decrease the wall stresses compared to solid ILT.**

A porous ILT was found to provide same protective role of a solid ILT and hence, if wall stress is required porosity could be neglected.

- **The porosity of the ILT transmits the blood pressure to the internal wall of AAA.**

A porous ILT allows the blood pressure to be transmitted to the internal wall without reduction.

- **The supportive role of the ILT is not a result of pressure drop on the wall, rather it is caused by the supportive role of the ILT reducing wall deformation.**

Porous and solid ILTs provide the same role of protection, although the porous ILT transmits all the pressure to the internal wall while the solid ILT does not. The reason for the supportive role of the ILT is its ability to reduce the deformation (strain) on the aneurysm wall.

- **Vortices of blood flow inside the aneurysm probably play an important role in the formation of the ILT and in the pathology of the AAA.**

Blood vortices may lead to platelet deposition causing a weakening and pathology to the affected region, and hence lead to thrombus formation.

- **AAA growth in some regions could be a function of mechanical forces.**

The growth of AAA is caused by many reasons, but it was found that blood flow inside the ILT at the distal end of the aneurysm may cause a concentration of some living cells within the thrombus that have a relationship to the pathology of AAA and lead to growth in those regions.

7.2 Future work

This work has discussed a number of the basic factors that may have relation to rupture, and some positive initial results were found that deserve more investigation. In particular, further work is recommended in the following areas:

Oxygen modelling within blood

It is thought that oxygen dysfunctioning is an important reason behind AAA pathology for aneurysms with the ILT. Oxygen should be included within the blood flow to take advantage of ILT porosity and its concentration should be checked at different sites of the ILT to understand how much this may increase the pathogenesis of the AAA.

Using patient specific models (realistic)

In reality, AAAs are not idealised shapes, they are more complex and irregular. To apply the findings of this thesis it is necessary to apply them to realistic shapes.

REFERENCES

Adolph R, Vorp DA, Steed DL, Webster MW, Kameneva MV, Watkins SC; (1997) Cellular content and permeability of intraluminal thrombus in abdominal aortic aneurysm. J Vasc Surg.;25(5):916–26

Ailawadi G, Eliason L, Upchurch R; (2003), Current concepts in the pathogenesis of abdominal aortic aneurysm, Journal of vascular surgery, 38: 584-588.

Alcorn G, Wolfson K, Sutton-tyrrell K, Kuller H, O'leary D; (1996), Risk factors for abdominal aortic aneurysms in older adults enrolled in the cardiovascular health study. Arterioscler thromb vasc biol, 16: 963-970.

Ashton J, Geest J, Bruce S, Haskett D; (2009), Compressive mechanical properties of the intraluminal thrombus in abdominal aortic aneurysms and fibrin-based thrombus mimics. J biomech, 42(3): 197–201.

Bargellini N, Petruzzi P, Cioni P, Vignali R, Sardella C, Ferrari G, Bartolozzi C; (2005), Type ii lumbar endoleaks: hemodynamic differentiation by contrast-enhanced ultrasound scanning and influence on aneurysm enlargement after endovascular aneurysm repair. Journal of vascular surgery, 41: 10-18.

Bhaskaran R; (2002), Introduction to CFD Basics, FLUENT.

Bieth J; (2001), The elastases, j soc biol, 195(2): 173-9.

Birkedal-Hansen H, Moore W, Bodden M, Windsor L, Birkedal-Hansen B, DeCarlo A, Engler JA; (1993), Matrix metalloproteinases: a review. Crit. Rev. Oral. Biol. Med, 4(2): 197-250.

Bonert M, Leask R, Butany J, Ethier C, Myers J, Johnston K, Ojha M; (2003), The relationship between wall shear stress distributions and intimal thickening in the human abdominal aorta. Biomedical engineering online,2,18.

Brady A, Simon G, Thompson G, Fowkes R, Greenhalgh J; (2004), Abdominal aortic aneurysm expansion, risk factors and time intervals for surveillance. Circulation,110:16-21.

Breeuwer M, Gotte U, Hoogeveen R, Wolters B, De putter S, Bosch H, Buth J, Rouet J, Laffargue F; (2004), Assessment of the rupture risk of abdominal aortic aneurysms by patient-specific hemodynamic modeling--initial results. International congress series, 1268, 1090.

British Heart Foundation (Government) Media News. http://www.bhf.org.uk/media/news-from-the-bhf/abdominal-aortic-aneurysms.aspx Accessed on 17 May, 2011

Buchanan J, Kleinstreuer R, Hyun C, Truskey G; (2003), Hemodynamics simulation and identification of susceptible sites of atherosclerotic lesion formation in a model abdominal aorta. Journal of biomechanics, 36: 1185-1196.

Budwig R, Elger D, Hooper H, Slippy J; (1993), Steady flow in abdominal aortic aneurysm models. J Biomech Eng, 115(4A):418-23.

Callanan A, Morris L, McGloughlin T; (2005), Prediction of abdominal aortic aneurysm (AAA) rupture using numerical and experimental techniques. Ir J Med Sci,174:S38.

Cheng Cheng P, Herfkens J, Taylor A; (2003b), Comparison of abdominal aortic hemodynamics between men and women at rest and during lower limb exercise. Journal of vascular surgery, 37: 118-123.

Cheng P, Herfkens J, Taylor A; (2003a), Abdominal aortic hemodynamic conditions in healthy subjects aged 50-70 at rest and during lower limb exercise: in vivo quantification using mri. Atherosclerosis, 168: 323-331.

Cowan J, Justin J, Dimick P, Henke J, Rectenwald J, Gilbert j; (2006), Epidemiology of Aortic Aneurysm Repair in the United States from 1993 to 2003. Ann. N.Y. Acad. Sci, 1085: 1–10.

Crawford C, Kristin H, Ernest T, Marley J; (2003), Abdominal aortic aneurysm: an illustrated narrative review. J manipulative physiol ther, 26:184-95.

Dalman L; (2003), Oxidative stress and abdominal aneurysms: how aortic hemodynamic conditions may influence aaa disease. Cardiovascular surgery, 11: 417-419.

Di Martino S, Guadagni G, Fumero A, Ballerini G, Spirito R, Biglioli P, Redaelli A; (2001), Fluid-structure interaction within realistic three-dimensional models of the aneurysmatic aorta as a guidance to assess the risk of rupture of the aneurysm. medical engineering & physics, 23: 647-655.

Doyle B, Coyle P, Kavanagh E, Grace P, McGloughlin T; (2010), A Finite Element Analysis Rupture Index (FEARI) Assessment of Electively Repaired and Symptomatic Ruptured Abdominal Aortic Aneurysms. IFMBE Proceedings, 31(3): 883-886.

Elger D, Blackketter D, Budwig R, Johansen K; (1996), The influence of shape on the stresses in model abdominal aortic aneurysms. Journal of biomechanical engineering, 118: 326–332.

Engellau A, Dahlstro M, Norgren A, Persson E, Larsson M; (2003), Measurements before endovascular repair of abdominal aortic aneurysms mr imaging with mra vs. Angiography and ct. Acta radiologica, 44: 177-184.

Ernst C; (1993), Abdominal aortic aneurysm, N engl j med, 328: 1167-1172.

Fagan M; (1992), Finite Element Analysis Theory and Practice. Longman Scientific and Technical.

Fillinger M, Marra F, Raghavan P, Kennedy E; (2003), Prediction of rupture risk in abdominal aortic aneurysm during observation: wall stress versus diameter. Journal of vascular surgery, 37: 724-732.

Fillinger M, Raghavan L, Marra P, Cronenwett L, Kennedy E; (2002), In vivo analysis of mechanical wall stress and abdominal aortic aneurysm rupture risk. Journal of vascular surgery, 36: 589-597.

Finol A, Amon H; (2001), Blood flow in abdominal aortic aneurysms: pulsatile flow hemodynamics. Transactions of the asme, 123: 474 - 484.

Fleischmann D, Hastie J, Dannegger C, Paik S, Tillich M, Zarins K, Rubin D; (2001), Quantitative determination of age-related geometric changes in the normal abdominal aorta. Journal of vascular surgery, 33: 97-105.

Fletcher C; (1990), Computational Techniques for Fluid Dynamics: Fundamental and general techniques, Springer.

Fung Y; (1993), Biomechanics: mechanical properties of living tissues, San Diego, Springer.

Gasser C, Görgülü G, Folkesson M, Swedenborg J; (2008), Failure properties of intraluminal thrombus in abdominal aortic aneurysm under static and pulsating mechanical loads, 48:179-188

Gasser Christian , Giampaolo Martufi, Martin Auer, Maggie Folkesson, Jesper Swedenborg (2010), Micromechanical Characterization of Intraluminal Thrombus Tissue from Abdominal Aortic Aneurysms, Annals of Biomedical Engineering, volume (38) 2, 371--379

Gray H; (1918), Anatomy of the human body, www.bartleby.com.

Hall C, You C, FACS R, Murray G, Benjamin E, Pantelis A; (2003) Mortality, Morbidity, and Costs of Ruptured and Elective Abdominal Aortic Aneurysm Repairs in Nova Scotia, Canada, Ann Vasc Surg, 17: 171-179.

Heller A, Weinberg A, Arons R, Krishnasastry K, Lyon R, Deitch J, Schulick H,Bush H, Kent C; (2000), Two decades of abdominal aortic aneurysm repair: have we made any progress?. Journal of vascular surgery, 32: 1091.

Hibbeler R; (2004) Mechanics of Materials, Prentice Hall.

Hollier L, Taylor L, Ochsner J; (1992), Recommended indication for operative treatment of abdominal aortic aneurysms. J. Vasc. Surg, 15:1046–1056.

Hua Johnson, Mower William R;(2001) Simple geometric characteristics fail to reliably predict abdominal aortic aneurysm wall stresses, J Vasc Surg. Aug;34(2):308-15.

Imray C; (2006), Managing an abdominal aortic aneurysm. Practical cardiovascular risk management, 4(2): 9 – 11.

Jamison R, Sheard G, Ryan K, Foura A; (2009), The validity of axisymmetric assumptions when investigating pulsatile biological flows, Austral. Mathematical Soc, 50: 713-728.

Karkos C, Mukhopadhyay U, Papakostas I, Ghosh J, Thomson G, Hughes R; (2000), Abdominal aortic aneurysm: the role of clinical examination and opportunistic detection. European journal of vascular and endovascular surgery,19:299-303.

Katz D, Littenberg B, Cronenwett J; (1992), Management of small abdominal aortic aneurysms. Early surgery vs watchful waiting. JAMA, 19:2678-86.

Kelly S, O'Rourke M; (2009), A two-system, single-analysis, fluid–structure interaction technique for modelling abdominal aortic aneurysms. Journal of Engineering in Medicine, 224: 0954-4119.

Khanafer K, Bull J, Berguer R; (2009), Fluid–structure interaction of turbulent pulsatile flow within a flexible wall axisymmetric aortic aneurysm model. Eur. J. Mech. – B/Fluids, 28, 88–102.

Lee Y, Keitzer W, Watson F, Liu H; (1982), Vascular geometry at the abdominal aortic bifurcation. J am med womens assoc, 37:77-81.

Lermusiaux P, Leroux C, Tasse J, Castellani C, Martinez R; (2001), Aortic aneurysm: onstruction of a life-size model by rapid prototyping. Annals of vascular surgery, 15, 131-135.

Leung J, Wright A, Cheshire N, Crane J, Thom S, Hughes A, Xu,Y; (2006) Fluid structure interaction of patient specific abdominal aortic aneurysms: a comparison with solid stress models. Biomed. Engng Online, 5: 33.

Li Z, Kleinstreuer C; (2006), Effects of blood flow and vessel geometry on wall stress and rupture risk of abdominal aortic aneurysms. J. Med. Engng Technol., 30(5): 283–297.

Liapis C, Kadoglou N; (2004), Matrix metalloproteinases: contribution to pathogenesis,diagnosis, surveillance and treatment of abdominal aortic aneurysms. Current medical research and opinion, 20(4): 419-432.

Logan D; (2006), A first course in finite element method, CL Engineering.

Lombardi J, Fairman R, Golden A, Carpenter P, Mitchell M, Barker C, Mcbride A, Velazquez C; (2004), The utility of commercially available endografts in the treatment of contained ruptured abdominal aortic aneurysm with hemodynamic stability. Journal of vascular surgery, 40: 154-160.

Meyer CA, Guivier-Curien C, Moore JE Jr; (2010), Trans-thrombus blood pressure effects in abdominal aortic aneurysms. J Biomech Eng. Jul;132(7):071005.

Morris L, O'Donnell P, Delassus P, McGloughlin T; (2004), Experimental assessment of stress patterns in abdominal aortic aneurysms using the photoelastic method. Strain,40:165–172.

Mower W, Baraff L, Sneyd J; (1993), Stress distribution in vascular aneurysms: factors affecting risk of aneurysm rupture. *Journal of Surgical Research*, 55:155-161.

Mower W, Quiňones W, Gambhir S; (1997), Effect of intraluminal thrombus on abdominal aortic aneurysm wall stress. *Journal of Vascular Surgery*, 26:602-8.

Outten J, Kruse K, Freeman M, Pacanowski J, Ragsdale J, Stevens S; (2003) Computational model of mechanical wall stress in abdominal aortic aneurysm one hour prior to rupture. In: Proceedings of the 2003 summer bioengineering conference, SBC2003, Key Biscayne, FL, 77-8.

Papaharilaou Y, Ekaterinaris J, Eirini M, Asterios K; (2007), A decoupled fluid structure approach for estimating wall stress in abdominal aortic aneurysms. Journal of Biomechanics, 40(2): 367-377.

Peattie A, Asbury L, Bluth I, Ruberti W; (1996), Steady flow in models of abdominal aortic aneurysms. Part i: investigation of the velocity patterns. J. Ultrasound med, 15: 679-688.

Peattie A, Riehle J, Bluth I; (2004), Pulsatile flow in fusiform models of abdoiminal aortic aneurysms: flow fields, velocity patterns and flow-induced wall stresses. Journal of biomechanical engineering, 126: 438-46.

Peppelenbosch N, Buth J, Harris L, Van marrewijk C, Fransen G; (2004), Diameter of abdominal aortic aneurysm and outcome of endovascular aneurysm repair: does size matter? A report from eurostar. Journal of vascular surgery, 39: 288.

Polzer S. and Bursa J.; (2010) Poroelastic Model of Intraluminal Thrombus in FEA of Aortic Aneurysm, 6th World Congress of Biomechanics . August 1-6, 2010 Singapore, IFMBE Proceedings, Volume 31, Part 3, 763-767.

Raghavan M, Vorp D, Federle M, Makaroun M, Webster W; (2000),Wall stress distribution on three-dimensionally reconstructed models of human abdominal aortic aneurysm. Journal of Vascular Surgery, 31:760–769.

Raghavan M, Kratzberg J, Castro M, Hanaoka M, Walker P, Da Silva E; (2006), Regional distribution of wall thickness and failure properties of human abdominal aortic, aneurysm. J. Biomech., 39(16): 3010–3016.

Raghavan M, Webster M, Vorp D; (1996), Ex-vivo biomechanical behavior of abdominal aortic aneurysm: assessment using a new mathematical model. Annals of Biomedical Engineering, 24(5):573-82.

Rodriguez J, Cristina R, Manuel D, Gerhard A; (2007), Mechanical stresses in abdominal aortic aneurysm. Material anisotropy a parametric study, IX Internatinal Conference on Computational Plasticity.

Sacks S, Vorp D, Raghavan M, Federle M, Webster M; (1999) in vivo three-dimensional surface geometry of abdominal aortic aneurysms. Annals of biomedical engineering, 27: 469-479.

Salsac Anne-Virginie, StevenR. Sparks, JuanC. Lasheras; (2004) Hemodynamic Changes Occurring during the Progressive Enlargement of Abdominal Aortic Aneurysms. Annals of Vascular Surgery, Volume 18, Number 1, 14-21

Sanfellipo P; (2003), Abdominal Aortic Aneurysm What we know, What we don't know-A review. International Journal of Angiology,12:145-152.

Sangiorgi G, D'averio R, Mauriello A, Bondio M, Pontillo M, Castelvecchio S, Trimarchi S, Tolva V, Nano G, Rampoldi V, Spagnoli G, IngleseG; (2001), Plasma levels of metalloproteinases-3 and -9 as markers of successful abdominal aortic aneurysm exclusion after endovascular graft treatment. Circulation, 104: 288-295.

Sayers R; (2002), Aortic aneurysms, inflammatory pathways and nitric oxide. Annals of the Royal College of Surgeons of England, 84:239–246.

Schurink G, Van Baalen J, Visser M, Van Bockel J; (2000), Thrombus within an aortic aneurysm does not reduce pressure on the aneurysmal wall. Journal of Vascular Surgery, 31:501-506 .

Scotti C, Alexander S, Satish M, Finol E; (2005), Fluid-structure interaction in abdominal aortic aneurysms: effects of asymmetry and wall thickness. Biomedical engineering online, 4:64.

Scotti C, Finol A; (2007), Compliant biomechanics of abdominal aortic aneurysms: a fluid– structure interaction study. Comput. Struct., 85(11–14): 1097–1113.

Speelman A, Bosboom E, Schurink G, Vande vosse F, Makaorun M, Vorp D; (2007), Effects of wall calcifications in patient-specific wall stress analyses of abdominal aortic aneurysms. Journal of biomechanical engineering, 129(1): 105-9.

Stringfellow M, Lawrence P, Stringfellow R; (1987), The infuence of aorta-aneurysm geometry upon stress in the aneurysm wall. *Journal of Surgical Research*,42:425–433.

Sun N, Leung W, Hughes J, Cheshire X; (2009), Computational analysis of oxygen transport in a patient-specific model of abdominal aortic aneurysm with intraluminal thrombus. The british journal of radiology, 82: s18–s23.

Takagi H, Yoshikawa S, Mizuno Y, Matsuno Y, Umeda Y, Fukumoto Y, Mori Y; (2005) Intrathrombotic pressure of a thrombosed abdominal aortic aneurysm. Ann Vasc Surg. Jan;19(1):108-12.

Taylor A, Thomas R, Zarins K; (1998), Finite element modeling of three-dimensional pulsatile flow in the abdominal aorta: relevance to atherosclerosis. Annals of biomedical engineering, 26: 975-987.

Taylor T, Yamaguchi T; (1994), Three-dimensional simulation of blood flow in an abdominal aortic aneurysm--steady and unsteady flow cases. *J Biomech Eng* 1994 , 116(1):89-97.

Thomas P, Stewart R; (1988), Abdominal aortic aneurysm. Br J Surg. Aug, 75(8):733-6.

Ujiie H, Tachibana H, Hiramatsu O, Hazel AL, Matsumoto T, Ogasawara Y, Nakajima H, Hori T, Takakura K, Kajiya F.; (1999) Effects of size and shape (aspect ratio) on the hemodynamics of saccular aneurysms: a possible index for surgical treatment of intracranial aneurysms. Neurosurgery. Jul;45(1):119-29.

Ujiie H, Tamano Y, Sasaki K, Hori T.; (2001) Is the aspect ratio a reliable index for predicting the rupture of a saccular aneurysm? Neurosurgery. Mar;48(3):495-502.

Van Dam E, Dams S, Peters G, Rutten M, Schurink G, Buth J, Van de V;(2006) , Determination of linear viscoelastic behavior of abdominal aortic aneurysm thrombus. Biorheology, 43: 695 –707.

Venkatasubramaniam A, Fagan M, Mehta T, Mylankal K, Ray B, Kuhan G, Chetter I, McCollum P; (2004) A Comparative Study of Aortic Wall Stress Using Finite Element Analysis for Ruptured and Non-ruptured Abdominal Aortic Aneurysms. Eur J Vasc Endovasc Surg., 28(2):168-76.

Versteeg H, Malasekera W; (1995),An Introduction to Computational Fluid Dynamics, John Visse R, Nagase H; (2003), Matrix metalloproteinases and tissue inhibitors of metalloproteinases: structure, function, and biochemistry. Circ res, 92(8): 827-839.

Vorp D, Lee C, Wang D, Makaroun S, Nemoto M, Ogawa S, Webster W; (2001), Association of intraluminal thrombus in abdominal aortic aneurysm with local hypoxia and wall weakening. Journal of vascular surgery, 34: 291.

Vorp D, Mandarino W, Webster W, Gorcsan J; (1996a) 3rd Potential influence of intraluminal thrombus on abdominal aortic aneurysm as assessed by a new non-invasive method. Cardiovascular Surgery,4:732–9.

Vorp D, Raghavan M, Muluk S, Makaroun M, Steed D, Shapiro R, Webster W; (1996b), Wall strength and stiffness of aneurysmal and nonaneurysmal abdominal aorta. Proceedings in Volume 800 in the Annals of the New York Academy of Sciences; United States.

Vorp D, Webster W, Federspiel W; (1998), Effect of intraluminal thrombus thickness and bulge diameter on the oxygen diffusion in abdominal aortic aneurysm. J biomech eng., 120: 579-83.

Vorp D; (2007), Biomechanics of abdominal aortic aneurysm. Journal of Biomechanics, 40(9):1887-1902.

Walsh W, Chin-quee S, Moore J; (2003), Flow changes in the aorta associated with the deployment of a aaa stent graft. Medical engineering & physics, 25: 299-307.

Wang D, Makaroun H, Webster M, Vorp D; (2002), Effect of intraluminal thrombus on wall stress in patient-specific models of abdominal aortic aneurysm. Journal of vascular surgery, 36: 1-7.

Wang D, Marshall W, Webster D, Vorp D; (2001), Mechanical properties and microstructure of intraluminal thrombus from abdominal aortic aneurysm. Transactions of the asme, 123: 536 - 539.

Wassef M, Timothy B, Chisholm R, Dalman F, Heinecke H, Kuivaniemi P, Pearce P; (2001); Pathogenesis of abdominal aortic aneurysms: a multidisciplinary research program supported by the national heart. J vasc surg, 34: 730-8.

Weir B, Amidei C, Kongable G, Findlay JM, Kassell NF, Kelly J, Dai L, Karrison TG;(2003) The aspect ratio (dome/neck) of ruptured and unruptured aneurysms. J Neurosurg. Sep;99(3):447-51.

Wilson R, Anderton M, Schwalbe E, Jones L, Furness P, Bell P, Thompson M; (2006), Matrix Metalloproteinase-8 and -9 Are Increased at the Site of Abdominal Aortic Aneurysm Rupture. *Circulation,*113:438-445.

Wolf Y and Bernstein E; (1994), A current perspective on the natural history of abdominal aortic aneurysms. Cardiovasc. Surg, 2:16–22.

Yu S, Ng H, Chua P; (1999), A numerical investigation on the steady and pulsatile flow characteristics in axi-symmetric abdominal aortic aneurysm models with some experimental evaluation. Journal of medical engineering & technology 23: 228 - 239.

Yu S; (2000), Steady and pulsatile flow studies in abdominal aortic aneurysm models using particle image velocimetry. International journal of heat and fluid flow, 21: 74-83.